



Aalborg Universitet

AALBORG UNIVERSITY
DENMARK

A Design & Optimization Framework for Valves in Digital Displacement Units

Bender, Niels Christian

Publication date:
2019

Document Version
Publisher's PDF, also known as Version of record

[Link to publication from Aalborg University](#)

Citation for published version (APA):

Bender, N. C. (2019). *A Design & Optimization Framework for Valves in Digital Displacement Units*. Aalborg Universitetsforlag. Ph.d.-serien for Det Ingeniør- og Naturvidenskabelige Fakultet, Aalborg Universitet

General rights

Copyright and moral rights for the publications made accessible in the public portal are retained by the authors and/or other copyright owners and it is a condition of accessing publications that users recognise and abide by the legal requirements associated with these rights.

- ? Users may download and print one copy of any publication from the public portal for the purpose of private study or research.
- ? You may not further distribute the material or use it for any profit-making activity or commercial gain
- ? You may freely distribute the URL identifying the publication in the public portal ?

Take down policy

If you believe that this document breaches copyright please contact us at vbn@aub.aau.dk providing details, and we will remove access to the work immediately and investigate your claim.

**A DESIGN & OPTIMIZATION
FRAMEWORK FOR VALVES IN DIGITAL
DISPLACEMENT[®] UNITS**

**BY
NIELS CHRISTIAN BENDER**

DISSERTATION SUBMITTED 2019



AALBORG UNIVERSITY
DENMARK

A Design & Optimization Framework for Valves in Digital Displacement[®] Units

Ph.D. Dissertation
Niels Christian Bender

Dissertation submitted August 16, 2019

Dissertation submitted: August 16, 2019

PhD supervisor: Prof. Henrik Clemmensen Pedersen
Aalborg University, Aalborg, Denmark

Assistant PhD supervisor: Assoc. Prof. Bernd Winkler
Linz Center of Mechatronics, Linz, Austria

PhD committee: Associate professor Henrik Sørensen (Chair)
Aalborg university
Professor Perry Li
University of Minnesota
Professor Petter Krus
Linköping University

PhD Series: Faculty of Engineering and Science, Aalborg University

Department: Department of Energy Technology

ISSN (online): 2446-1636
ISBN (online): 978-87-7210-474-4

Published by:
Aalborg University Press
Langagervej 2
DK – 9220 Aalborg Ø
Phone: +45 99407140
aauf@forlag.aau.dk
forlag.aau.dk

© Copyright: Niels Christian Bender

Printed in Denmark by Rosendahls, 2019

Preface

This dissertation has been submitted as an extended summary and collection of papers to the Faculty of Engineering and Science at Aalborg University in partial fulfilment of the requirements for the degree of Doctor of Philosophy. This work was funded by the Danish Council for Strategic Research via the HyDrive-project (case no. 1305-00038B) and the research has been conducted at the Department of Energy Technology at Aalborg University with a research study at Linz Center of Mechatronics (LCM) GmbH lasting three months.

This work is largely motivated by the results and discussions of the Ph.D. dissertations by Daniel B. Rømer and Christian Nørgård. I would like to thank both of them for their inputs and contributions related to the topic of my work.

Both Jeppe H. Christensen and Michael M. Bech have been extremely kind in supporting with laboratory support regarding the test-rig. For that I thank you. Also, the entire team at LCM made a great effort to make my research abroad enjoyable, which I am forever grateful.

My supervisor Henrik C. Pedersen deserves a special thanks for leading me along the way when critical decisions were to be made. His expertise and assistance has influenced this work greatly.

I am thanking all of the above mentioned, my office buddies Per Johansen and Remzija Cerimagic and fellow PhD students for being part of this journey and for their social support. Finally, thanks to my family, friends and girlfriend for being both patient and supportive.

Niels Christian Bender
Aalborg University, August 16, 2019

Preface

Abstract

This thesis deals with various aspects related to the design and optimization of fast switching valves used in Digital Displacement[®] machines. Here, the focus is primarily on developing model-based methods to predict the fluid dynamics during valve switching, because this is essential for predicting the performance of such machines.

The need for more detailed simulation tools is related to the time consuming process of developing new technologies/products in hydraulic systems. This applies to both performance and durability. One of the latest proposals for a more efficient pump technology has therefore driven the motivation for developing design methodologies and prototypes of so-called "digital valves".

Based on a valve concept and state-of-the-art design methodologies, a set of equations has been established to describe the motion of the valve plunger. The method is based on an interaction between equations solved analytically and numerically, to describe the influence of the flow geometry on the switching time and the fluid dynamic energy loss. During the optimization process, the simpler models are used to find a dimensioning that fits the purpose. Here, there is special focus on mechanisms that lower the speed of the plunger before it is stopped by the valve seat.

The primary conclusions regarding the flow geometry are drawn on the basis of transient and dynamic CFD simulations. The formulation of this simulation model is novel in the manner the dynamic mesh is updated and how the maximum time step is limited as a function of the current plunger position.

Several valve prototypes have been tested under various circumstances to investigate the extent to which the developed simulation tools are useful. Here there is a proper correlation between theory and practice, however, it has proven difficult to determine the exact velocity profile near mechanical collision between plunger and seat.

The industry demands methods for predicting lifetime as well as the consequences of long-term wear on system performance. This field is rapidly developing at the time of writing, but generic methods are not yet available to predict the effects of changes on valve design or operating conditions. In

Abstract

this thesis, the possible wear phenomena that are thought to occur in the designed seat valves are elaborated. Wear marks near the mechanical contact surfaces are documented experimentally. This is attributed, among other things, to the rapid shift time. It is still unclear what consequences the high number of switching cycles at the desired pressure may have on the long-term durability of the valves. Before this can be tested, the activating mechanism must be replaced with something more durable.

In total, this research has contributed to a deeper understanding of transient fluid dynamic phenomena in fast switching valves. In addition, initial wear studies have shown that the mechanical design is durable, although clear surface changes have been observed.

Resumé

Denne afhandling omhandler diverse aspekter relateret til design og optimering af hurtigt skiftende ventiler anvendt i Digital Displacement[®] maskiner. Her er fokuset primært på at udvikle modelbaserede metoder til at forudsige fluiddynamikken under ventil-omskiftning, fordi dette er afgørende for at forudsige ydeevnen af sådanne maskiner.

Behovet for mere detaljerede simuleringstværværktøjer hænger sammen med den tidskrævende proces det er at udvikle nye teknologier/produkter inden for hydrauliske systemer. Dette gælder både mht. ydeevne og holdbarhed. Et af de seneste bud på en mere effektiv pumpe teknologi har derfor drevet motivationen for at udvikle designmetodikker og prototyper af såkaldte 'digitale ventiler'.

Med udgangspunkt i ét ventil koncept samt state-of-the-art designmetodikker, er der blevet opstillet et sæt af ligninger som beskriver bevægelsen af ventilens glider. Metoden bygger på et samspil mellem ligninger løst analytisk og numerisk, for at beskrive sammenhængen mellem strømningsgeometrien og skifte-hastigheden samt det fluid-dynamiske-energitab. Under optimeringsprocessen benyttes simple modeller for at finde frem til en dimensionering som passer til formålet. Her er der specielt fokus på mekanismer som sænker hastigheden af glideren inden denne stoppes af ventilsædet.

De primære konklusioner vedrørende strømningsgeometrien er draget på baggrund af CFD simuleringer der simulerer det transiente og dynamiske forløb. Formuleringen af denne simuleringmodel er speciel ift. hvordan det dynamiske mesh opdateres og hvordan det maksimale tidsskridt begrænses som funktion af den øjeblikkelige glider-position.

Flere ventil-prototyper er blevet testet under forskellige omstændigheder for at undersøge i hvilken grad de udviklede simuleringstværværktøjer er brugbare. Her er der en tilpas sammenhæng mellem teori og praksis. Dog har det vist sig vanskeligt at bestemme den nøjagtige hastighedsprofil nær mekanisk kollision mellem glider og sæde.

Industrien efterspørger metoder til at forudsige levetider samt konsekvenser af langvarig slid på systemers ydeevne. Dette felt er i skrivende stund under hastig udvikling, hvor generiske metoder endnu ikke er tilgængelige til

Resumé

at forudsige indvirkningerne fra ændringer af ventil design eller driftsbetingelserne. I denne afhandling uddybes de mulige slid-fænomener som menes at kunne opstå i de designede sædeventiler. Slid-mærker nær de mekaniske kontakt flader er dokumenteret eksperimentelt. Dette tilskrives blandt andet den hurtige skiftetid. Det er stadig uklart hvilke konsekvenser det høje antal af skiftecyklusser ved det ønskede tryk kan have for den langvarige holdbarhed af ventilerne. Før dette kan testet må den aktiverende mekanisme erstattes med noget mere holdbart.

I alt har denne forskning bidraget til en dybere forståelse af transient fluid dynamiske fænomener i hurtigt-skiftende ventiler. Desuden har indledende slid studier påvist at det mekaniske design er holdbart, selvom tydelige overflade ændringer er blevet observeret.

A Design & Optimization Framework for Valves in Digital Displacement Units

This present report combined with the listed scientific papers has been submitted for assessment in partial fulfilment of the PhD degree. The documented thesis is mainly based on the above listed papers, where parts of these papers are directly used are properly cited. The thesis is not in its present form acceptable for open publication but only in limited and closed circulation as the copyright may not be ensured.

List of published and submitted papers:

- A Experimental Validation of Flow Force Models for Fast Switching Valves, Niels C. Bender, Henrik C. Pedersen and Christian Nørgård, in *Proceedings of the ASME/BATH Symposium on Fluid Power and Motion Control*, 2017
- B Reliability Analysis of a Hydraulic On/Off Fast Switching Valve, Niels C. Bender, Henrik C. Pedersen, Andreas Plöckinger and Bernd Winkler, in *The Ninth Workshop on Digital Fluid Power*, 2017
- C Towards a modelling framework for designing active check valves – a review of state-of-the-art, Niels C. Bender, Henrik C. Pedersen, Andreas Plöckinger and Bernd Winkler, in *Int. J. Fluid Power*, vol 19(1), pp 49-64, 2017
- D Evaluating the Influence of Leaking Active Check Valves in Digital Displacement Units, Niels C. Bender, Henrik C. Pedersen, Andreas Plöckinger and Bernd Winkler, in *IEEE Global Fluid Power Society PhD Symposium*, 2018
- E Numerical Investigation of Switching Features of a Hydraulic Seat Valve with Annular Flow Geometry, Niels C. Bender, Henrik C. Pedersen, Andreas Plöckinger and Bernd Winkler, in *Int. J. Fluid Power*, vol 19(3), pp 152-164, 2018
- F A Multi-Agent Evolution Algorithm Used for Input Shaping of a Repetitive Non-Linear Dynamic System, in *Proceedings of the ASME/BATH Symposium on Fluid Power and Motion Control*, 2018
- G Experimental Study of a Digital Displacement Machine Utilizing a Cushioning Valve Topology, Niels C. Bender, Jeppe H. Christensen, Michael M. Bech and Henrik C. Pedersen, in *The Tenth Workshop on Digital Fluid Power*, 2018
- H Measurements of a Novel Digital Hydraulic Valve Comprising a Cushioning Feature, Niels C. Bender, Andreas Plöckinger, Paul Foschum, Bernd Winkler and Henrik C. Pedersen, in *Journal of Dynamic Systems*,

Resumé

Measurement, and Control, accepted for publication - under going second review process, 2019

I Feasibility of Deep Neural Network Surrogate Models in Fluid Dynamics, Niels C. Bender, Torben O. Andersen and Henrik C. Pedersen, in *Modeling, Identification and Control: A Norwegian Research Bulletin vol 40(2) pp 71-87, 2019*

J Parameter Correlation by Static and Dynamic Evaluations Utilizing a Mechatronic Design Procedure for a Digital Displacement Unit, Niels C. Bender, Torben O. Andersen and Henrik C. Pedersen, under review at *IEEE/ASME Transactions on Mechatronics, 2019*

Other papers:

A Investigation of squeeze film damping and associated loads, Per Johansen, Niels C. Bender, Anders H. Hansen and Lasse Schmidt, in *Proceedings of the ASME/BATH Symposium on Fluid Power and Motion Control, 2017*

"It ain't what you don't know that gets you into trouble. It's what you know for sure that just ain't so."

– Mark Twain (1835 – 1910)

"To finish the moment, to find the journey's end in every step of the road, to live the greatest number of good hours, is wisdom."

– Ralph Waldo Emerson (1803 – 1882)

Contents

Preface	iii
Abstract	v
Resumé	vii
Nomenclature	xv
I Extended Summary	1
1 Introduction	3
1.1 Preliminaries and Terminology	4
1.1.1 Working Principles of DDU	5
1.2 State-of-the-art	7
1.2.1 Digital Displacement [®] Technology	7
1.2.2 Design Methodologies Relevant for Mechatronic Sys- tem Design	17
1.3 Research Objectives	19
1.4 Main Contributions	20
1.5 Outline of Papers	22
1.6 Reading Guidelines	25
2 Developed Valve as Used in a DDU	27
2.1 The Machine	27
2.2 The Developed and Optimized Valve	28
2.2.1 Design Possibilities to Reduce Impact Loads	29
2.2.2 Achieved Theoretical Performance	31
3 The Design Framework	35
3.1 Flow Diagram of the Framework	35
3.2 Simplified DDU Equations	36

Contents

3.3	Digital Valve	40
3.3.1	The Dynamic Computational Fluid Dynamics (CFD) Framework	40
3.4	Valve Fluid Flow & Forces, F_f	47
3.4.1	Steady-state Flow Force, F_{flow}	48
3.4.2	Transient Flow Force, F_t	49
3.4.3	Valve Flow	50
3.4.4	Valve Fluid Inertia	52
3.4.5	Sensitivity of Flow and Force Predictions	54
3.4.6	Movement-Induced Flow and Force, F_{MI}	55
3.4.7	Squeeze-film and stiction force, F_e	59
3.5	Comparison of CFD and LPM	62
3.5.1	LPM vs CFD of the Optimum Valve	66
3.6	Mechanical End-stop and Spring Forces, $F_m + F_s$	67
3.7	Valve Energy Losses in a DDU	68
3.7.1	Efficiency	69
3.7.2	Analytical Integration	71
3.7.3	Valve Dimensioning at Certain Operating Conditions	72
3.7.4	Energy Dissipated during Switching	73
3.8	Stresses in the Plunger and Seat	74
3.9	Hydraulic Circuit Design	75
3.9.1	Analysis of the Fluid Dynamics	75
3.10	Summary	79
4	Validation of the Framework	81
4.1	Purpose of the Experiments	81
4.2	Experimental Test-rigs	82
4.2.1	Test-rig Concept I	82
4.2.2	Test-rig Concept II	83
4.2.3	Test-rig Concept III	84
4.3	Results	85
4.3.1	Valve Switching Results	85
4.3.2	Valve Switching Results - With a Cushion Groove	87
4.3.3	Valves Tested in a DDU	91
4.3.4	Run-in Wear	93
4.4	Summary	97
5	Closing Remarks	101
5.1	Conclusions	101
5.2	Future Work	103
	References	104

Contents

I	Design Optimization	113
I.1	Objectives	113
I.2	Design Variables and Constraints	114
I.3	Results	117
II	Plunger Surface Scans	121
II	Papers	127
A	Experimental Validation of Flow Force Models for Fast Switching Valves	129
B	Reliability Analysis of a Hydraulic on/off Fast Switching Valve	141
C	Towards a modelling framework for designing active check valves a review of state of the art	161
D	Evaluating the Influence of Leaking Active Check Valves in Digital Displacement[®] Units	179
E	Numerical Investigation of Switching Features of a Hydraulic Seat Valve with Annular Flow Geometry	191
F	A Multi-agent Evolution Algorithm used for Input Shaping of a Repetitive Non-linear Dynamic System	205
G	Experimental Study of a Digital Displacement Machine Utilizing a Cushion Valve Topology	217
H	Measurements of a Novel Digital Hydraulic Valve Comprising a Cushioning Feature	237
I	Feasibility of Deep Neural Network Surrogate Models in Fluid Dynamics	251
J	Parameter Correlation by Static and Dynamic Evaluations Utilizing a Mechatronic Design Procedure for a Digital Displacement Unit	271

Contents

Nomenclature

Table 1: Applied nomenclature in this dissertation

Abbreviation	Explanation	Unit
2D & 3D	2- & 3-dimensions	
AAU	Aalborg University	
ACV	Active Check Valve	
AIP	Artemis Intelligent Power	
ANN	Artificial Neural Network	
BC	Boundary Conditions	
CFD	Computational Fluid Dynamics	
DDP	Digital Displacement Pump	
DDT	Digital Displacement Technology	
DDU	Digital Displacement Unit	
DFCU	Digital Flow Control Unit	
DFR	Design for Reliability	
FEA	Finite Element Analysis	
GDE	Generalized Differential Evolution	
HPV & LPV	High & Low Pressure Valve	
LPM	Lumped Parameter Model	
MIF	Movement Induced (MI) Flow	
MCV	Moving Coil Valve	
MMV	Moving Magnet Valve	
ODE	Ordinary Differential Equation	
PDE	Partial Differential Equation	
MTTF	Mean Time to Failure	
PE	Power Electronics	
RANS	Reynolds Averaged Navier Stokes	
ROM	Reduced Order Model	
SEM	Scanning Electron Microscope	
SOTA	State Of The Art	
CC/rev	Cubic Centimetres per revolution	
L/min	Liter per minute	
RPM	Rounds per Minute	
Variables		
C_d	Discharge coefficient	[-]
E	Energy	[J]
F	Force (normally only the z-component)	[N]
P	Power	[W]
p	Pressure	[Pa]
Q	Flow	[m ³ /s]
i	Current in e.g. HPV and LPV actuator	[A]
u	Voltage in e.g. HPV and LPV actuator	[V]
W	Mechanical Work	[J]
x, y, z	Coordinates in a coordinate reference system	[m]
t	Time	[s]
Δt	Step-time	[s]

Nomenclature

β	Bulk modulus	[bar ⁻¹]
γ	Jet angle	[rad]
η	Efficiency	[-]
θ	Shaft position	[rad]
μ	Dynamic viscosity	[N s m ⁻²]
ν	Kinematic viscosity	[m ² s ⁻¹]
ρ	Density	[kg m ⁻³]
ψ	DDU displacement fraction	[-]
Parameters		
A	Area	[m ²]
c	Fitting coefficients	[-]
E	Young's modulus	[Pa]
h	Height	[m]
k	Parametric coefficient	[-]
L	Hydraulic inductance	[m ⁻³ s ² Pa ¹]
l	Length	[m]
m	Mass of moving part	[kg]
N	Integer number	[-]
S	Distance	[m]
R	Major radius of plunger	[m]
Re	Reynold's number	[-]
r	Radius	[m]
V	Volume	[m ³]
w	Width	[m]
α	Dynamic mesh factor	[-]
ϵ	Machine epsilon	[-]
ν	Poisson's ratio	[-]
λ	Eigenvalue	[-]
ρ	Spearman's correlation rank	[-]
σ	Standard deviation	[-]
ϕ	Offset angle	[rad]
χ	Hydraulic resistance	[Pa m ⁻³ s]
Operators		
\sqrt{x}	$\sqrt{ x sgn(x)}$	
\dot{x}	$\frac{dx}{dt}$	
\ddot{x}	$\frac{d^2x}{dt^2}$	
\bar{x}	Time averaged/approximated value	
\tilde{x}	Residual: $x_1 - x_2$	

The variables and parameters only explain the 'macro' meaning of each symbol. During the report proper index explanation are given whenever an unexplained symbol is used. This is done since the notations used in the papers are not necessarily the exact same, which may lead to confusion.

Part I

Extended Summary

Chapter 1

Introduction

The pursuit of an optimal solution is something that not only concerns the field of engineering, but also resonates with most processes in nature. Whether it being within; business, sports, diets, finance, gastronomy, living organisms, etc. all share the same simple structure: "*What is my goal? What parameters can I change to achieve this goal? What am I (not) allowed to do?*". Some formulations have a constant environment; others change over time, e.g. a temperature change, a humidity change or a change in a social norm. The available parameters to tune can vary over time, e.g. if a material or disruptive technology are invented/discovered. Political regulations and laws can influence what you are allowed to do, and the spatial dimensions of a system constrains the size of the components. The interpretation of what is optimal can vary through time, e.g. speed over accuracy or efficiency, environmental- or political- changes that requires a redefinition of the '*goal*'. At the time of writing, the main interest of society lies in creating efficient energy conversion solutions.

The main objective of this dissertation is to develop and validate a framework for design & optimization of the mechanical topology of valves used in Digital Displacement Units (DDU). This type of machine offers high part-load efficiency compared to other fluid power machinery, and performs just as good or even better at high rotational speeds. The technology can potentially reach out to the mobile hydraulics industry [30, 109], wind power transmission systems [101], winch drives [49] or wave energy & tidal current energy converters [79], where high power density and robustness are prioritized. The development of new fluid power technology is typically a long and costly process, e.g. the first known DDU prototype was developed around 1989 [85] and the first commercial machine is currently just being deployed. Therefore, any contribution towards virtual prototyping is relevant in order

to mature a fluid power technology faster and make it competitive to e.g. electrical alternatives. Virtual prototyping is achieved through model-based design where the principles of system modelling can be combined with optimization theory to find the design that performs optimally within the problem definition. This model-based approach also helps to understand complex processes in a system, which are otherwise difficult to measure directly.

1.1 Preliminaries and Terminology

The terminology in fluid power can be misleading and the community has not yet reached consensus on which terms to use for some concepts. Brief definitions of the essential terms used in the present report are given here.

Fluid power machine: has the objective of converting a mechanical torque to hydraulic power and vice versa. This may be done with a fixed or variable displacement unit.

Digital Fluid Power (DFP): when fluid power machines are using concepts from switching electronics, i.e. system states attain discrete values and are controlled by digital valves instead of proportional valves.

As pointed out in [1] this formulation is vague and can be challenged on a number of points. It is argued that since a DC-motor is not digital electronics it makes no sense to claim a pump to be digital simply because the principle is discontinuous. The definition is therefore not rigid, but since this work relates to the DD[®] Technology (DDT) this terminology is adapted regardless of its sanity.

Digital valve: is for hydraulics what the transistor (MOSFET or IGBT) is for power electronics, i.e. a component acting to open/close a conducting pathway in a circuit. This is a mechatronic component that is operating with some actuating mechanism that can move a mechanical part (e.g. a plunger), towards a stationary mechanical part (e.g. a seat). This will respectively open and close the connection between flow/pressure ports. The valve is thus digital in the sense that it will either be on or off, with some switching time in between. Acronyms of the term includes: On/Off valve, Fast Switching Valve (FSV), High Speed On/Off Valve (HSV).

Switching time: the time between a switching signal is sent until the digital valve has transitioned from one binary state to another. Opening and closing times may vary significantly and depend on the flow conditions.

Digital Displacement (DD): is a trademark of Artemis Intelligent Power (AIP) and refers to controlling the displacement in discrete steps. A pressure chamber enclosed by a moving piston can attain two different 'discrete' pressure levels.

1.1.1 Working Principles of DDU

The concept of a DDU utilizing Active Check Valves (ACV) is shown in Fig. 1.1a. Control signals are sent when the machine has a certain angular position (θ), where the state of the valves may be determined from the chamber pressure (p_C) or direct position measurement. This is used to control the machine displacement as detailed by Pedersen (2018) [81], or used in a timing control scheme, e.g. as proposed in [Paper E] or [110]. The valve's plunger movement (\dot{z}), the fluid force (F_f) and the maximum fluid pressure (p_{max}) have been analyzed under various flow rates by the Computational Fluid Dynamics (CFD) framework developed in this work. These results are plotted in Fig. 1.1b.

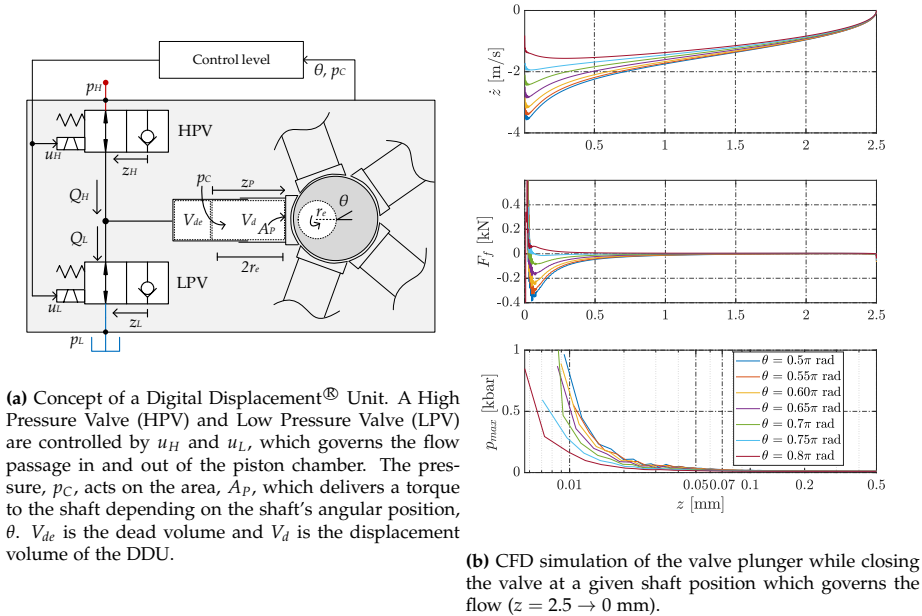


Fig. 1.1: The relevant dynamics of the HPV and LPV are plotted to illustrate how the fluid force (F_f) scales as the flow is increased during closing. This leads to significant differences in the velocity profile and the maximum pressure occurs earlier as valve switching approaches $\theta = 0.5\pi$. This fluid pressure reaches the yield strength of the used materials and may become problematic for the long-term durability.

The machine is functional when either HPV or LPV is on, or while both are off which allows increasing or decreasing p_C . Both valves are not intended to be on simultaneously. The graphs of Fig. 1.1 shows how much the switching time is dependent on the shaft position. The velocity is primarily affected as the plunger nears the seat where the maximum fluid pressure rises

drastically. The pressure magnitude nears 1 GPa, which indicates that an assumption of rigid bodies is not sufficient near impact. Prediction of F_f is an essential topic of this work as this both influences the dynamic performance, but also impact speed and hence durability.

The efficiency as function of shaft speed and displacement of a DDU compared to a bent-axis and swash-plate pump are shown in Fig. 1.2. These graphs are for pumping operation. The reference pumps have similar rated power output, and the documented efficiencies are the primary motivation to research the DDT.

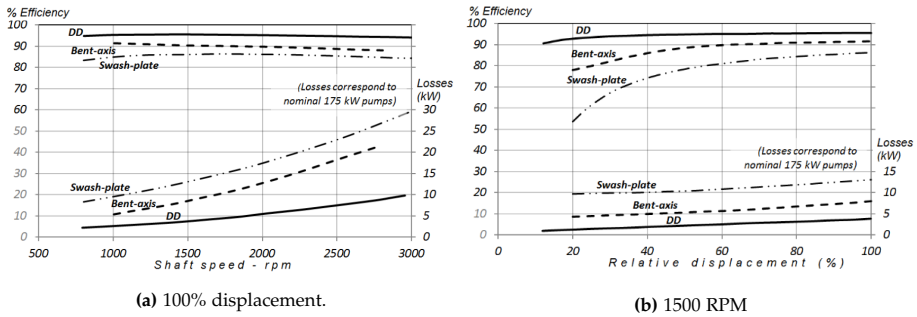


Fig. 1.2: Losses and efficiencies against shaft speed and displacement of hydraulic pumps. Graphs are from [109].

The configuration of a DDU can be constructed in a number of ways as illustrated by Fig. 1.3. Configuration **A** is only valid for pumping mode since high pressure fluid can only leave the piston chamber, while **B-E** operates in all four quadrants. Here **C** and **E** are able to open against high pressures without overloading the actuator, thus allowing cold-start, this however eliminates the safety functionality of check valves which means either more requirements to reliable control or the use of a pressure relief valve.

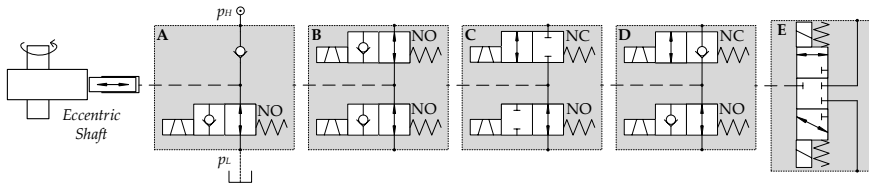


Fig. 1.3: Some examples of valve configurations enabling different variants of DD operation, inspired by Noergaard (2017) [68].

This work focusses on Actively controlled Check Valves (ACV) and configuration **B** is therefore of primary interest as is also illustrated in Fig. 1.1a.

1.2 State-of-the-art

The literature review is divided into two categories to cover the current SOTA of the DDT, i.e. the current state of digital valve design, and the modelling techniques which may/have been used to predict valve performance. The second one covers the SOTA of the relevant design methodologies.

1.2.1 Digital Displacement[®] Technology

The concept of DDT was formed in the 1980s by a research group at Edinburgh University led by Stephen Salter. In 1994 the group formed the company Artemis Intelligent Power (AIP) Ltd based on various patents on DDT [99, 100], and on the specific valves e.g. [62, 86, 111]. Their 12 piston E-dyn 96 CC/rev, suitable for mobile applications, is shown in Fig. 1.4 (up to 1800 RPM and 350 bar) and the efficiency curves of a smaller machine is shown in Fig. 1.5 at different pressures. The higher pressures mean more power, but also increased leakage and pressure dependent friction. This causes the 400 bar curve to deteriorate at low speeds. A pressure difference in the range of 200-300 bar seems beneficial for the specific mechanical design in order to achieve highest efficiency. The academia has formed various research groups to contribute in the development of the technology where the most prominent are: The University of Edinburgh [19, 85, 87], Tampere University of Technology [32], The University of Minnesota [110, 113], Purdue University [63], University of Agder [74] and Aalborg University [37, 68, 81, 98].

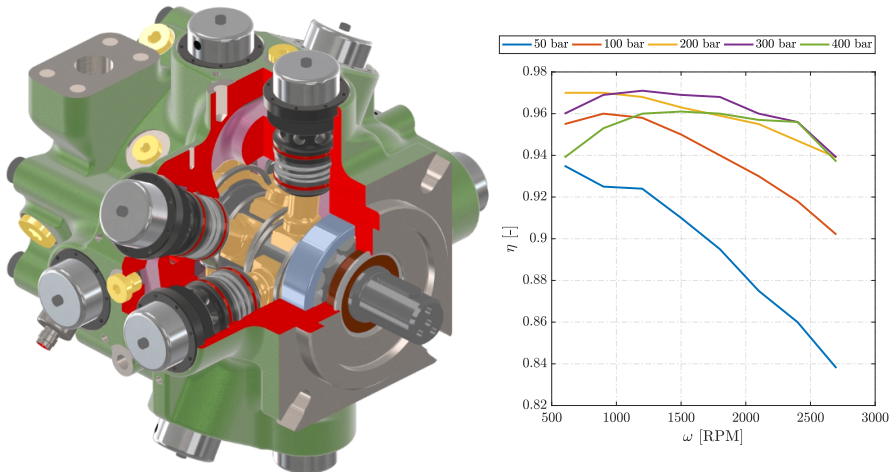


Fig. 1.4: Configuration of the E-dyn96 DDP by AIP (11.8CC/rev) running with full displacement. Reconstruction of picture from [82].

Fig. 1.5: Overall efficiency of a DDP (11.8CC/rev) running with full displacement. Reconstruction of picture from [18].

Furthermore, a small Norwegian based company called Diinef is compet-

ing on delivering the future of fluid power machines within DDT, with their "Digital Distributor valve systems". Both companies (AIP and Diinef) uses a radial piston configuration where two on/off valves are used to control each piston chamber. The exact designs are yet intellectual property reserved for the companies, but the concepts have served as inspiration for much of the research done at e.g. AAU. The main reason that AAU has adopted the use of two ACV with an annular flow geometry is that these have a relatively low throttling loss, fast switching (without excessive power consumption due to aiding flow forces) and the inherit check valve safety feature that avoids over-pressure.

In October 2018 the majority of the shares in AIP was acquired by Danfoss Power Solutions, which is a signal that the technology may finally be ready for mainstream adaptation.

Since the DDU is sparsely tested in the industry there is little knowledge about possible issues and necessary design considerations. The various research projects at AAU [37,68,81,98] including this dissertation thus serves to enhance the knowledge of the achievable performance and design of DDU. Quotes from Roemer (2014) [98] has among others served as motivation for further studies:

- *"Assuming satisfactory tolerances of the valve plunger, the prototype tests include submerging in oil and pressurization in order to validate the simulated switching time and examine stiction/squeeze effects when operating the valve at higher pressures."*
- *"Next large study is on the durability of the valve, in particular wear and fatigue at the valve seat."*

Noergaard (2017) [68] presented several prototype designs. Experimental findings of the first iteration MCVi1.0 [65,73] showed some problems with either mechanical or fluid friction and that 200 bar fluid pressure increased the switching time from 2 to 3 ms (either from change in viscosity or pressure dependent friction). As part of this research the next generation, MCVi2.0 was tested under oil submersion and later applied by Noergaard (2018) in [70] showing a strong correlation between experiment and simulation. The conclusion about the actual end-damping of the design was not convincing and the influence of the movement-induced flow was not included in the applied test-rig. Therefore, measurement of the plunger position under conditions similar to those when implemented in a DDU with pressure corresponding to the LPV has been relevant research in regards to verifying the predicted velocity profile during impact with the seat. Furthermore, the stiction characteristics of the valve, i.e. opening, had not been analyzed in depth along with possible wear formations and probability of critical failures. As pointed out by Noergaard (2017), [68]:

“Long term testing of the valves in DD operation is needed to determine and improve the reliability of the designs.”

There has been a concern that the digital valves are susceptible to long-term damage and this has therefore been a relevant research field, with the objective of better understanding the failure mechanisms of digital valves used in DDU.

Regarding Digital Valve Design

The following review is largely inspired by the work done in [Paper C] and several sections are paraphrased here to make it fit into the broader perspective along with the new contributions since the publication of [Paper C].

The rise of DFP technology has introduced new design criteria for digital valves. This is mainly on the switching period, the pressure loss across the valve (i.e. throttling) and the required number of switching cycles before failure. In short the evaluation metrics of a digital valve are: throttling loss/flow capacity, switching time, price, lifetime (function of switching cycles) and weight. The relevance of these are application dependent. An overview of digital valve technology branches is provided in Fig. 1.6.

The mind map visualizes that research has been done to optimize and improve all of the most prominent and well-known valve configurations. Furthermore, examples of each valve category has been implemented in a DDU where in general the most efficient solutions utilize an annular seat type design.

Valve requirements while used in DDU have been discussed in [68, 90], i.e. demands on switching times, electrical energy for switching, durability etc. In this research, those findings have been used as inspiration to establish the requirements.

Two valve plungers with different elasticity, various hardening and coating combinations applied in a water hydraulic valve have been studied experimentally by Paloniitty et al. (2016) [76]. The findings showed significant wear on the contacting surfaces of all the proposed designs and no significant improvements were found by using a more elastic design, which could indicate that not only impact is an issue, but also micro-sliding in the seat region may contribute to wear. Water hydraulics suffers under poor lubricating properties, low viscosity and is generally a more aggressive fluid from a corrosive and chemical point of view. In comparison, most oil hydraulic valves have less wear, but this is an indication that similar concepts are not worth pursuing at present moment.

A micro valve package utilizing 128 independent needle valves is optimized by Linjama et al. (2015) [56]. This is done with static CFD to achieve higher flow rates and by Finite Element Analysis (FEA) on the solenoid actuator to evaluate the switching response. For comparison a very similar

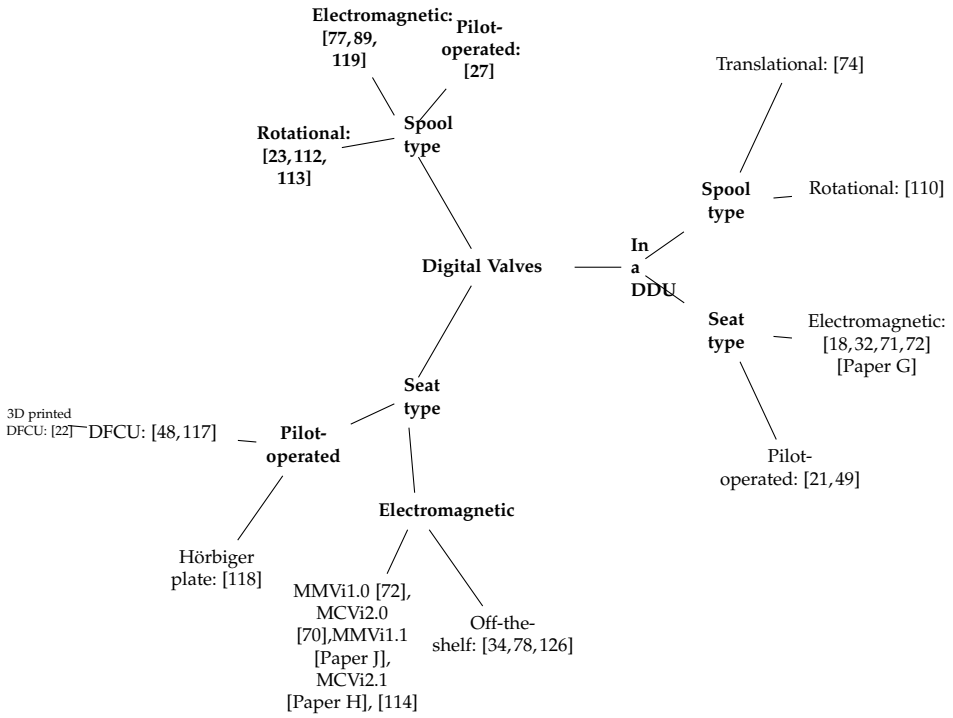


Fig. 1.6: State-of-the-art (SOTA) of digital valve designs, where abbreviations are: Digital Flow Control Unit (DFCU), Moving Magnet Valve (MMV) and Moving Coil Valve (MCV). The valves are divided into two main classes and further divided based on the actuating mechanism and one branch is allocated to show the different research that has tested valves in a DDU. The figure illustrates which areas have been touched upon by this research.

concept of a miniature valve for high-flow is presented by Lantela & Pietola (2017) [48] where 32 pilot operated valves (with four increments on size) are used to control four independent metering edges. The manifold used for this valve design is laminated, which gives significant fluid friction losses, and the total mass is around 9 kg. However, the design freedom of mechanical systems has been expanded with the invention of 3D metal printing, which is relevant in valve design and manifolds. Most recently Chekurov & Lantela (2017) [22] presented a laser melted digital valve, discussing the possible improvements compared with the laminated design of [48]. The authors utilized an iterative design procedure with static CFD to find sub-optimal flow paths (comparison of measurement and CFD was within 10%). They highlighted that: flow paths and edges could be manufactured with a high ‘smoothness’ (reducing fluid friction with around 50% and increased flow capacity by 30%). The improvement on compactness is not discussed but the figures clearly show a more compact design compared to the laminated one. Fur-

1.2. State-of-the-art

thermore, the increased hardness of the melted material is argued to improve the durability of the seat due to an increased energy absorption, and generally harder surfaces are prone to less wear, as follows from Archard's wear law. The major drawback is the cost of manufacturing with this method (in the above example one manifold was priced at 901€) and therefore mainly relevant in high-fidelity applications.

The majority of the literature focusses on the actuating part when designing digital valves [66–68,70,73,98,121]. Here various types of electromagnetic actuators have been optimized by a combination of FEA and Lumped Parameter Models (LPM). The primary focus is on axisymmetric designs which enables rapid computational evaluation of the designs, and generates designs which are normally easy to manufacture due to the symmetries. An equivalent electric circuit model is used to search the fitness landscape aided by static FEA, and for the last stages of the optimization a transient FEA is applied to verify the performance. The optimized valve designs w.r.t. the actuator are summarized in Fig. 1.7.

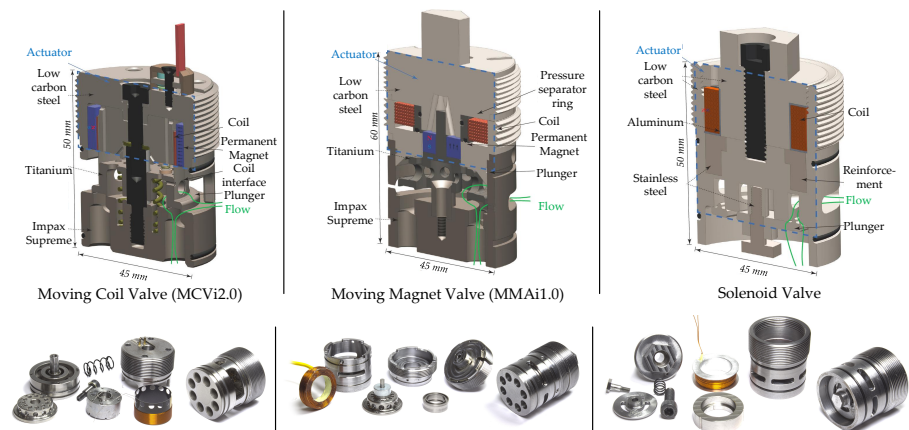
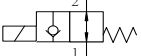
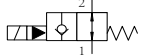
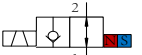
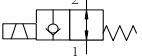


Fig. 1.7: Valve CAD and actual prototypes from AAU, picture from [71]. In this work only the Moving Coil Valve (MCVi2.0) and the Moving Magnet Valve (MMVi1.0) will be considered due to their more rapid force build-up.

The amount of topological studies of the mechanical poppet/plunger regarding end-damping features and durability is limited. One study [93] attempts to reduce the mechanical stress through optimization of the shape of the contacting surfaces where FEA is used to evaluate this stress. However, it does not consider the impact stress. One of the latest proposals is to reduce the impact stresses by a "cushioning design" [104]. A fluid is entrapped in a groove as the plunger approaches the seat. This fluid must travel through a narrow gap which builds up pressure in the groove. The consequence of this geometrical design was analyzed theoretically in [104] showing the depen-

Chapter 1. Introduction

Table 1.1: Active check valve specifications where * indicates industrial product and ** indicates scientific prototype.

Valve type	T_s [ms]	m [kg]	$MTTF_D$ [years]	$\Delta p@120$ L/min [bar]	p/Q [bar min/L]
 HYDAC WS16YR-01* [34]	35	0.65	150<	2/5	350/100
 PARKER DSH161NR* [78]	45	0.34	-	6/6	350/150
 AAU MMVi1.0** [72]	2/6	0.60	-	0.15	350/125
 AAU MCVi2.0** [70]	< 3	0.41	<1	0.18/0.48	350/125

dependencies of both impact and stiction on lift and velocity. Patented solutions of progressive springs applied to dampen the armature or plunger is another opportunity, e.g. as given in [62].

The SOTA in available valves shows that the key specifications of leak-free bi-directional 2/2 one-way check valves with fast switching are as presented in Table 1.1. Here T_s is the switching time, $MTTF$ is the Mean Time to Failure, m is the mass of the valve without oil, $\Delta p@120$ is the port differential pressure with a flow of 120 L/min ($1 \rightarrow 2/2 \rightarrow 1$) and p/Q is the ratio between the rated pressure and flow.

The numbers clearly show that the valves designed specifically for DDU performs better than the commercial options (similar valves can be found from Comatrol, Eaton and Bosch but performance is worse and the above are thus the obvious alternatives). However, the lifetimes of the prototypes are so far not documented and the preliminary studies in this dissertation suggest a lifetime below 1 year for the MCVi2.1. Unfortunately, specifications of the valves designed by AIP as used in a DDU are not available.

Generally, the commercial valves that allow high flow rates are associated

1.2. State-of-the-art

with switching times around 50-100 ms, which is not enough for running a DDU at medium speeds. Some commercial spool type valves do have switching times below 5 ms, opens against high pressure and support the required flow rates. The pressure losses are significant, are not leak-free and do not support check valve functionality.

Based on the findings from above it is expected that an increase of durability can be achieved by lowering the impact speed. Thereby lowering the mechanical stresses and noise occurring from impact collision. For the valve considered in the present work the actual limit is unknown, but a simulation study of dry mechanical impact in the valve was carried out in [Paper J]. This study revealed a velocity threshold in the range of 1.5 m/s for all points in the design space when considering peak von Mises stresses to be maintained below 350 MPa. The requirements for the considered valve in the present work are:

- The peak flow force at rated speed must be cancelled by the counteracting mechanism to ensure a normally open valve.
- Combined power losses in the valves should not exceed around 1% of the rated power output.
- The switching time of the valve must be a significant factor shorter than the DDU rotation period at rated speed.
- An impact velocity of 1.5 m/s or below.
- The fluid pressure peak near end-stop should be below the yield strength of the materials.

Modelling Techniques for Fluid Dynamics

The solution to Navier Stoke's (NS's) equations with possible multi-physical phenomena such as varying viscosity from pressure or temperature changes, along with compressible fluids, cavitation and viscous Eddies is so far only achievable by numerical computations where the gold standard for many problems, including hydraulic valves, is the CFD framework with a Reynolds Averaged NS (RANS) form. For specific types of fluid mechanical systems, Reduced-Order-Models (ROM) have been derived, which have accuracy limitations but reduced time required for analysis. The branches of relevant simulation models are summarized in Fig. 1.8.

CFD

The first published full 3D CFD analysis of a hydraulic valve was presented in [3] where the flow force in a proportional valve was simulated. The method has since been applied widely to support hypotheses about specific designs

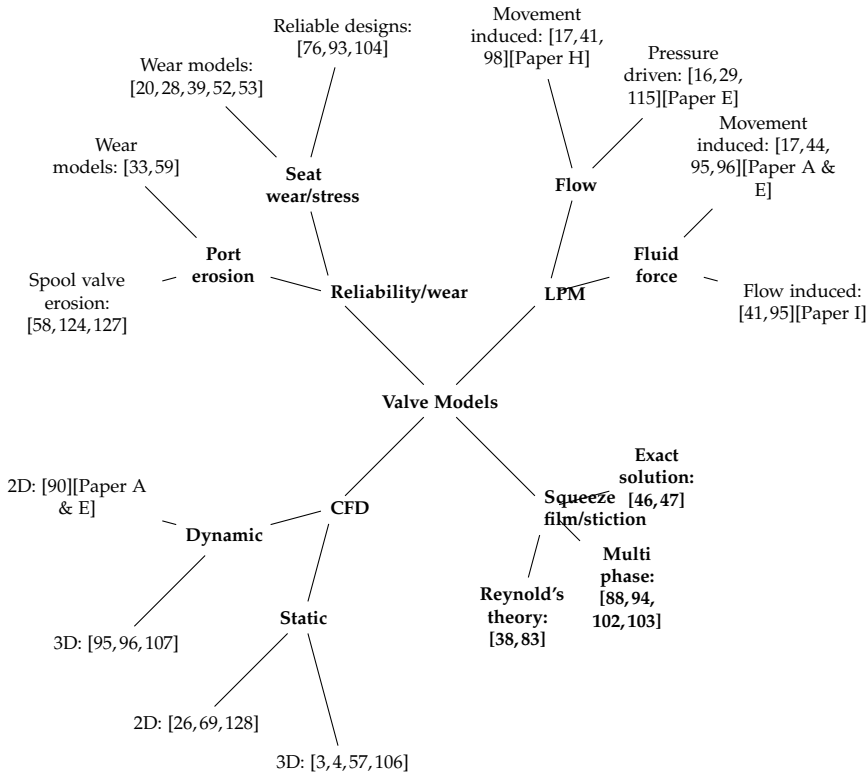


Fig. 1.8: State-of-the-art (SOTA) in modelling fluid dynamics/tribology for valves. The LPM includes various methods for reducing the model order by lumping parameters, where the Squeeze film/stiction branch is a specific ROM that applies to situations of thin films between flat surfaces. The CFD branch is on general topics that relate valve design to CFD analysis and in the reliability/wear branch various experimental findings on valve wear and promising wear prediction models are summarized.

or to evaluate some performance parameter used in optimization, see e.g. [4,57,106].

Studies of seat valves often reduces the 3D geometry into an axisymmetric 2D geometry, which reduces the model order significantly. The validation of such an approach either requires running both the 3D and 2D model and comparing results, which may lead to only partially accurate conclusions since the integrated quantities such as fluid force and throttling loss may be accurately predicted, while ignoring symmetry breaking phenomena that cause locally higher flow rates or circulation zones. For the study of valve switching performance the acting fluid force is essential and experimental data, 3D and 2D CFD results of an annular seat type valve from [69] supports the hypothesis that 2D axisymmetric analysis with a laminar CFD model is

sufficient. Similar but less comprehensive studies of flow fields in seat valves include [26, 128].

The above solves the flow field in a static environment, but as the spool or plunger moves through the fluid some dynamic- and history- effects will occur in a viscous fluid. A seat valve with a plunger immersed in an initially still fluid is studied in the two similar publications [95,96]. Various conditions are simulated to construct a LPM based on a linearized form of the NS equations. This can be derived analytically for a sphere moving through a fluid as discussed in [96]. In contrast to the analytic solution, CFD simulations show that the friction coefficients depend on the plunger position (z), where the added mass from the fluid dominates the Movement-Induced (MI) force and viscous terms dominates during end-stop. Pressure driven flow is predicted with a quadratic model with two look-up coefficients (that depend on z) and a similar form is used to represent the flow-induced force where CFD results are used. The LPM is constructed by adding the derived terms and compared to a full dynamic CFD simulation in [96] (no flow is present), where the largest error is observed as the plunger is near the seat. This MI force model is thus relevant to study further and other approaches to determine the model coefficients are considered necessary if damping forces should be predicted more accurately and effectively. Furthermore, the consequence of a non-zero flow is relevant to study.

LPM

The prediction of a pressure driven flow normally takes the form of the orifice equation. Depending on the flow condition either a purely turbulent form or a form correcting for laminar conditions can be applied [16, 115]. This model form was used in [95] with a linear and quadratic term, but the coefficients were determined by CFD. As shown in [29] there is a transient response time of orifices.

The flow force arising from movement of fluid around the valves plunger (flow-induced force) is also a topic that concerns the switching performance of digital valves. For spool type valves this is normally predicted by a momentum consideration where the derivations of such flow-induced forces goes back to 1952 [50] and more extensively in 1967 [64]. An annular seat valve is constructed in a quite different manner and a parametric expression of a flow-induced force is not straight-forward.

The Movement Induced (MI) flow and force that arises from moving a solid body in a fluid have been solved analytically for simple geometries in e.g. [17, 44]. These simple models breaks down when other solid bodies are interacting, such as the seat in a valve. Also, complicated geometries makes the derivation of general expressions difficult. A few techniques utilizing CFD simulations have been shown in [95,96] to remedy this, but conclusions

about the MI-flow and of the impact region are sparse. A deeper understanding of the fluid dynamics in such situations are considered highly relevant to understand the switching situation in digital valves.

Squeeze film/stiction

The separation of two solid bodies with a viscous boundary lubrication layer does introduce a resistive force proportional to the separation velocity and inversely proportional to the cube of the gap height [94]. The magnitude of this force is governed by the actual tensile strength of the liquid, i.e. when/if cavitation occurs, the force will be reduced [88,102,103], which is observed experimentally where the Stefan force is sufficient as long as the absolute pressure is above the vapor pressure. Typically when separation velocities are low. Surface topography may lead to different contact areas than expected when surfaces are assumed flat. These effects are not modelled in a manner suitable for optimization in the literature.

An exact and approximate solution to the transient squeeze film problem for a disc approaching a flat plate is derived in [47]. The local acceleration of the fluid is shown to have a significant effect for low viscosity fluids. Experimental evidence in [46] confirms the theoretical pressure predictions at the center of the plates from [47]. The contributions from the inertial and viscous components of the pressure rise depends on the fluid viscosity, and both water and 80% aqueous glycerol solutions are tested. The results shows that the convective acceleration is negligible, and for a high viscosity fluid the local acceleration is not as significant as the viscous component.

Reliability/wear

Studies of hydraulic valve wear mainly focus on predicting the internal leakage of spool valves caused by eroding edges [58,124,127]. The erosion rates of the bushing and spool are predicted by CFD and Edward's erosion equation in [127] for various port openings and a given amount of particles with given sizes. This method is useful to give an idea of how severe this is for a given design, although the amount, sizes and shapes of contaminants are seldom known for a real system.

Degradation of combustion engine valves is the topic of [20,28,52,53], where [52,53] presents valve recession results of the same test-rig and results of varying impact velocity and load force are illustrated. Tests of impact speed below 1 m/s showed little to no wear in the seat region [53]. The most interesting conclusion of [52,53] is that a small steady supply of lubricating oil causes valve recession to be almost non-existent compared to dry impact situations where a significant wear is observed. A similar conclusion is presented in [28] where an oil residue tribofilm is observed via light optical microscopy and for more detailed images a Zeiss 1550 SEM was used.

The oil acts as a protective layer by smoothing the contacting surfaces and minimizing stresses at asperities. The study of [20] is aimed at a numerical and experimental technique to determine valve wear upon dry impact with an adhesive wear law and FEA. This technique is interesting in hydraulic valves, but due to the lubricating properties in hydraulics it is not considered directly applicable. Also, a formulation of a simple model that accounts for impact wear and sliding wear is established in [53]. Shortcomings include inaccurate predictions when material combinations are changed and when surface geometries change, i.e. the model relies on experimental coefficients.

1.2.2 Design Methodologies Relevant for Mechatronic System Design

The optimization of a hydraulic valve is normally done by splitting the system up into its subcomponents. Choosing one configuration of the actuator, plunger, spool or spring (etc.) will pose constraints on the possible configurations of other subcomponents. Accurate simulation tools for each component are essential, where explicit function evaluations are preferred, but often it is necessary to formulate the problem using implicit functions.

The accessibility of computational power and software tools has made multiphysics, or at least numerical computation based design approaches feasible, for applications where coupled Ordinary Differential Equations (ODE) & Partial Differential Equations (PDE) govern the system. This is exactly the case when designing valves.

A series of design tasks solved by employing numerical analysis like FEA or CFD in collaboration with Lumped Parameter Models (LPM) have been identified [25,36,51,108,122].

Several examples of actuator optimization while used in electromagnetic actuated valves also use a LPM that is supported by FEA and experiments, e.g. [66–68,70,73,98,121,122].

Most mechatronic systems involve controlling certain system states via exogenous inputs and the control performance is inherently correlated to the system design, where choice of actuators, moving parts and stiffness of these play an essential role. This motivates holistic design methodologies that consider the synergy of the entire system [60,84]. In case of a DDU the available control strategies will be restricted by the applied valve [80], also the dimensioning of the actuator, plunger, DDU displacement and rotation speed couples the various sub-systems and must be considered in the design process.

The standard form of the above is to use high-fidelity models to construct and/or validate simpler models that are used in optimization. The prototype is then manufactured and the measured performance compared to the predicted.

Design for Reliability

One of the latest trends in system design is to apply statistical tools on large data sets describing failures and faults. In this manner the product can be designed to serve a desired lifetime and avoid over dimensioned costly products, i.e. Design for Reliability (DfR). The relevant environmental- and operating-conditions for the system are used when predicting the reliability and therefore detailed knowledge/experience about the components and the physics governing wear-out is required. This has been widely and successfully applied in the Power Electronics (PE) field, although this is yet not trivial as discussed in [123]. One physical based model of wear-out supported by empirical data of several tests cases on IGBTs was revealed in [105], where thermal cycles along with empirical constants predicts the lifetime.

In tribological and mechanical systems the wear and fatigue behavior have been studied for decades without any clear understanding of the various processes. A review of this field was given in [Paper C] where it becomes clear that the concept of predicting damage or irreversible degradation is an inherently difficult problem. Citing Williams (2005) [116]: “For the relatively elementary case of two loaded surfaces, one hard the other softer, sliding over one another we might suppose that the loss of linear dimension, say w , in the wearing surface will depend on the applied load P , the imposed sliding speed V , the coefficient of friction μ , the hardness of the softer surface H , the time they slide together t and the size of the contact measured by some representative length dimension R .” This reveals

$$w = f(P, V, \mu, H, t, R)$$

where simple dependence of w and μ are yet to be discovered. The most recent progress in this field is the discovery of a critical length scale which controls the severity of adhesive wear [2]. This is demonstrated by an atomistic model where large junction sizes produce debris by fracture, and smaller junctions causes asperities to smooth out plastically. This is a clear leap towards a physical understanding of wear, although restricted only to that of dry sliding motion. Paper C continues to discuss the concepts and prediction difficulties related to gigacycle fatigue behavior and wear mechanisms observed in seat type valves, which was paraphrased earlier in this chapter.

The purely statistical models are only useful in well-defined situation, due to the high amount of potential influencing variables, i.e. geometrical changes, material choices, surface treatments (like coatings or hardening), manufacturing, lubrication additives, thermal stresses, mechanical stresses and environmental conditions. The physics of wear-out in hydraulic systems is complicated, where reliability is to a great extend based on the manufacturers MTTF or on the currently only handbook as discussed by Liniger (2015) [55], namely the *Handbook of reliability prediction procedures for mechani-*

1.3. Research Objectives

cal equipment [39]. The possible pitfalls of this handbook were briefly studied in the dissertation [54], where a clear mismatch between modern field data and reliability predictions was illustrated. One reason is argued to be erroneous model structure of applying the MTTF where essential contributors are omitted, another possible reason is the fact that the empirical basis of [39] dates back to the 1960's which means advances in manufacturing techniques, material science, component design and quality of lubricant over the last decades makes today's components much more reliable. To demonstrate a conservative estimate on reliability the methods from [39] have been applied for a digital valve in this research as explained in [Paper B].

Suitable Optimization Algorithms

Intuitively, a powerful actuator will add both mass, cost, and power consumption in exchange of potentially faster response time. Increasing the flow area will reduce throttling loss while changing the fluid forces during switching, this will also add more mass to the overall system and a heavy plunger will change the switching time of the valve. Furthermore, a larger plunger increases the contact stress when the contacting area is not scaled accordingly. The optimal design of a valve is therefore a complex multi-objective problem with conflicting objectives. Based on this, the valve's fitness landscape is expected to be non-convex and to contain several discrete design variables such as choice of topology or number of coil turns. This leaves out gradient based optimization concepts and means evolution algorithms or Monte Carlo algorithms are preferred. The general concepts and SOTA of differential evolution are given in [24], where it is obvious that a vast amount of algorithms have been proposed without any clear superior approach. Digital valves have successfully been optimized in [5,66,97] with the Generalized Differential Evolution (GDE3) algorithm created by Kukkonen (2012) [43]. The GDE3 is not sensitive to the initial parameters and due to its characteristics of pruning designs into the Pareto front it is well suited for design tasks with conflicting objectives.

1.3 Research Objectives

As stated in the introduction the research objective is: "to develop and validate a framework for design & optimization of the mechanical topology of valves used in DDU."

This translates to the following hypothesis: *It is possible to advance and validate the current SOTA modelling framework describing the relevant fluid dynamics of digital valves and reduce the impact loads.*

To investigate the hypothesis, the following objectives are addressed:

- To define the structure of a framework relevant for digital valve design.
- To develop and validate a set of models useful for design and optimization, i.e. that predicts the physical properties/phenomena that are determining for the performance of the valve.
 - Predict the energy losses associated with the valve.
 - Predict the fluid forces to a degree for which the impact velocity can be approximated.
- To optimize the valve with the revised framework.

Based on the SOTA a series of gaps were identified in the knowledge required to set up a framework for designing digital valves. There is a need to analyze the trade-off between using different fluid dynamical models for valves, i.e. cost of accuracy vs. required time for analysis. This implies that even though an optimization algorithm manages to find the fittest designs within its allowed search time, this design may only be sub-optimal or simply wrong if phenomenological effects are left out in the modelling framework. The fluid dynamics during fast switching must therefore be analyzed.

It was identified that designs with end-damping may enhance valve durability while reducing noise. Therefore, the transient fluid dynamics during switching for the type of valve are essential to understand, since this is associated with both the switching losses and the switching trajectory. This has not been investigated in depth prior, and therefore investigation of designs that takes end-damping into consideration and modelling this damping accurately are relevant.

Attempts of simplifying the models describing the flow geometry have been presented in the literature. This work will elaborate those approaches by analyzing the accuracy by using ROM (such as simplified physics) to construct LPM, and comparing these to the other available high-fidelity formulations.

The valve objectives have been established in prior research with a main focus on modelling and validating the actuating component [68,98], looking mainly at valve switching time vs DDU efficiency. This means that dynamic models for the interaction with the fluid have only been studied sparsely, and an accurate description of this may be useful to formulate other objectives or to provide new optimum designs of the mechanical topology.

1.4 Main Contributions

This project has in total contributed towards faster development of digital valves by identifying and evaluating the fluid dynamical quantities, which directly affect the performance of such valves when used in a DDU.

1.4. Main Contributions

- An extensive SOTA analysis has been performed to identify the available possibilities for creating a digital valve design framework.
- A CFD framework has been established in order to investigate the switching situation of a digital valve.
- Gaps in modelling of; flow-induced force, MI flow and MI force have been elaborated by a series of strategic CFD simulations to show the tendencies of the various coefficients useful for simpler models. This was derived for a baseline design and the accuracy of the LPM vs CFD was demonstrated while a flow was present during switching. A parametric model of the combined fluid force was required and a proposal of such is provided in this work.
- Two approaches to validate the MI -flow and -force were realized. Both test-rigs showed that the MI force (prediction of the switching profile) is sufficiently approximated. The magnitude of the MI flow have been difficult to verify. Flow sensors does not support the 40 L/min flow rate with a period of only 2 ms, which is why the integrated value (fluid volume) has been measured. This has given an indication that the phenomenon is real, but the quantification is concerned with a significant uncertainty.
- Experimental data of cushioning plunger designs have been used to verify models used to design such. This includes the pressure build-up inside the cushioning groove and the end-damping profile. This test was done with a still pressurized fluid. Hereafter, the valve was proven to function properly in a DDU. The surface topographies of the sealing surfaces were studied after run-in to check for any obvious wear zones or design flaws finding mild wear marks. It is unclear if this will develop more severely over the course of billions of operation cycles, but is nevertheless premature evidence of the wear that can be expected in the infant lifetime of a similar DDU.
- An overall design framework has been formulated. The structure of the modelling framework uses simple design rules to check certain constraints of a design before this is evaluated by the LPM. If the design is feasible and optimal it is simulated in the highest-fidelity CFD model. An optimal design was found by utilizing this approach, where knowledge from previous valve designs was used to redefine the success criteria and the design space. The optimal design has lower impact speeds according to simulation and maintains the same level of DDU output energy.

1.5 Outline of Papers

This dissertation is comprised by an extended summary and collection of papers. Each paper is a contribution to solve the modelling challenges for a digital valve used in a DDU. This is a multidisciplinary task consisting of fluid dynamics, electromagnetism, fluid power, tribology and structural mechanics. The content of the modelling framework depends on the investigated valve concept and when experimental evidence is available this may be applied to revise the models into the next iteration, i.e. (*version.concept.iteration*) as depicted in the flowchart of Fig. 1.9. The current models for the actuator and fluid dynamics have been shown to agree well with measurement of several manufactured prototypes.

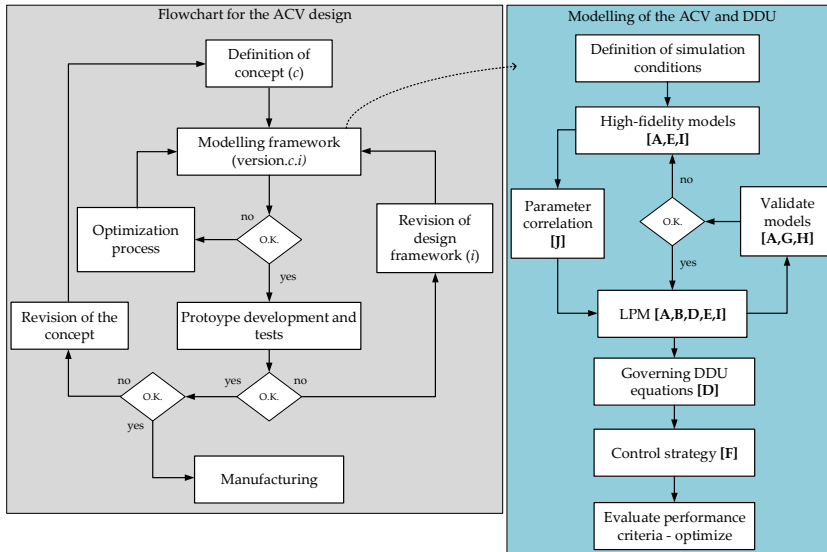


Fig. 1.9: Flowchart of the process to develop the mechanical concept of a digital Active Check Valve (ACV). The fluid dynamics in the modelling framework and revision of this is of primary interest in this work. The published scientific papers [A-J] are assigned to the boxes in the modelling framework where they contribute.

The figure illustrates how an appropriate modelling framework is sought by restricting high-fidelity models into a more rapid executable LPM. This has been done by using parameter correlation to locate dominating parameters and then comparing the predictions of the LPM to that of the high-fidelity model. The papers elaborate the high-fidelity and low-fidelity models and are shortly summarized here.

1.5. Outline of Papers

Paper A [10]

This paper aims at validating the fluid force predicted by the developed CFD framework while switching in an initially still fluid. A prototype valve was manufactured at AAU and this was used to measure the switching dynamics of the valve with air or oil as the fluid. This was performed at three different voltage levels and three different oil temperatures. The results of various models and experiment are compared in the paper and conclusions made hereof.

Paper B [11]

This paper presents a conservative estimate of the life-expectancy of a digital valve by applying the available failure rate models. These are from the reliability handbook for hydraulic components: *Handbook of reliability prediction procedures for mechanical equipment* [39]. The presented analysis concerns the mechanical spring and the sealing feature of a seat valve. To investigate the sealing feature further a FEA was carried out to estimate the contact stresses that occur in the seat due to a static pressure difference and this was compared to a simple Hertz stress model.

Paper C [12]

A SOTA relevant for hydraulic valve design is presented to establish the methodology for a design framework and identify the relevant physics. The methods that are applicable for the relevant physics are reviewed to show what is currently possible and what is not. A gap is identified in understanding the interaction between fluid and solid during a switching cycle of fast switching valves, i.e. how MI-flow, MI-force and pressure/flow relation behave. Thus also expressions of the design parameters that affect the outputs the most are missing. Furthermore, the prediction of long-term wear in digital valves is considered infeasible to quantify with the SOTA knowledge.

Paper D [13]

The reliability results of [Paper B] yielded a risk of internal leakage developing over time, which is why this paper presents a study of internal leakage in DDU. A generic simulation model is presented and a hypothetical situation simulated, where the amount of valve switching cycles and leakage are correlated by a wear propagation function. This is used to show how leakage affects the efficiency curve of a DDU over time. A time-averaged simplification of the dynamic model is presented, which decreases simulation time significantly while predicting similar performance. This static model has

since been re-formulated in [Paper J] with a more realistic description of the throttling loss.

Paper E [14]

Due to the potential importance of knowing the velocity near mechanical end-stop, a series of numerical experiments using the CFD framework are presented in the present paper. The specific details of dynamic meshing and implementation of plunger movement are presented in the paper. Major findings includes quantification of the MI-flow and -forces as function of plunger lift and velocity. Furthermore, a significant transient build-up of flow is found when solving the equations by an un-steady solver and with constant pressure boundary conditions on both inlet and outlet for an initially still fluid.

Paper F [9]

This paper presents a strategy for shaping the input voltage of the switching valves to reduce impact loads while enhancing efficiency. A simulation study is presented for two different optimization algorithms and this shows how much the performance can be affected theoretically from shaping the input. The design space is potentially huge, and it is not considered feasible to apply the presented strategy directly while optimizing the valve design.

Paper G [8]

This paper shows experimental data from a DDU test-rig when a new plunger concept featuring a cushion end-damping (MCVi2.1) is used as the HPV. The valves energy loss, impact speeds, opening and closing times are estimated over different operating pressures and rotation speeds, and the performance features of the MCVi2.0 and MCVi2.1 prototypes are compared. Microscope images of the valves contacting surface and actuator after a few hours of motor operation have later been used to understand the possible wear areas.

Paper H [15]

This paper presents experimental evidence to validate models used for the design of the plunger concept used in [Paper G] (MCVi2.1). This includes, pressure change in the cushioning groove, MI-flow and the general switching characteristics. This new test situation emulates a DDU environment better than the approach used in [Paper A]. The position is measured with an Eddy-current transducer, and the fluid pressurized to 5 bar. Two methods to validate the MIF are proposed.

Paper I [7]

This paper elaborates on the fluid forces acting on the valve plunger, where a few experimental data points are used to verify the sanity of different models. Three different models for predicting the flow-induced force are presented, using either CFD, simplified physics or a neural network surrogate. The resulting valve switching profile from these models are compared to investigate their relevance. A reduction of computational time of the high-fidelity model is sought by varying the amount of iterations allowed for the dynamical CFD solution, hence allowing partially converged solutions. A sweet-spot is observed where the level of convergence is sufficient to ensure a stable solution over time. However, this is not enough of an improvement to make the high-fidelity model suited for optimization.

Paper J [6]

A mechatronic design procedure for digital valves in DDU is presented with a focus on the methods that has been applied to simplify the design task of the flow delivering design. Rough design rules are formulated to remove infeasible designs from dynamical function evaluation. This means the computation time will be spent on more feasible designs and the simple dynamic models used to filter the design space into a few candidates. This will be evaluated by a full dynamical CFD routine to verify the performance, to ensure that the LPM is sufficient. Parameter correlation is used to illustrate dominating parameters which are important when defining the LPM.

1.6 Reading Guidelines

The output of the optimization framework, i.e. the digital valve, is presented in Chapter 2. The predicted valve performance when used in a DDU is presented. This chapter is not related to any research papers.

Chapter 3 presents all the relevant steps and equations of the design framework. This is a mixture of several research papers (A,D,E,I,J) summarized into one analysis of the relevant characteristics of digital valves operating in a DDU.

Chapter 4 shows the coherence between various simulated states of the valve and the ones that have been measured from different test-rigs. The approaches taken in the corresponding research papers are discussed and the relevant conclusions and findings are summarized.

The main conclusions of this work are presented in Chapter 5 and the contribution of each paper summarized. A final section presents the perspective for future work in the field of research and design of digital valves for DDU.

Chapter 1. Introduction

Appendix I applies the validated framework to locate optimal designs. A brief discussion is given about how the problem may be formulated.

Appendix II presents images of the relevant contacting surfaces of a few plunger designs both by using ultrasound and optical microscope.

Chapter 2

Developed Valve as Used in a DDU

"It's not hard to make decisions when you know what your values are."

– Roy E. Disney (1930 – 2009)

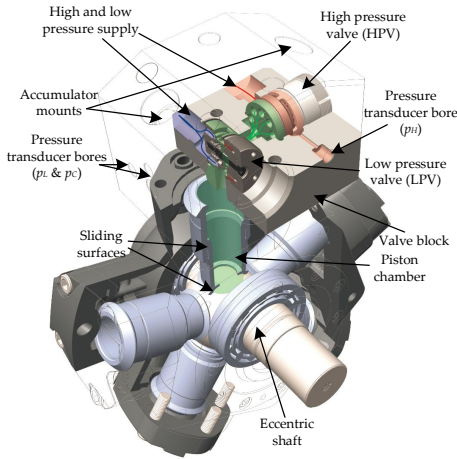
An energy efficient, light and durable machine will mean lower costs for the environment and the user. This chapter presents the proposed valve design to realize this.

2.1 The Machine

The design phases of a mechatronic system consists of identifying the requirements, possibilities, new ideas and experience to arrive at a preliminary design. Hereafter, the performance of the design must be expressed mathematically so that either implicit or explicit functions can be applied to evaluate the feasibility of various designs.

The machine used as test environment with the proposed DD modification is illustrated in Fig. 2.1 with corresponding key specifications.

The energy conversion in the hydraulic valve is one of the major topics of this work and roughly speaking decomposes into: energy required to move the plunger, energy converted to a fluid force (both dampening and accelerating the plunger) and the pressure throttling loss across the plunger/seat. This means the flow conditions must be known during switching (determined by the DDU piston), the actuating force must be known to predict the significance of fluid forces, but otherwise the mechanical topology can be analyzed as an isolated system.



DDU	
Rated Speed	800 RPM
Chamber displacement	50 CC/rev
Chambers	5
Peak flow rate	125 L/min
Rated pressure	250 bar
Weight	50 kg
Rated power	110 kW
Valves	
Switching time	2-4 ms
Avg. actuator power	40.5 W
Avg. hydraulic loss	23.2 W
Plunger radius (R)	11.8 mm
Plunger width (w_{in})	7.1 mm
Stroke length (l_s)	2.8 mm
Moving mass	20 g
Valve mass	0.47 kg

Fig. 2.1: Design proposal for a DDU by modifying an existing Parker CALZONI radial piston machine.

2.2 The Developed and Optimized Valve

The choice of plunger concept was that of a seat type valve with one annular flow path. This has been chosen since this concept fulfils the requirement when considering a hydrostatic transmission system for wind turbines as the application where the DDU are used. Instead of analyzing several concepts and topologies, the objective has been to study one concept in depth.

The valve was optimized to reduce the impact speeds in the switching valves and to reduce the energy not converted into mechanical work in the motoring DDU. The force response of an actuator optimized for use in digital valves have been used based on the findings of [68], leaving the design of parts governing for the fluid dynamics to be of interest. The problem has been defined as elaborated in Appendix I where the proposed valve has the configuration as shown in Fig. 2.2.

A copper wire is wound into a coil with $N = 117$ turns and wire diameter $d = 0.6$ mm. This is separated from the hydraulic part of the valve by a pressure-separator ring. The coil is bonded by cyanoacrylate glue. The two housing parts are fastened with bolts from the side. An axially magnetized Permanent Magnet (PM) is mounted in the top-center of the plunger to make bi-directional actuator force possible. In the center of the plunger a pipe allows fluid transport from the top chamber of the PM to the rest of the system. The clearance between the PM and the housing is proposed to have round grooves to allow faster pressure dissipation in the clearance, thereby reducing tilting and mechanical contact. As the plunger moves in negative

2.2. The Developed and Optimized Valve

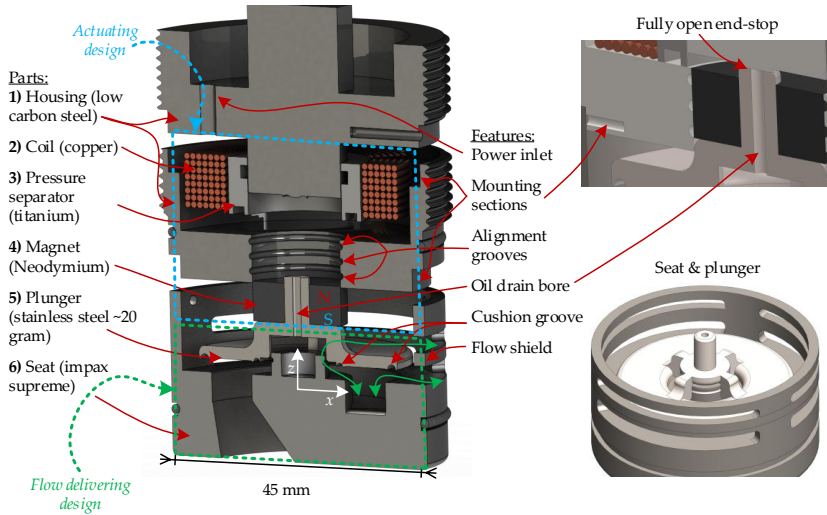


Fig. 2.2: Isometric exploded cross-sectional view revealing the proposed MMVi.1 design. A close-up view of the end-stop mechanism of a fully open valve is displayed. The seat & plunger are shown from another perspective to clarify the design.

z-direction the damping force rises, simultaneously the flow force rises due to the restriction of the flow path. The plunger seals the annular flow path, this flow is converted to a circular flow path to make manifold manufacturing easier. The O-rings are installed to prevent leakage to atmosphere and between the piston chamber and manifold.

The valve design has the benefit of avoiding any need to supply the moving parts with electricity. This makes it robust, and also the amount of individual parts is maintained low. Besides, the actuating force meets the requirements for switching time.

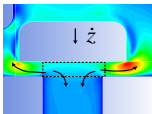
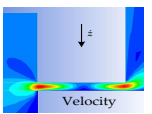
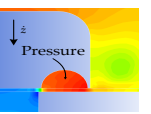
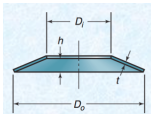
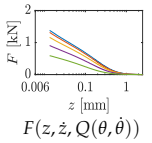
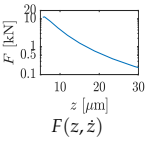
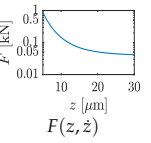
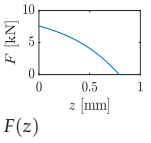
The shape of the plunger, seat, venting bores, alignment grooves and housing have been done to ensure that the valve is compact while easy to assemble. This is to a great extent aided by experience from previous valve prototypes. Some of the design parameters governing for the plunger have been determined by optimization (see Appendix I), and generally the remaining parts are designed by best-practices and ingenuity. FEA has been used to verify that material stresses are reasonably low. During this project a few different design solutions to reduce the impact loads have been considered.

2.2.1 Design Possibilities to Reduce Impact Loads

Upon a mechanical impact a significant stress may propagate through the materials, which may be a limiting factor in the valve's lifetime. One possibility is to use special materials and coatings which are able to absorb this

impact energy. This is associated with increased costs. Another solution is to make design modifications to limit the impact speed. The physics governing for the impact speed and design modifications have been studied during this research and the proposals are summarized in Table 2.1.

Table 2.1: Ways of realizing end-damping

	Movement Induced Flow (MIF)	Flat surface	Cushioning groove	Belleville spring washer
Concept				
Force	 $F(z, \dot{z}, Q(\theta, \dot{\theta}))$	 $F(z, \dot{z})$	 $F(z, \dot{z})$	 $F(z)$
Synergy	This source of damping can be achieved in combination with all the other options. The force becomes more dominating as z approaches zero.	This force is active approximately at $z = 0.1l_c$ where l_c is the length of contacting surfaces.	This force is active approximately at $z = 0.1l_g$ where l_g is the length of cushion groove.	Depending on spring dimensions the active interval can be varied and the force profile altered. The energy is stored and will be released when opening.
Design consequences	This is a natural feature of the plunger due to its shadow area, which will give rise to fluid being displaced. Adjusting this causes changes to the moving mass.	The sealing surfaces will inherently comprise a squeeze film damping which can be freely designed. It comes with the cost of a stiction force.	Including a groove in the sealing region means that high precision modifications must be made to the plunger.	The layout need to consider a logical integration of the spring. Risk of making the valve dysfunctional if actuator- and fluid-forces are lower than anticipated, thus making the valve impossible to close.

The first two concepts are an inherent part of a poppet-type valve with a flat contact zone and are therefore in-direct ways of providing end-damping, where the moving mass is also altered. The geometric changes to govern the MIF is radius and width of the plunger. This force starts to develop from around 1 mm and has a significant influence. The origin of this force comes by a reduction in the flow-induced force.

The flat surface damping comes with the drawback of correspondingly increased stiction. Both stiction and squeeze-film effects are difficult to model because cavitation and inertial fluid effects becomes relevant when surfaces

2.2. The Developed and Optimized Valve

are separated rapidly, i.e. as discussed in [88]. Furthermore, CFD simulations of the impact situation have yielded pressures in the range of GPa which obviously will cause local deformations of the solid, i.e. preventing the fluid pressure to rise that drastically. A deeper understanding of this calls for more multi-physical couplings than what has been studied in this research.

The cushion groove widens the plunger along with the radial length of the orifice in order to achieve a damping force profile with no significant stiction added as discussed in [104]. The design change does not store the impact energy and depending on the size of the specimens there may occur difficulties with tolerances to create these grooves. It has been possible to add two individual grooves to the plunger, which according to simulations add the necessary force to provide a soft-landing.

The introduction of an end-damping spring stores the impact energy and releases it to open the valve. However, it may introduce the consequence that the valve cannot fully close without the synergistic flow forces coming from the DDU, i.e. the acting forces must be known with high certainty. The dimensioning of the spring must be tailored to the specific size of the DDU and the actuator for the valve to be able to switch at full displacement (i.e. switch when flow is low). Therefore, it is not necessarily possible to dimension the end-damping force to absorb the required energy when closing at partial stroke where the instantaneous flow will peak. The optimization algorithm has handled this trade-off between energy capacity of the spring and the impact energy, and as the results have revealed the spring is not necessary for the chosen design. A lot of feasible design points have been located which utilize both cushioning grooves and an end-damping spring. A design without the spring has been chosen since this makes the design simpler and puts a softer demand on the modelling accuracy.

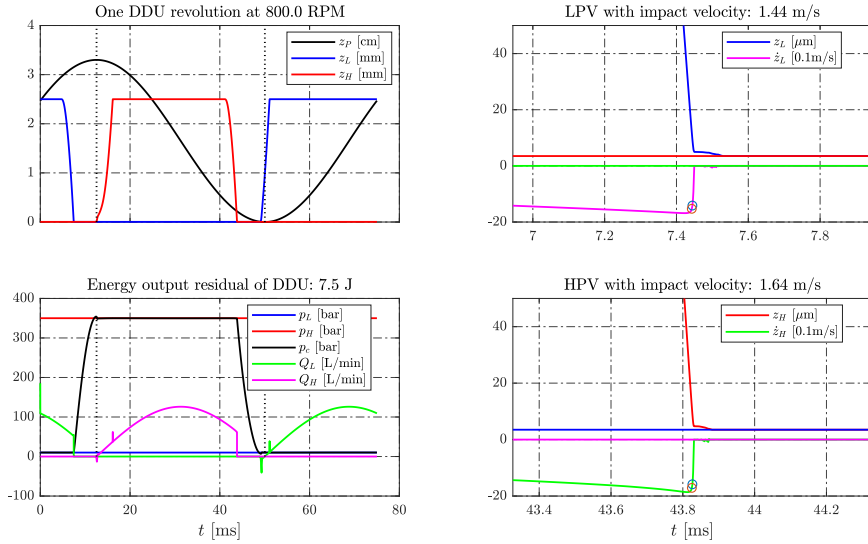
Finally, the opportunity of reversing the actuator force during switching may be taken to introduce soft landing control. This either requires knowledge about the work done by the fluid and actuator, on-line position measurement or an on-line optimization algorithm tuning the switching signals of the valves. The latter was attempted in [Paper F] but not been tested since the optimal design achieves the desired impact velocity, without reversing the actuating force.

2.2.2 Achieved Theoretical Performance

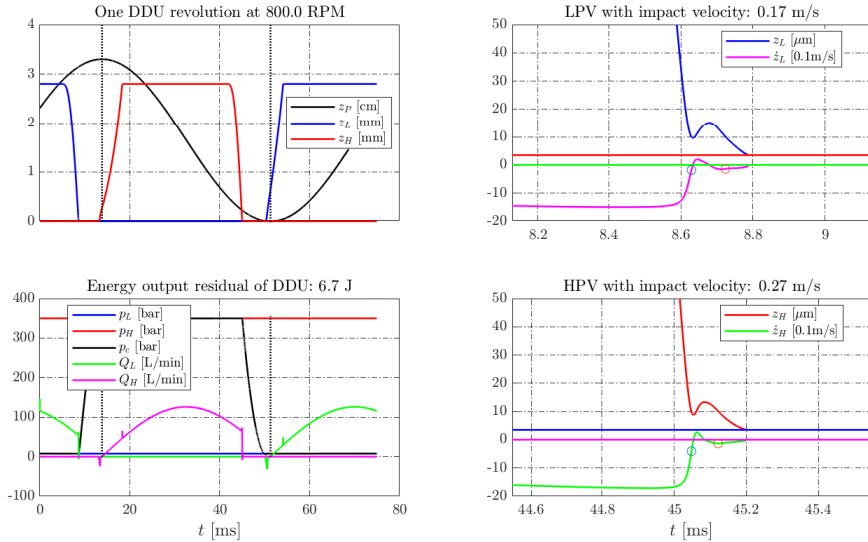
The simulation model developed in this work has been used to evaluate the performance of the DDU with either the previous valve (MCVi2.0) or the new valve design (MMAi1.1). The performance is summarized for comparative purposes in Fig. 2.3.

The energy losses associated with the valves are given in the two figures along with the velocity profile near impact. These have been the objectives of

Chapter 2. Developed Valve as Used in a DDU



(a) Performance of MCVi2.0 (titanium plunger).



(b) Performance of MMVi1.1 (stainless steel plunger).

Fig. 2.3: Simulation results of a DDU with the previous valve prototype developed at AAU (MCVi2.0) and with the new optimized design (MMVi1.1). Impact speed is evaluated at $10 \mu\text{m}$ to be conservative and account for possible plunger misalignment. The two dots mark the interval in which $z = 10 \mu\text{m}$ and the impact velocity is interpolated between these two points.

2.2. The Developed and Optimized Valve

optimization. The performance is presented here to show the improvements and to illustrate that the new plunger can be realized in stainless steel and still reach the necessary switching requirement. This is cheaper than the titanium plunger otherwise used, and the material is researched more in depth. This simulation shows that the flow force is low enough for the valve to be normally open and that the combined valve energy loss is 6.7 J out of 1.61 kJ output energy for each revolution. The switching times are satisfactory and the impact velocities are well below the threshold of 1.5 m/s, i.e. surface coatings can be avoided. The pressure peak in the HPV cushioning groove is around 200 bar relative to p_H , which is sufficiently lower than the materials yield strength.

The above is the output of the proposed optimization formulation and the next chapter is devoted to explain the design framework used to predict this performance.

Chapter 2. Developed Valve as Used in a DDU

Chapter 3

The Design Framework

“All models are wrong, some are useful.”

– George E. P. Box (1919 – 2013)

The design framework must in short be able to predict the performance of a digital valve in a given DDU environment. This includes: dynamic response, flow characteristics, fluid force, energy required to switch and stresses. These are governed by various design parameters and this chapter summarizes the proposed solutions to the challenges of making a design framework.

3.1 Flow Diagram of the Framework

The developed design framework is created to evaluate the performance of a specific valve concept where three levels of model fidelity are used: only static evaluations, dynamic evaluations (including ODEs) and finally including PDEs in the form of Navier Stoke’s equations.

The first step is to establish rough design rules to do a preliminary assessment of a given designs dimensioning. This is the pre-modelling phase and the formulation of these design rules, i.e. static evaluations, requires some engineering judgement.

Based on literature and experience from steady and transient CFD simulations of the design, a dynamic LPM has been formulated consisting of coupled ODEs which are solved numerically.

Finally, the designs that are found optimal by the LPM are considered for manufacturing by running full transient CFD and/or FEA (either 3D or 2D axisymmetry). The initial thoughts on the framework structure was presented in [Paper C]. The updated version, presented in [Paper J] is shown in

Fig. 3.1.

Figure 3.1 illustrates that the choice of various concepts to some extent couples to each other. This decision process is for the engineer to perform. It may be decided in a qualitative manner by consulting the literature and studying obvious design consequences. Based on the choices, the system can be parametrized and the relevant modelling techniques identified. This identification is explained by the steps in the '*Define modelling techniques & optimize*' block where the time consumed to simplify the problem must not exceed the time spent by just applying the highest fidelity models. This depends on the amount of required function evaluations, which to some extent is a function of the design parameters. In this work there are around 30 parameters and to open the possibility of testing various objectives and constraints model simplifications are essential.

The remainder of this chapter focusses on the modelling-work since this is the primary research contribution. Figure 3.2 gives an overview of the HPV simulation model and couplings of the system variables.

The specific equations used to create the model are elaborated in this chapter, where the two grey boxes in Fig. 3.2 include novel contributions from this work.

3.2 Simplified DDU Equations

The performance criteria discussed in this research relates to DDU efficiency and durability. Besides, certain requirements must be met in the functionality of the machine. The task of this work thus consists of establishing accurate models to evaluate the machine performance.

Piston Kinematics

The rotation of a DDU may be described purely by kinematics and thus only requires knowledge about the rotating shaft velocity. This can be translated to piston displacements and velocities

$$z_{P,i} = r_e \cos(\theta + \phi_i) + r_e \quad (3.1)$$

$$\dot{z}_{P,i} = -\dot{\theta} r_e \sin(\theta + \phi_i) \quad (3.2)$$

where r_e is the radius of the eccentric, θ is the shaft angle, ϕ_i is the angle which offsets piston i from the other pistons relative to θ , and z_P denotes the displacement of the piston. All these are defined as shown in Fig. 1.1a where $\phi_1 = \pi/2$.

The DDU is a multi-body system with possible local deformations from force and torque equilibriums meaning that pressure, flow and leakages all

3.2. Simplified DDU Equations

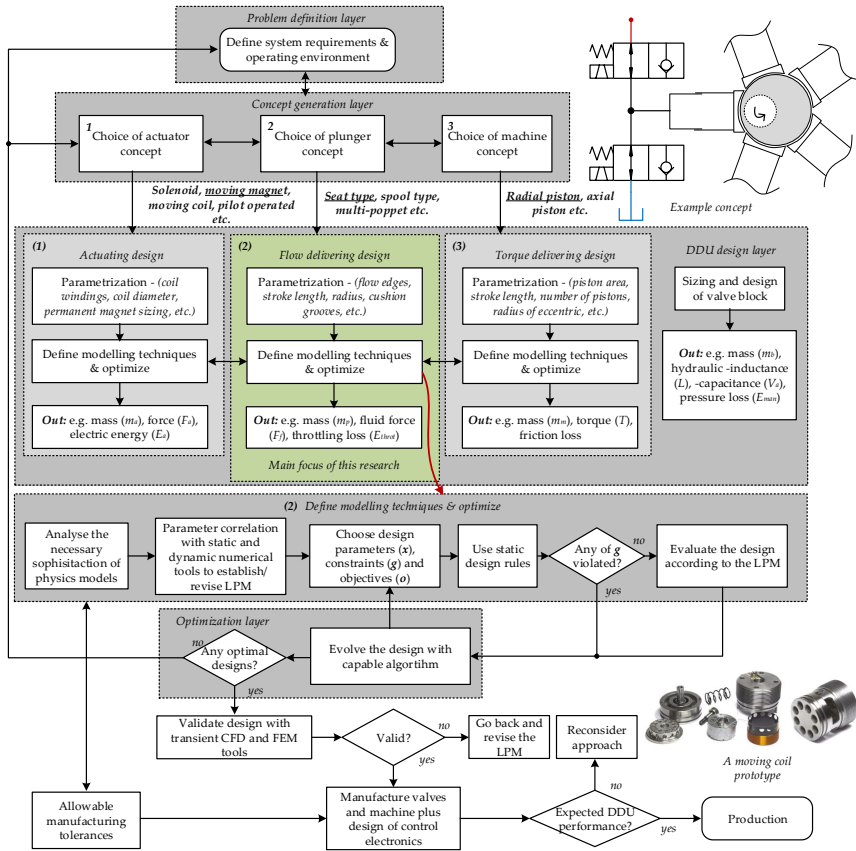


Fig. 3.1: Flow diagram of the proposed DDU design framework. Figure is from [Paper J]. The user defines the environment and the requirements which normally are continually adjusted by the user, based on these a series of qualitative decisions must be taken. The identification of necessary physics is largely based on the state-of-the-art, hereafter parameter correlation is used to analyze the proposed geometry and from this construct Lumped Parameter Models (LPM). Integrated quantities like fluid force, valve throttling loss and machine efficiency may be defined as performance metrics. The static design rules and LPM are used in synergy to locate optimal designs, and the chosen design is validated by transient CFD analysis before manufacturing.

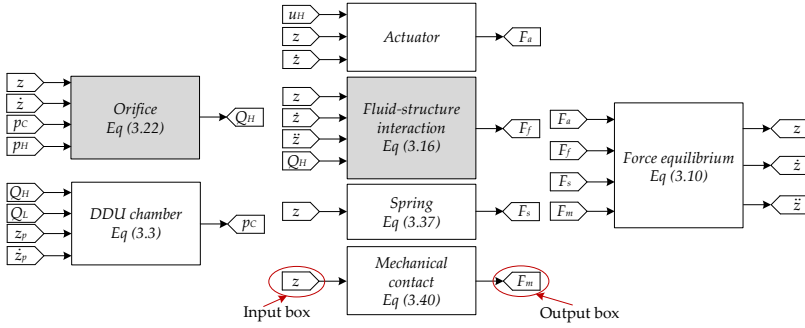


Fig. 3.2: Simulation model of the interaction between the HPV and the piston chamber, where the valve flow (Q_H and Q_L) and chamber pressure (p_C) couples the sub-systems. The two grey boxes indicate the areas where this work has contributed. The model is similar for the LPV, but the model inputs p_H , Q_H and u_H are with subscript L .

determine how fast the machine rotates in motoring mode. This dissertation focuses on the framework describing the valves and therefore a rapid solution (both in computation and programming) is preferred, also the above mentioned phenomena does not couple to the valve performance.

Chamber Pressure Dynamics

The produced torque of the DDU is related to the pressure in the piston chamber. The pressure dynamics of the piston chamber is described by a continuity equation as

$$\dot{p}_C = \frac{\beta_{eff}}{V_{de} + A_p z_P} (Q_H - Q_L - A_p \dot{z}_P) \quad (3.3)$$

where β_{eff} is the pressure dependent effective bulk modulus of the oil, expression discussed in [40] is applied, Q_H and Q_L are the flow through HPV and LPV respectively, A_p is the piston area and V_{de} is the dead volume of the piston chamber as shown in Fig. 1.1a.

The effective bulk modulus is governed by the mechanical construction and the fluid, and it plays a role in describing the losses occurring during pressurization and de-pressurization. In other words, the time required to change the pressure will decrease with a decrease in volume and/or with an increase in stiffness, and vice versa. This contributes to the amount of energy converted for every shaft revolution.

Hose Model

The connecting hoses are modelled by continuity equations and regular parametric expressions for the hose inductance and laminar Poiseuille flow (due

3.2. Simplified DDU Equations

to dimensioning ensuring laminar flow). A hose is divided into several control volumes to describe the time derivative of flow and pressure. The equations used are inspired by [31] whom uses the model for a similar problem.

$$L_h = \frac{\rho F l_h}{N_e r_h} \quad (3.4)$$

$$\chi_h = \frac{8\mu_F l_h}{N_e \pi r_h^4} \quad (3.5)$$

$$\dot{p}_k = \frac{N_e \beta_{eff,h}}{l_h \pi r_h^2} (Q_{k-1} - Q_k) \quad (3.6)$$

$$\dot{Q}_k = L_h^{-1} (p_k - p_{k+1} - \Delta p_{fric,k}) \quad (3.7)$$

$$\Delta p_{fric,k} = Q_k \chi_h \quad (3.8)$$

Here the index k denotes the quantity related to the element number k with a total number of elements of $N_e = 5$, $\beta_{eff,h}$ is the effective bulk modulus of the hose (kept constant at 5000 bar), l_h and r_h are hose length and radius respectively. These ODEs are solved by using the boundary pressures to give in- and out-going flow. The pressures are attenuated by accumulators as illustrated by Fig. 3.3. The pump is assumed to be ideal and deliver a flow to maintain a constant p_p . This value may be substituted with measurements for validation purposes.

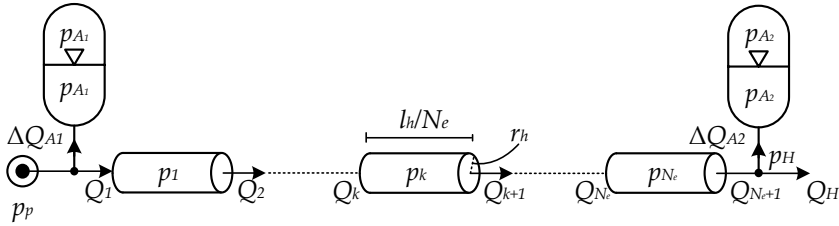


Fig. 3.3: Hydraulic schematic of the interconnection between accumulators and hose (divided into N_e elements.)

The length of the hose plays a role in avoiding pressure pulsations and water hammer phenomena and since relatively fast valve switching (a few milliseconds) is desired the hose should in general be as short as possible. This gives lower inductance and lower resistance. The pressure waves travels quite fast relative to the desired switching frequency of the digital valves and resonance of these pressure waves is therefore not expected to occur.

Accumulator Model

Accumulators stores hydraulic energy and releases this when needed. The accumulators used in the test-rig are diaphragm-types which have low inertia

and a gas-spring stiffness much lower than that of the hydraulic fluid. The process is considered adiabatic and the pressure change can be expressed by [42]

$$\dot{p}_A = \frac{p_A^\kappa}{V_A \left(p_{pre,g} p_A^{-1} \right)^{\kappa-1}} Q_A \quad (3.9)$$

where κ is the polytropic exponent of the gas, $p_{pre,g}$ is the pre-charge pressure of the gas, V_A is the volume of the accumulator and Q_A is the flow to the accumulator.

The response of the diaphragm is considered immediate and the pressure of the gas and liquid side are always equal.

3.3 Digital Valve

The valve switching dynamics is found from the acting forces as summarized in the equilibrium of forces

$$\ddot{z} = m^{-1} \left(F_a - F_f + F_s + F_m \right) \quad (3.10)$$

where F_a is the force of the actuator, F_f is the fluid force from interaction between the fluid and the plunger, F_s is the total spring force, and F_m is the mechanical end-stop force from seat and plunger contact. These forces, as shown in the free-body-diagram of the plunger in Fig. 3.4a, are discussed in the following.

3.3.1 The Dynamic Computational Fluid Dynamics (CFD) Framework

Early on in the project a dynamic and to some extent generic CFD framework was identified to be essential in order to understand the switching behavior of digital valves. The following test cases of the valve have been studied:

- Switching under constant velocity, and fluid is initially still
- Switching under constant acceleration, and fluid is initially still
- Switching under varying acceleration, and varying boundary flow
- A non-zero pressure differential on the boundaries, and fluid is initially still

The focus ended up on a 2D axisymmetric formulation to allow rapid generation of geometry, meshing and analysis at the cost of restricting designs to be symmetric and disregarding possible symmetry breaking phenomena.

3.3. Digital Valve

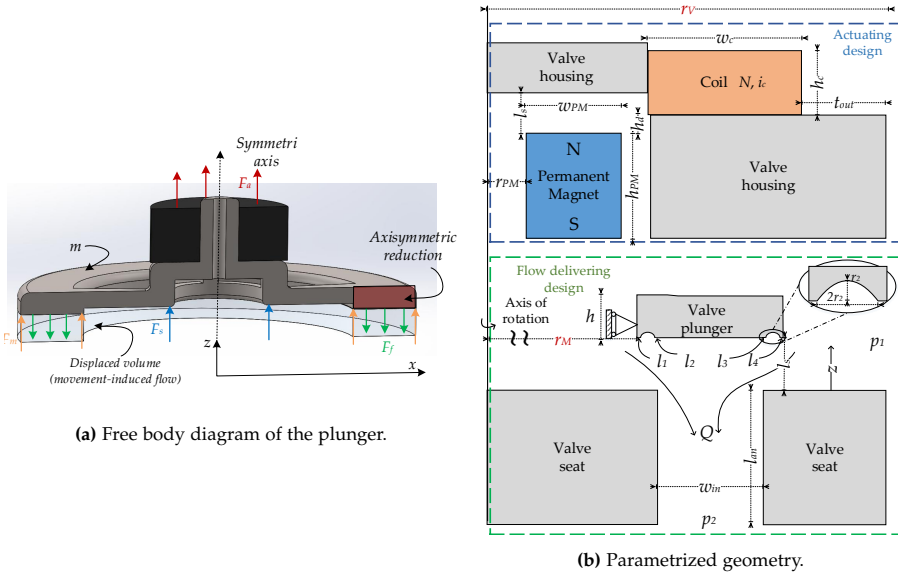


Fig. 3.4: The figure illustrates the plunger in 3D and the approximate locations of each force. The motion is along the z -axis and forces assumed to act uniformly on the entire body. This 3D design along with the valve housing and seat have been reduced to the 2D axisymmetric parametric geometry of Fig. 3.4b where the most relevant parameters and variables are denoted. $r_M = R - w_{in}/2 - l_1 - l_2 - 2r_1$

The validity of this approach was ensured by consulting measurements of the valve prototype. The approach requires only one dynamic meshing technique, the layering technique, because only rectilinear motion is considered. The CFD approach has been validated for simple test situations as discussed in [Paper A and H]. The developed framework is elaborated in [Paper E] and the most relevant details are summarized here with some additional discussions.

The problems solved to realize the dynamic CFD simulation are; formulating a proper mesh given the applied discretization schemes, setting up the dynamic mesh zones, time-stepping algorithms and describing the motion of the moving walls. Details about the mesh can be found in [Paper A & E].

The layering technique requires a quadrilateral mesh structure in order to either collapse or expand the mesh orthogonally to the moving surface. This method preserves the original mesh, compared to the other methods available and metrics such as skewness is therefore not worsened while simulating. The concept is illustrated in Fig. 3.5 where the mesh height shrinks for each time step according to the motion of the plunger, and the element either expands or collapses when one of the constraints of (3.11) are violated. A limit of the time step-size may be defined to avoid jumping through several

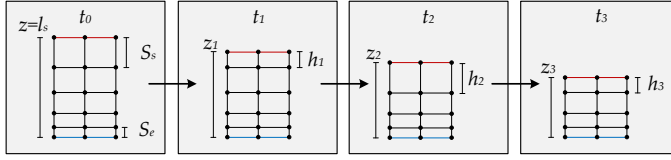


Fig. 3.5: Time incrementing of a dynamic biased mesh by the layering method. The red-line is a moving wall-boundary and the blue is a fixed wall-boundary. Black lines are regular element edges.

elements of the mesh in one time step (causing negative cell volume) and the allowed height (h_{id}) of the elements on a boundary can be changed with time.

$$h > \alpha_c h_{id} \quad ; \quad h < (1 + \alpha_s) h_{id} \quad (3.11)$$

Where h is the current height of the mesh element on the moving wall, α_c and α_s are the collapse and split factors respectively. The maximum allowed step-size is defined as

$$\Delta t_{max} = \frac{\Delta S}{2|\dot{z}| + \epsilon} \quad (3.12)$$

where ϵ is a small number to avoid dividing by zero, and the allowed distance, ΔS corresponds to the length of one element in the z -direction. The element size varies as a function of z as shown in Fig. 3.5, and ΔS is therefore defined as a variable. This ensures that the time step is restricted to avoid negative cell volumes when the mesh is updated. This distance is defined as

$$\Delta S = \begin{cases} S_e - \frac{S_e}{I_s} z & \text{if } z < z_{lim} \\ \frac{S_e - S_s}{I_s} z + S_e & \text{otherwise} \end{cases} \quad (3.13)$$

where z_{lim} is a user-defined position at which the non-linearity of the fluid force becomes significant compared to other forces. To capture this sudden rise in damping force, low step-sizes are necessary. For each time step the allowed maximum step-size is updated and the actual step-size is determined by the solver algorithm in ANSYS Fluent based on the numerical truncation error of the fluid dynamical equations. Therefore, this does not account for the numerical error introduced by integration of the plunger's acceleration.

Several issues with negative cell volumes have been experienced when the value of ΔS was poorly defined. Furthermore, the value of h_{id} is preferably dependent on z , but a sufficient formulation has not been found to give reasonable results, therefore it has been kept constant.

Examples of two spatial solutions at given time instants during valve switching are shown in Fig. 3.6.

The contours of the graphs show the interpolated fluid pressures and the streamlines show the velocity vectors of the fluid. This illustrates circulation

3.3. Digital Valve

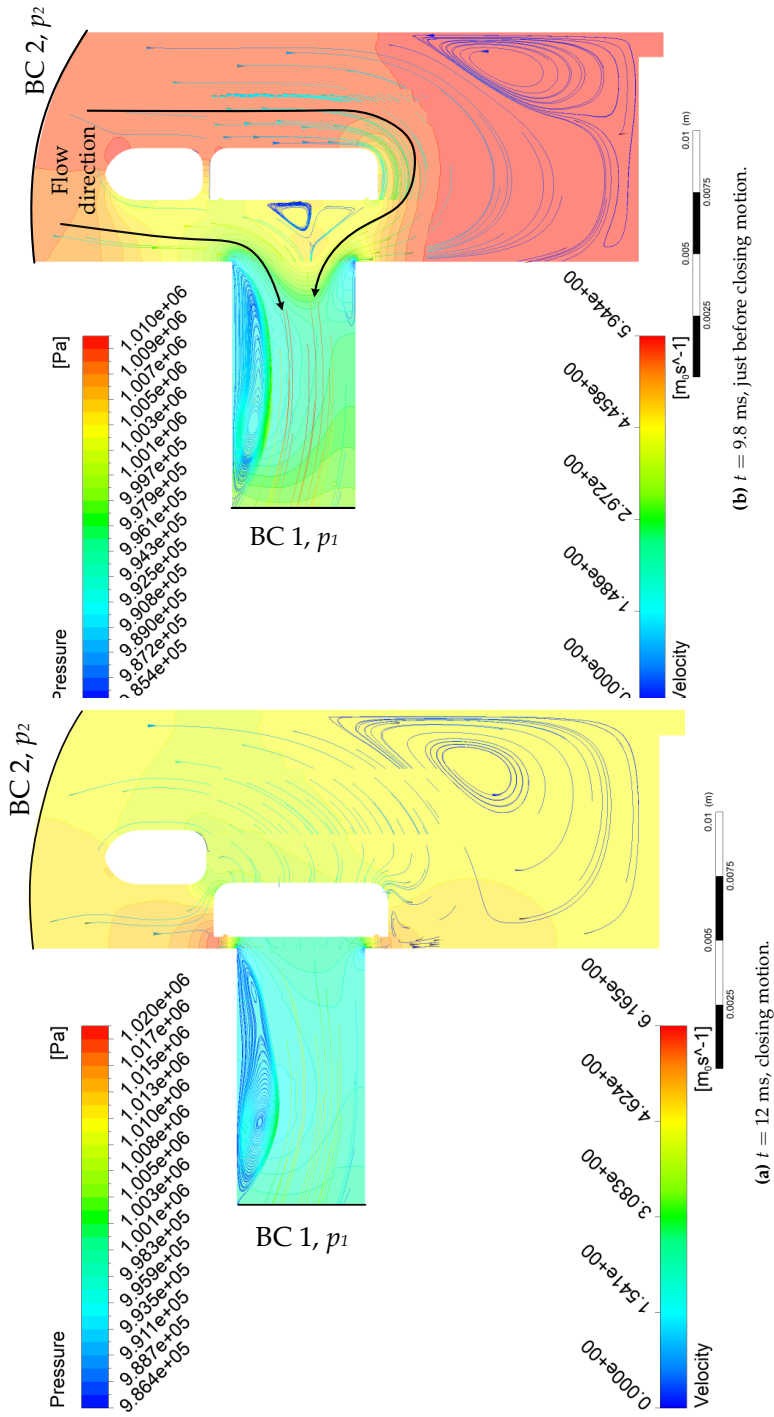


Fig. 3.6: Merger of spatial pressure and velocity solutions to the fluid flow problem. The plunger is actuated after 10 ms and the figures show the situation before and after the initiation of movement. White areas are solid bodies, coloured areas are fluid and the black lines denotes the edges where Boundary Conditions (BC) are defined.

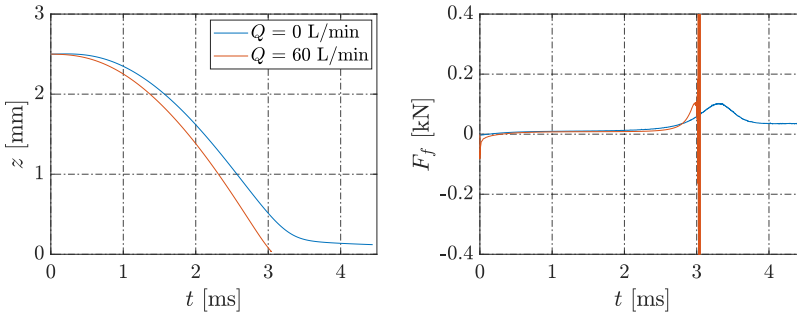


Fig. 3.7: Position (z) and fluid force (F_f) during valve switching. The boundary conditions either allow a flow of 0 or 60 L/min. Two quite different switching characteristics are observed and the fluid force becomes unstable when $Q = 60$ L/min.

zones, but more importantly the pressures on the surface of the plunger may be integrated to find the fluid force. The mass flow rate at the boundaries compared to the pressure drop at the two boundaries can be used to describe the flow characteristics. The pressure levels shows that the flow does not cause much pressure change around the plunger when z is high, but as z decreases the interaction changes.

During the switching instant, the boundary conditions can be defined in various ways, which significantly affects the solution. One case is to have no flow allowed across the boundary edges, i.e. the expanded fluid volume must be filled by the compressed one. Another one is to enforce a constant flow condition that is non-zero, e.g. 60 L/min. The difference of these two situations when observing plunger position and the fluid force is visualized in Fig. 3.7.

Figure 3.7 reveals a significant change in the damping forces of the two situations. At zero flow the plunger is gradually decelerated, whereas the 60 L/min causes the impact to occur at a higher velocity. This conclusion has been supported by the experimental observations that were shown in [Paper A & H]. The fluid force solution diverges as $z \rightarrow 0$ when $Q = 60$ L/min, which is either attributed to ill-conditioned equations from the compressed mesh or due to a too large step-size. To study this further a series of varying flow conditions have been simulated with CFD and the fluid force (F_f) near end-stop computed. These are plotted in Fig. 3.8.

The graphs of Fig. 3.8 shows how F_f depends on z and the flow, i.e. on the position of the DDU shaft (θ) and the rotation speed ($\dot{\theta} = 800$ RPM). The smoothing of the results shows that F_f rises fast as $z \approx 50 \mu\text{m}$ and also that it is highly non-linear. The force oscillation influences the plunger movement, hence feeding back to the solution for F_f and this causes instability and at some point this causes divergence and the simulation is terminated. Study of

3.3. Digital Valve

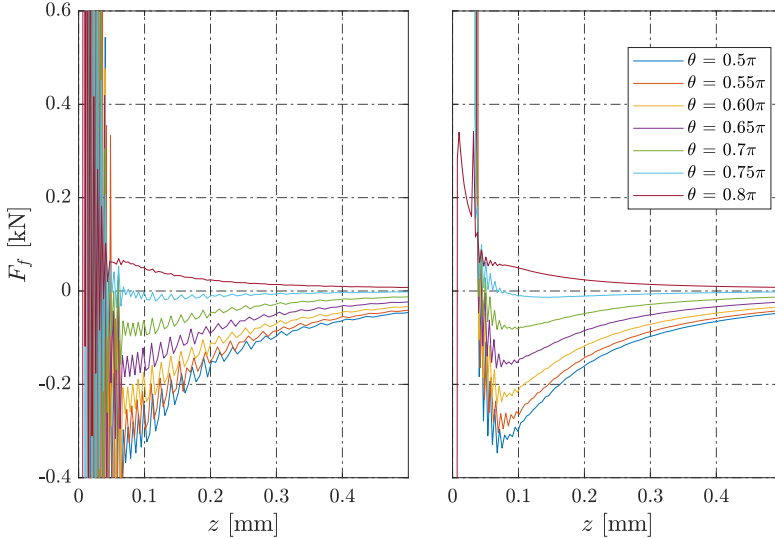


Fig. 3.8: Switching at different shaft angles and constant rotating speed causing different flow conditions according to (3.2). The results of the two plots are identical, but the graphs to the left have not been smoothed whereas the ones to the right are smoothed over 20 values.

the impact situation is thus not entirely possible with the current settings of the CFD framework.

The maximum step-size and the ideal height of the layering mesh have been adjusted to remedy the unstable force results. The step-size constraint makes it possible to include the end-damping forces and evaluate valve switching down to $2 \mu\text{m}$ when the flow conditions are at its peak (125 L/min), but at the cost of additional computational burden. The resulting graphs are shown in Fig. 3.9.

The introduction of dynamic limits to the step-size gives a more stable solution. Whether this is caused by improving stability of the discretized RANS equations or of the discretized equation of motion is difficult to say since these are coupled. However, the stability of the numerical integration has been analyzed by studying the eigenvalues of a mass-spring-damper system which is similar to a digital valve. An increase of the fluid damping force means a requirement of lower step-size to ensure a stable solution as shown in the following.

Importance of Step-size for Stability

The acceleration is integrated numerically to obtain velocity and position in the CFD framework. This is done by the forward-Euler method. The

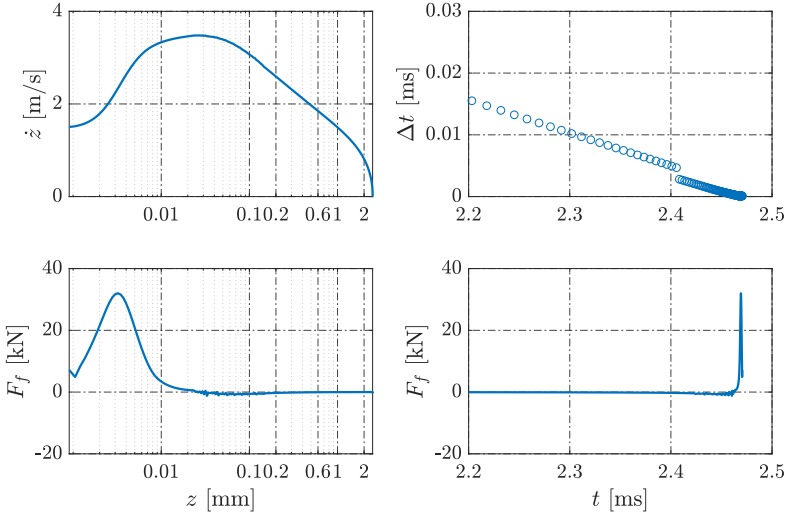


Fig. 3.9: Switching at $\theta = \pi/2$ meaning $Q = 125$ L/min. The results are shown as function of the plunger position (z) and the time step-size plus fluid force are plotted over time to show how rapidly the damping force rises.

major drawback of this method is that it is only a first order solver, and small step-sizes may be necessary to give stable solutions. The reason for not using higher order integration is because F_f is found from CFD, where the mesh is updated for each iteration. If e.g. the 4th order Runge-Kutta method was desired, this would require four CFD iterations to integrate the acceleration. After these iterations it would be necessary to re-initialize the mesh and the solution space to the instant before these four iterations and then the actual time step update may be performed. This is a computational and programming challenge and has not been considered a more feasible approach for the problem at hand.

Stability of forward-Euler integration can be evaluated by looking at the eigenvalues of the system. Using the linear test equation ($\dot{y} = \lambda y$ with a non-zero initial condition) it can be shown that the solution is stable if

$$|1 + \lambda \Delta t| \leq 1 \quad (3.14)$$

In this analysis the valve is approximated by a mass-spring-damper system, which means the drag term is not included and neither is the position dependent damping nor the flow-induced force. The eigenvalues of a mass-spring-damper system are

$$\lambda = -\frac{k_v}{m} \pm \frac{\sqrt{\frac{k_v^2}{m^2} - \frac{4k_s}{m}}}{2} \quad (3.15)$$

3.4. Valve Fluid Flow & Forces, F_f

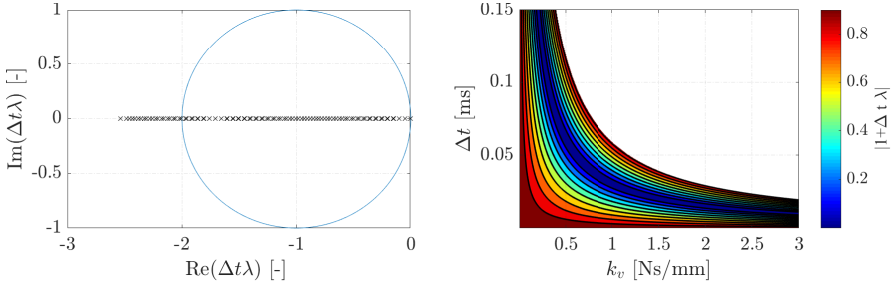


Fig. 3.10: *Left:* is the stability region (the blue line) according to (3.14) and step-size multiplied by eigenvalues from (3.15) (shown as crosses). The eigenvalues are $-16.4e3$ and $-16.9e3$ when $m = 30$ g, $k_s = 2.22$ N/mm, $k_v = 0.5$ Ns/mm, i.e a step-size, $\Delta t < 0.119$ ms is necessary for the discrete equations to be stable. The step-size is varied from $1e^{-5}$ to 0.15 ms in the plot. *Right:* shows the distance between each eigenvalue and the point $(-1,0)$.

Since the mass (m) and spring stiffness (k_s) are fixed for a given design, the stability region can be evaluated at different time step-sizes (Δt) and damping (k_v) to reveal Fig. 3.10.

The stability region reveals that a low damping means large steps can be used, and when the damping increases the allowable step-size decreases. If all the velocity dependent forces are linearized in the region near the seat, the equivalent k_v coefficient is 0.1 Ns/mm and the solution should therefore be stable for steps-sizes in the order of 0.1 ms. This is a quite large step-size, which is why the forward-Euler method should be sufficient. Furthermore, added mass from the fluid means that the stable region widens.

However, as observed in the above simulations the fluid force did become unstable as the opening area decreased (around $z = 0.1$ mm) where the non-linear term of the fluid force dominates. Therefore, the maximum step-size decreases linearly with a steeper gradient near the end-stop as defined by (3.13). This approach is not guaranteed to be stable since it depends on the values of S_e and z_{lim} and changing the valve design may move the necessary value of z_{lim} .

3.4 Valve Fluid Flow & Forces, F_f

The force that arises from the interaction between a moving fluid and a moving solid plays a significant role in predicting the valve performance, see [Paper A, E, H & I]. The force is governed by the plunger wall boundary pressures and these are affected by movement and acceleration of the fluid and/or body. The earlier iterations of the MCVi1.0 and MCVi2.0 [66,90] were primarily designed with respect to the actuator and a non-parametric fluid force model used to include the fluid force of one design. Design changes to

the flow geometry was therefore not included in e.g. [90, 96]. The total fluid force has been divided as

$$F_f = F_{flow} + F_t + F_{MI} + F_e \quad (3.16)$$

where F_{flow} is the steady-state flow force, F_t is the transient flow force, F_{MI} is the Movement-Induced (MI) force from plunger movement and F_e is the fluid force occurring near end-stop.

3.4.1 Steady-state Flow Force, F_{flow}

F_{flow} has been studied by CFD in [Paper E & I] and also experimentally in [69] for the same valve design. The currently most accurate parametric form for the considered valve concept is

$$F_{flow} = \begin{cases} F_p - \rho_F \frac{Q^2}{c_c A_o} \sin(\gamma) & \text{if } \Delta p \geq 0, \\ F_p & \text{else} \end{cases}, \quad (3.17)$$

where

$$F_p = A_p \Delta p \quad (3.18)$$

$$\Delta p = p_2 - p_1$$

$$\gamma = \tan^{-1} \left(\frac{c_1 z^{c_2}}{w_{in}^{c_3}} \right) \quad (3.19)$$

$$A_o = \min(4\pi Rz, \underbrace{2\pi R w_{in}}_{A_p}), \quad (3.20)$$

and where γ is the angle used to describe the influence of the Vena-Contracta (VC) as discussed in [Paper I]. This angle is determined based on the relation between the plunger displacement (z) and seat width (w_{in}), which have been identified to be dominating for F_{flow} . The further away the plunger is from the seat, the lower F_{flow} becomes for positive flow. In the considered flow range, a negative flow causes F_{flow} to become almost independent of z . The force F_p occurs from having a differential pressure across the valve and for a positive flow this force is reduced depending on the jet angle. As A_o goes to zero a singularity arises in (3.16) which is avoided by having $z_{min} = 2 \mu\text{m}$ and $Q = 0$ at z_{min} .

The tuning parameters (c_1, c_2, c_3) are determined from minimizing the Mean Absolute Error (MAE) of F_{flow} between LPM and CFD simulations. The remainders are purely defined by the plunger's dimensions and the fluid's density. The value of F_{flow} is used to assess if a given design is normally open at peak flow conditions, if not this design is not further evaluated.

3.4. Valve Fluid Flow & Forces, F_f

At positive flow, F_{flow} is sensitive to z when the value of this is below $0.5w_{in}$. For values higher than this the flow force still decays as $\gamma \rightarrow \pi/2$ but with a low gradient. Plots of [Paper I] show agreements between the flow force and pressure/flow relation from the various models, with an example given in Fig. 3.11. The correlation between Δp and F_{flow} is clear from the graphs as well as the non-linear flow relation.

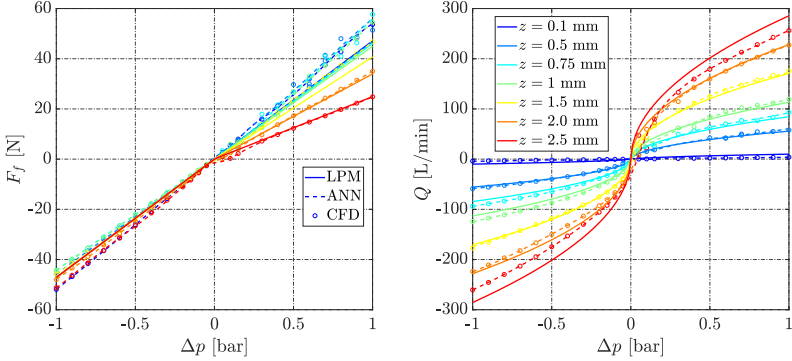


Fig. 3.11: Flow force and flow computation from CFD, LPM and LPM aided by ANN for various values of z . Figure is from [Paper I] and values are for the baseline design, $R = 15$ mm and $w_{in} = 5$ mm.

Artificial Neural Network Surrogate Model

The above model for the flow force is derived from a simplified physical understanding of hydraulic valves. This has the risk of omitting certain characteristics and dependencies, which would be captured by a CFD analysis. Therefore, the possibility of constructing an Artificial Neural Network (ANN) surrogate model based on CFD results has been investigated in [Paper I].

The paper investigated the feasibility of applying ANN as a surrogate by using the LPM of (3.23) and (3.16) together with CFD data. The relations between inputs ($\Delta p, z, R, w_{in}$) and outputs (F_f, Q) were compared to understand the requirements for data diversity and size. If analytical expressions are impossible to derive it makes sense to look at a surrogate like the ANN. However, the computational burden in obtaining training data is heavy for the transient and dynamic problem. Hence for the considered type of problem, a parameter correlation is considered as a stronger tool to reduce the fluid flow problem into a set of coupled ODEs.

3.4.2 Transient Flow Force, F_t

The transient flow force (F_t) is a consequence of a change in flow, i.e. changing the fluid momentum means changing the pressure around the plunger.

This force is modelled in spool type valves as being mass times acceleration of the fluid volume of interest. This translates to the expression

$$F_t = -\rho_F l_d \dot{Q}_t = -2w_{in} \rho_F \dot{Q}_t \quad (3.21)$$

where the damping length (l_d) is governed by the geometry and for seat type valves normally equal to the hydraulic diameter and \dot{Q}_t is the change of the transient flow, i.e. including Movement-Induced flow (3.32) and flow gradient through the valve. Using the orifice equation to describe the flow, means that the above term becomes a drag force proportional to the velocity of the plunger.

3.4.3 Valve Flow

The flow through the valve is determined by the opening area of the valve, the current pressure difference, the current flow and by the speed of the plunger. The total flow is

$$Q_t = Q + Q_{MIF} \quad (3.22)$$

where the two separate flow contributions are described by (3.23) and (3.32). Normally, the flow through a valve is described solely by the orifice equation (3.23). Several models that apply to both laminar and turbulent cases have been proposed in the literature where reasonable results have been shown with the parametric version from [16]

$$\Delta p = \underbrace{\frac{\rho_F}{2(A_o C_d)^2}}_{k_{f1}} Q|Q| + \underbrace{\frac{Re_t \mu_F}{2A_o D_H}}_{k_{f2}} Q \quad (3.23)$$

where A_o is the orifice opening area, D_H is the hydraulic diameter of the orifice, ρ_F and μ_F are the fluid's density and dynamic viscosity respectively, Re_t is the Reynold's transition number, C_d is the discharge coefficient at turbulent conditions. Best fit for C_d and Re_t when compared with CFD results are $C_d = 0.67$ and $Re_t = 58$. The coefficients k_{f1} and k_{f2} account for both turbulent and laminar flow conditions. These coefficients play a role in determining the throttling loss in a DDU.

The LPM requires knowledge about the discharge of the flow area (C_d) and the transition number from laminar to turbulent (Re_t). These may be determined based on common values, CFD simulations or from measurement. The discharge coefficient of orifices has been studied for decades (e.g. [35, 64, 115]), and commonly it depends on the Reynolds number. The maximum Reynolds number of an annular valve occurs in the annular flow path or in the gap between the plunger and the seat. These can be approximated by [69]

$$Re = \max(Re_{ann}, Re_{seat}) \quad ; \quad Re_{ann} = \frac{Q}{2\pi R V_F} \quad ; \quad Re_{seat} = \frac{Q w_{in}}{2\pi z R V_F} \quad (3.24)$$

3.4. Valve Fluid Flow & Forces, F_f

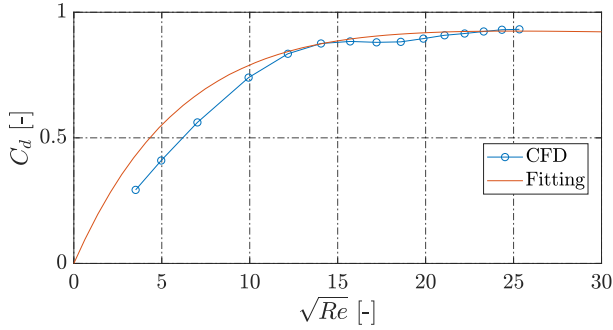


Fig. 3.12: Discharge coefficients estimated with CFD results when the flow is varied within a range expected for a DDU. The expression of (3.25) is plotted and referred to as "Fitting".

The expected flow resulting from a pressure difference can be calculated from CFD and (3.23) can be applied to calculate the value of C_d for the relation to hold.

It is best practice to make C_d dependent on the Reynolds number like [120]

$$C_d = C_{d,\infty} \left(1 + c_4 e^{-c_6 C_{d,\infty}^{-1} \sqrt{Re}} + c_5 e^{-c_7 C_{d,\infty}^{-1} \sqrt{Re}} \right) \quad (3.25)$$

where $c_4 \dots c_7$ are fitting parameters and $C_{d,\infty}$ is the turbulent discharge coefficient. This expression holds sufficiently as observed from Fig. 3.12 where the geometrical parameters are unchanged and only Q is varied during CFD simulation of the digital valve.

This is indicating that the CFD model is sufficient, and that C_d can be parametrized for the baseline design as a function of Q . However, to test this further a series of different flows and plunger positions have been simulated for four different designs (R and w_{in} are varied) revealing the values in Fig. 3.13 here Re_{seat} is largest for all the design points.

The graphs illustrates that changing both R, w_{in} and z does result in significantly different dependencies on the Reynolds number. Low Re numbers comes at large z which gives coefficients close to and even slightly above 1 at one instant. This happens since the size of z becomes greater than w_{in} which means the region of minimum flow area is not near the plunger. In this situation the geometry is not similar to a regular orifice and the traditional models are not necessarily meaningful.

The graphs also show that the flow direction influences the value of C_d . The tendencies of the coefficient do not resemble the classical dependency between C_d and the Reynolds number, i.e. applying (3.25) and (3.24) is not expected to be useful as a parametric expression for this design.

In the case of designing a motor the flow is primarily positive, this means the range of C_d is 0.44-0.8. The discharge coefficient is kept constant for all

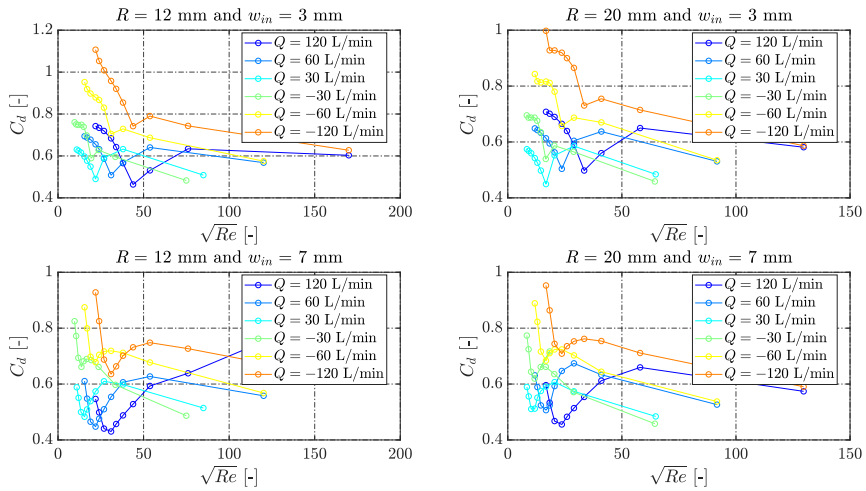


Fig. 3.13: Discharge coefficients estimated by CFD predictions and inserting into (3.23) where Reynolds number found from (3.24). Both Q and $z \in [06]$ mm are variables in each graph.

designs during optimization knowing that this does introduce an inaccurate throttling loss and flow force. However, this will eliminate the requirement of CFD simulations for each parametric update.

Valve Leakage

In [Paper D] a framework was presented to quickly assess the consequences of a leaking valve and also when leakage occurs as a function of switching cycles. A leakage between 0-1% of maximum flow is investigated, the loss increases linearly with increase of leakage as presented in the paper. A Poiseuille flow consideration between two flat parallel plates results in a 0.03% leakage flow relative to peak flow when the leakage path gap height is $2 \mu\text{m}$ and the length of the gap is 0.1 mm. This length is the lower bound of the design space and thus gives the highest leakage flow. This loss is insignificant compared to the machine output and therefore leakage predictions are not included. Besides seat type valves are normally leak-free.

3.4.4 Valve Fluid Inertia

Evaluation of the un-steady pressure driven flow through a valve was one of the topics studied by CFD analysis in [Paper E]. This revealed a transient period in which the fluid needed to accelerate from rest to the steady value predicted by the pressure flow relation. This is not surprising from the equation of momentum, and in digital hydraulics this parasitic inductance is something that is relevant to consider due to the fast switching of the control

3.4. Valve Fluid Flow & Forces, F_f

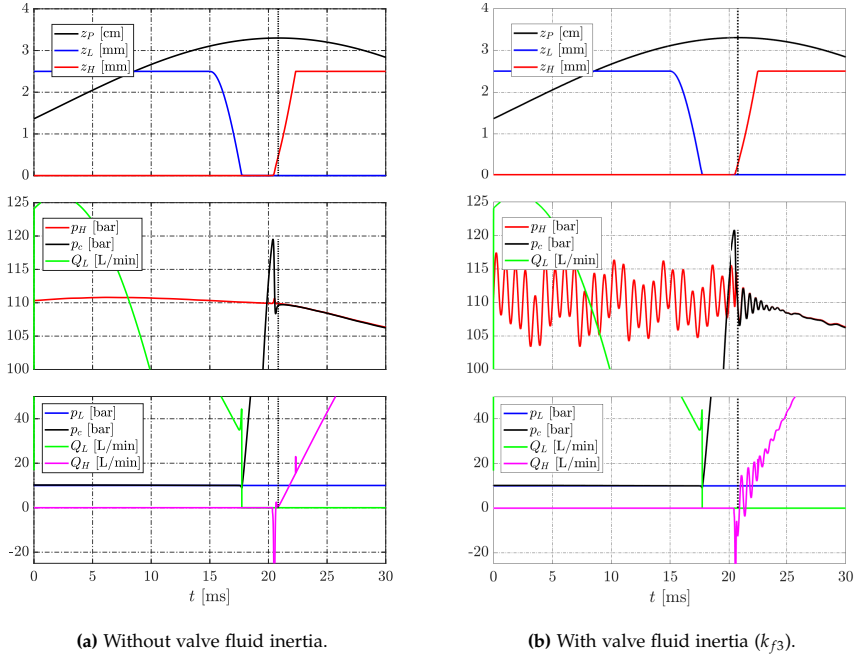


Fig. 3.14: Simulation results of a DDU operating in motor mode showing the consequence of one modelling adjustment.

valves. An approach was demonstrated in [29] using the mean flow velocity through an orifice and applying the continuity- and momentum- equation, which resulted in the equation

$$\Delta p = k_{f1}Q|Q| + k_{f2}Q + k_{f3}\dot{Q} \quad (3.26)$$

where the third fluid coefficient k_{f3} is the valve inductance. The time dependent term describes acceleration and deceleration of the fluid going through the orifice, and for a steady-state flow the equation reduces to the orifice equation presented in (3.23). The lumped parameter, k_{f3} was proposed by [29] to be governed by

$$k_{f3} = \frac{\rho_F}{\sqrt{\frac{\pi C_d A_o}{2}}} \quad (3.27)$$

This additional term has been used to describe the movement of the fluid between the accumulator and the piston chamber. Simulations of a DDU with and without the fluid inertia have been performed revealing the graphs of Fig. 3.14.

The graphs show how the introduction of fluid inertia between accumulator and valve causes oscillations on both the high pressure (p_H) and the

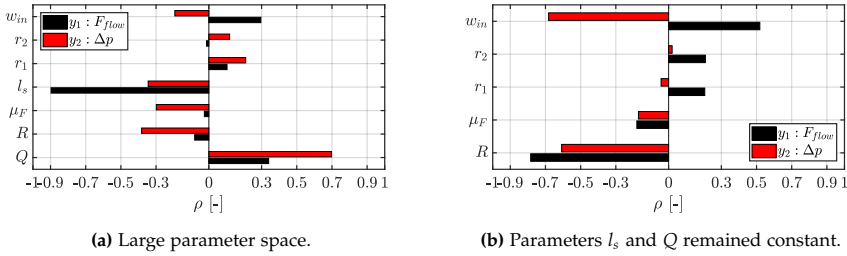


Fig. 3.15: Parameter correlation values of the two static fluid dynamical output parameters, flow force and pressure drop. Results from [Paper G] but Fig. 3.15b is presented here for the first time.

chamber pressure (p_C). Attenuation of this should be ensured by the accumulator.

A 3D CFD analysis from [92] of a DDU piston chamber with two relatively large digital valves revealed an oscillating pressure in the piston chamber whereas the constructed LPM of [91] did not. A similar pressure oscillation was observed experimentally in the DDU test-rig as explained in sec. 4.3.3. The oscillation had a frequency of 0.7 kHz and attenuated after 15 ms and therefore similar but not identical to the one shown in Fig. 3.14b, which is 1.7 kHz and attenuated after 5 ms.

3.4.5 Sensitivity of Flow and Force Predictions

Paper J elaborates the developed framework, and illustrates the parameter correlations in the flow delivering design. The LPM of flow and force include the parameters l_s, μ_F, R, Q and w_{in} . The parameter correlation reveals the significant correlations with respect to the chosen outputs, and therefore also the remaining irrelevant parameters. One example was shown in the paper where Q and l_s dominated the outputs (Fig. 3.15a), maintaining these two parameters constant reveals the correlations of Fig. 3.15b. The correlation of $l_1, l_2, l_3, l_4, r_1, r_2$ was found to be irrelevant w.r.t the defined outputs. However, R, w_{in} and to some degree μ_F correlates with the outputs.

The solutions found by static CFD along with the same design points used in the LPM have been used to compare the sensitivity and residual of the predictions from the two models. Spearman's correlation metric and the residual between CFD and LPM are computed to yield that the correlations of the models are similar. In addition, the MAE of residuals for the force predictions is 1.5 N and for the pressure to flow prediction a MAE of 2 kPa is found.

3.4.6 Movement-Induced Flow and Force, F_{MI}

In resemblance to the forces arising from flow conditions around the plunger, a force will occur when the plunger moves relative to the fluid. This is referred to as a Movement-Induced (MI) force and this movement will furthermore cause a flow referred to as a MI Flow (MIF). The behavior of the MI force was studied with 3D CFD simulations by Roemer et al. (2015) [95,96]. The authors argued that due to switching in the millisecond range no 'complicated' flow phenomena will have time to develop from the initially still fluid and thereby convective acceleration are eliminated from the incompressible NS equations reducing it to its linearized form. The MI force therefore takes the approximate form for rectilinear motion

$$F_{MI} = \underbrace{k_a \ddot{z}}_{\text{Added mass}} + \underbrace{k_v \dot{z}}_{\text{Viscous}} + \underbrace{k_d \dot{z} |\dot{z}|}_{\text{Drag}} + \underbrace{k_h \int_0^t \frac{dz}{\sqrt{t-\tau}} d\tau}_{\text{History}} \quad (3.28)$$

where k_a, k_v, k_d, k_h are fluid friction coefficients that are constant for the original expression, but due to the nearby boundary walls these coefficients are dependent on z . Sometimes this fluid friction is called "drag". In the following a small distinction is made, a viscous term is proportional to velocity and a drag term is proportional to the square of velocity. The added mass determines the work necessary to change the kinetic energy of the fluid. This work is done by the plunger and since the resisting force is proportional to the acceleration of the body it is referred to as an "added mass", although it more accurately describes the change in kinetic energy of all the fluid [17]. The viscous friction and history terms are also derived from the Stokes-flow drag on a circular disk [44]. The drag term is not part of the Stokes-flow solution, but is a term of the Morison's equation [17]. This additional term has been shown to be necessary in order to represent the force results of CFD analysis. The values of the coefficients were presented in [Paper E] and the analysis is extended here for clarification of the approach for finding these and how accurate the model is when the underlying assumptions are challenged. The significance of the history term was tested in [Paper A] and for the studied valve this term is insignificant, largely because switching is in the ms range. For the other contributions the following cases may be considered.

Condition I, a low constant velocity: For the case where the acceleration is zero, both history- and the added mass terms are zero. Equation (3.28) reduces to

$$F_{MI} = k_v \dot{z} + k_d \dot{z} |\dot{z}| \approx 0 \quad (3.29)$$

where the drag term goes to zero due to the square of velocity. This means k_v can be isolated and calculated by CFD simulations. However, CFD simulation resulted in a high damping when the plunger movement was initiated.

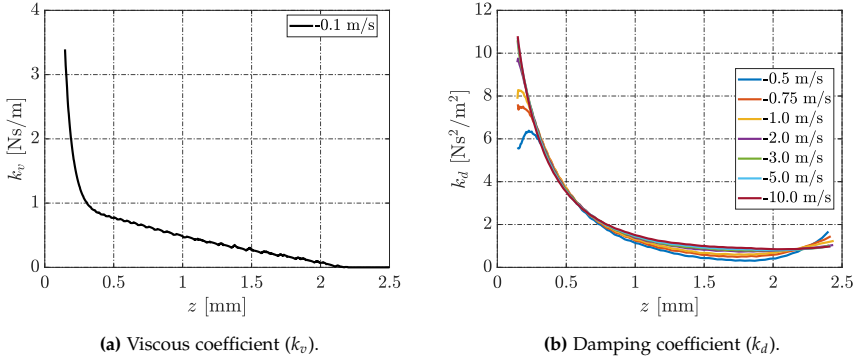


Fig. 3.16: Friction coefficients found by the described approach where the value of k_v is used to find k_d . The velocities are negative, i.e. z goes to zero.

This is because of the impulse drag that arises when changing a velocity instantaneously from 0 to \dot{z}_i as derived in [45] which means (3.29) must be reformulated to find the actual k_v

$$F_{MI} = \left(k_v + \frac{k_I}{\sqrt{t}} \right) \dot{z}_i \quad (3.30)$$

where k_I is an impulse drag factor which only exists when a body is accelerated from rest to a constant velocity infinitely fast. This leaves two unknowns, but since the inverse of the time are related to the impulse drag, this force will dominate in the first few time-steps where $t \approx 0$ and the magnitude of k_v is not important to estimate the value of k_I . This leaves one unknown and k_v can be calculated for the remainder of the data points as shown in Fig. 3.16a.

Condition II, several high constant velocities: Since both k_I and k_v have been determined it is now possible to find values for k_d . This is done for various velocities to test its dependence on this. Ideally it will be zero at all times, i.e. if the fluid friction (F_{MI}) is only proportional to velocity. The CFD results have, however, yielded that a quadratic term is necessary and the calculated coefficients of k_d for various velocities are summarized in Fig. 3.16b.

Studies of fluid friction of a flat circular disk moving in an initially still, incompressible, viscous fluid were elaborated in [Paper A]. The analytically parametric expressions of the MI-terms was presented, where the viscous coefficient of $k_{v,plate} = 16\mu_F r_{plate}$, setting the plate radius equal to the outer radius of the plunger gives $k_v = 0.01$ which is quite insignificant. The value only fits the value predicted from CFD when $z > 2$ mm. As z decreases the introduced error becomes significant. The drag coefficient of a flat plate is given as $k_d = 0.5\rho_F C_f \pi r_{plate}^2$ where C_f is shape dependent and equal to 1.1 for a circular disk. The value of $k_d = 0.3$ for the considered design, which is in the correct range when z is around 2 mm.

3.4. Valve Fluid Flow & Forces, F_f

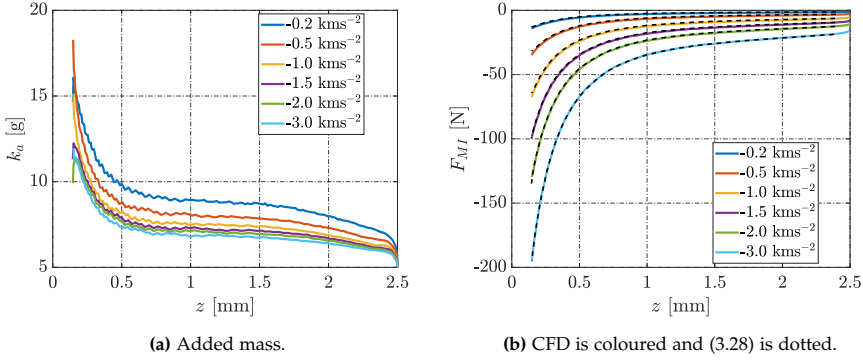


Fig. 3.17: Added mass coefficient for various accelerations and putting it all together to compare the CFD force with the one predicted by (3.28). For this comparison k_a from the CFD simulation of -3 kms^{-2} is applied.

Condition III, several constant accelerations: As described above the history term of (3.28) may be omitted without introducing a significant error. Since the remaining coefficients have been determined it is possible to derive the added mass by simulating a constant plunger acceleration.

$$k_a = \frac{k_v \dot{z} + k_d \dot{z} |\dot{z}| - F_{MI}}{\ddot{z}} \quad (3.31)$$

The results of the added mass and the value of F_{MI} are given in Fig. 3.17.

The added masses are ideally independent on the acceleration magnitude, which is also the trend as the acceleration rises. The total force predictions from the two modelling approaches yield almost identical results and the form of the LPM is sufficient for the considered example.

Studies of the added mass of a flat circular disk moving in an initially still, incompressible, viscous fluid reveals a parametrized added mass of $k_{a,plate} = 8/3\rho_F r_{plate}^3$. Setting the plate radius equal to the outer radius of the plunger gives $k_a = 12 \text{ g}$, which is not far from that predicted by CFD and may be used as an alternative. If instead the added mass of a plate of radius r_{out} and a smaller plate of radius r_{in} are subtracted ($r_{out} > r_{in}$) with each other, the formula $k_{a,annulus} = 8/3\rho_F(r_{out}^3 - r_{in}^3)$ is obtained. This resembles the plunger geometry better and gives $k_a = 9.5 \text{ g}$, which is also closer to the value predicted by CFD.

The Movement Induced Flow (MIF) of the valve concept considered in this work has not been investigated by neither simulation nor experiment prior to this research. The MIF relates to the velocity of the plunger, but also to the current position of it as shown in [Paper E]. This indicates that the plunger's shadow area cannot merely be multiplied the velocity to find this flow as prior believed [41,68,98]. Instead the area varies with z as illustrated

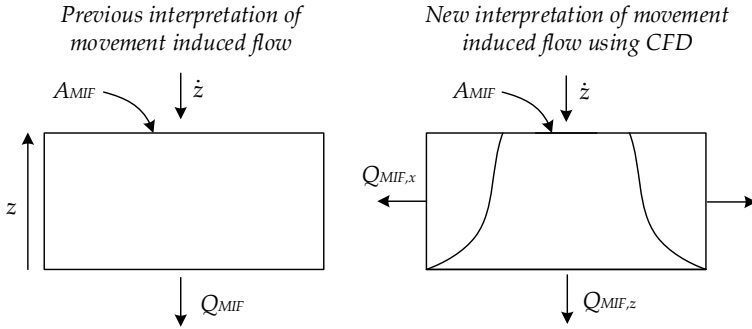


Fig. 3.18: Conceptual difference in the interpretation of the MIF. The new method considers the flow in both x and z -direction.

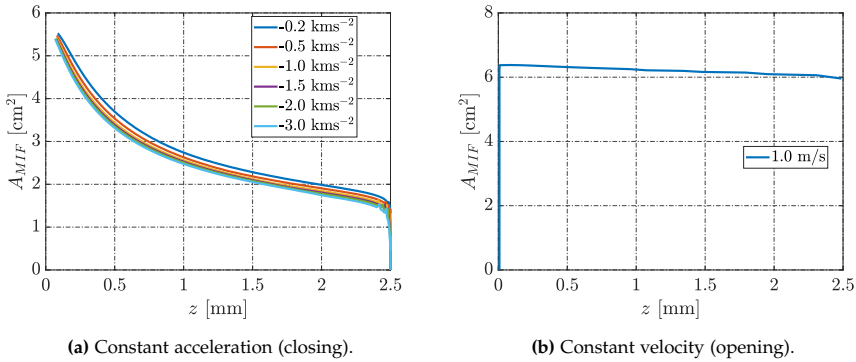


Fig. 3.19: Effective areas of the MI Flow (MIF).

by the dotted line in Fig. 3.18.

The MIF is determined based on the plunger's velocity and an effective area (A_{MIF}). This may be determined by CFD simulations, i.e. by dividing the mass flow rate by the plunger velocity at each time step, yielding the areas of the graphs shown in Fig. 3.19. Several constant accelerations are simulated for the closing motion, and due to the independence on \dot{z} the flow area is only evaluated for one data point during opening. This results in a higher A_{MIF} for the entire range of z as shown in Fig. 3.19b. The area in general depends on z and not significantly on \dot{z} or \ddot{z} .

The MIF is described by

$$Q_{MIF} = k_{MIF} A_{MIF} \dot{z} \quad (3.32)$$

where the effective area $A_{MIF} \approx A_p = 6.4 \text{ cm}^2$ as z is close to zero. A parametric version of this may be achieved simply by scaling the area with

3.4. Valve Fluid Flow & Forces, F_f

the change in shadow area as, i.e. $k_{MIF} = A_p A_{p,ref}^{-1}$, where $A_{p,ref}$ is the area of the reference design and A_p the shadow area of the new design. This is simply a necessary approach since the position dependency of A_{MIF} cannot be derived analytically, but since $A_{MIF} \approx A_p$ when $z = 0$ this is considered a fair approach to make the expression parametric.

The approach for the MI force requires at least three dynamic CFD simulations for each new plunger design. This is not feasible in parametric analysis, which is why an approach similar to the MIF has been taken. The final form of the MI force applies the parametric relations of k_a , k_d and k_v discussed in the text. This means the outer and inner radius of the annulus scales the coefficients found by CFD for the reference point given above as

$$F_{MI} = \frac{r_{out}^3 - r_{in}^3}{r_{out,ref}^3 - r_{in,ref}^3} k_a \ddot{z} + \frac{\mu_F (r_{out} - r_{in})}{\mu_{F,ref} (r_{out,ref} - r_{in,ref})} k_v \dot{z} + k_{MIF} k_d \dot{z} |\dot{z}| \quad (3.33)$$

k_a , k_v , k_d are look-up tables with input of z . When a design change is proposed during optimization these coefficients are then scaled according to the radius of the annulus. The drag term has the same dependency on geometry as the MIF described in (3.32), i.e. radius squared. This makes the model parametric, while introducing modelling uncertainty.

In a system like a digital valve the fluid is seldom still. The added mass is valid although the fluid is moving relative to the body. However, if the fluid is accelerated together with the body this will change the force. This effect is partially included by the transient flow-force from (3.21), which should compensate for this. This simplification is one source of modelling uncertainty. When the fluid moves relative to the body this may potentially change the dampening forces discussed in the above. This is compensated by the flow force of (3.17), but is a source of modelling uncertainty. All of the above proposals to create a LPM has been tested by comparing CFD to the LPM looking at fluid force and plunger velocity. The analysis is presented in the following pages, and ends up showing that the correct magnitudes are predicted for the reference design when all models are tested together. The parametric relations are tested in a few data points where the velocity magnitudes fits sufficiently between CFD and LPM when considering the purpose of the LPM.

3.4.7 Squeeze-film and stiction force, F_e

The quick separation or adhesion of solid bodies with a fluid in between is the cause of local pressure changes, generating either a dampening or suction like force. The phenomena is an inherent property of seat type valves and the exact prediction of this force has been shown in literature to be a comprehensive task since surface roughness and possible cavitation can be the cause of

a significant deviation from the expected force. Cavitation of the fluid occurs at a certain pressure depending on the tensile properties of the fluid. This may be governed by the purity of the fluid and the level of air content. These multiphase conditions can be simulated to some degree via CFD and analytical solutions have also been proposed as discussed in the SOTA in Chapter. 1. However, for physical systems the quality of the oil is seldom known, where nano bubbles and other particles may be present. The cavitation phenomena is mainly considered plausible when opening the LPV. Accurate modelling of this may open the possibility of pushing the DDU performance further by reducing the stiction period. However, a conservative and rapid executable approach has been preferred since experiments have not shown signs of stiction being a severe issue.

The approach chosen is to introduce a switch condition in the region near end-stop. The MI force is dominated by squeeze-film damping or stiction in this region where the most simple solution is to use the Stefan force, which is sufficient when cavitation does not occur. This model ignores intake losses, cavitation and inertia of the fluid as discussed for a flat plate in [88].

The flow between the flat plates separating the cushioning groove and the fluid domain have been described by a Poiseuille flow as discussed in [Paper H]. In the same paper the combined fluid force near end-stop is elaborated. The cushion force is found by applying the continuity equation to the fluid volume inside the groove and multiplying the pressure by the shadow area. The force takes the form

$$F_e = C_{on?}F_c + F_s \quad (3.34)$$

$$F_s = \begin{cases} 2\pi \sum_{i=1}^{N_f} r_{M,i} \frac{l_i((2p_1 - p_{1,i} - p_{2,i})z^3 + 8\mu_F z l_i^2)}{z^3} & \text{if } z_{min} < z \leq l_g \\ 0 & \text{otherwise} \end{cases} \quad (3.35)$$

$$F_c = \sum_{i=1}^{N_g} p_{c,i} A_i \quad (3.36)$$

where $C_{on?}$ determines if a cushion groove is present or not, N_g and N_f denotes the amount of grooves and flat surfaces. See Fig. 3.20 for the visualization of the above variables and parameters, and consult [Paper H] for more detailed explanations of the model. This paper shows that the model is able to predict the cushion groove pressure to a sufficient degree and that experimental stiction periods are also possible to predict.

The fluid force resulting from quick separation of the valve plunger from the seat has been evaluated with the LPM and CFD model to visualize the difference. A constant value of $\dot{z} = 1$ m/s is applied. The initial plunger position is $8 \mu\text{m}$. This is chosen since lower initial positions give numerical divergence in the CFD model. The velocity magnitude is in a range realistic to occur in digital valves used in DDU, but is in the high end compared to how

3.4. Valve Fluid Flow & Forces, F_f

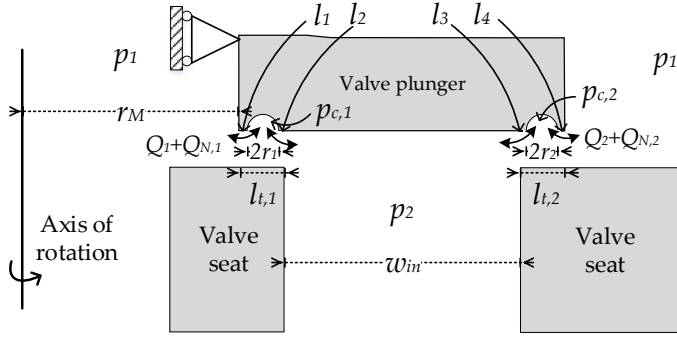


Fig. 3.20: Relevant parameters of cushion plunger concept. $r_M = R - w_{in}/2 - l_1 - l_2 - 2r_1$.

near the plunger and seat are to each other. The simulations are repeated with and without cushioning grooves, and one set of CFD simulations is presented where the fluid can exist in multiple phases. The results are given in Fig. 3.21.

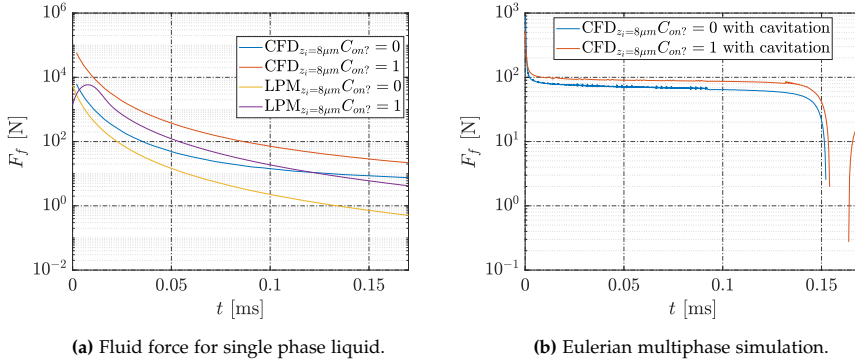


Fig. 3.21: Stiction forces from CFD and LPM for a flat and cushion design with and without cavitation in the fluid. Notice log-scale on y -axis.

Oil compressibility causes the cushion stiction force to develop over a longer time in the LPM than that of the CFD, however after 0.01 ms this effect has vanished. The forces decay with similar gradients thus indicating that the order of the model is sufficient. The predictions of the flat contact design show disagreement on how fast the force becomes insignificant, i.e. omitting in-take losses and inertial forces causes the LPM to predict quicker opening than that of the CFD, i.e. a lower stiction force.

The introduction of a cavitation threshold of 1 Pa gives rise to a much more constant resisting force in the cushioning design. The fluid vaporization

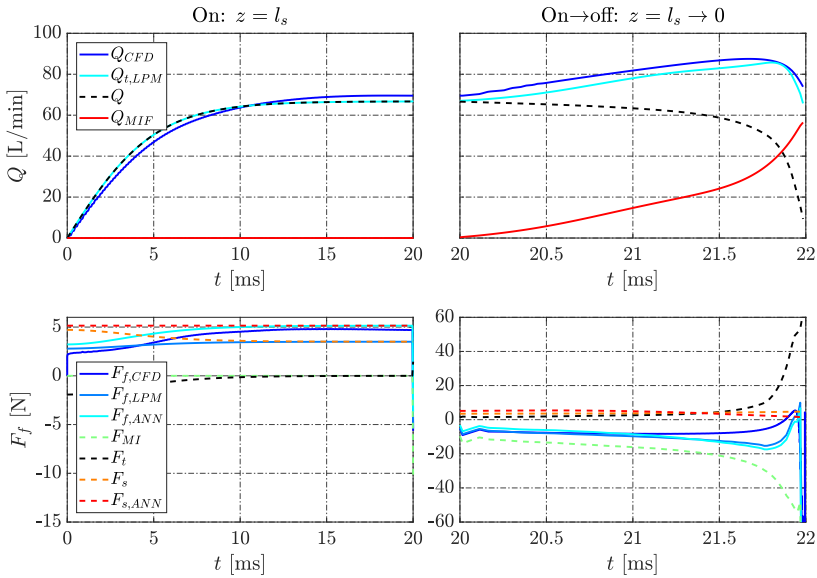


Fig. 3.22: CFD analysis with a constant boundary pressure differential of 0.1 bar leading to a build-up of flow. The valve is initially open and initiates closing after 20 ms. $F_{f,ANN}$ uses the ANN model to predict F_{flow} . This force is F_s in the graphs, which is denoted as $F_{s,ANN}$ for the ANN. Notation and graph from [Paper I]). The acceleration, velocity and position from the CFD simulation are used directly in the LPM.

causes the pressure of the cavitation zone to saturate at 1 Pa. The fluid forces decay rapidly around 0.15 ms in Fig. 3.21b and becomes negative. This must be caused by the shrinkage of the cavitation zone, thus according to this cavitation model the energy release from the phase change contributes with a force acting to open the valve. If cavitation occurs the valve is thus expected to open quicker in reality than predicted by the LPM. This rapid change and oscillation of the stiction force has also been observed experimentally for a flat disk in e.g. [88].

3.5 Comparison of CFD and LPM

The LPM is constructed by all the mentioned terms of the above, where these terms may only be valid for the special case under which they were derived. Therefore, the models related to the fluid force acting on the plunger have been tested under different conditions.

In [Paper I] the different force contributions during a switching cycle with a 0.1 bar pressure differential were computed by the LPM and compared to the total fluid force from the CFD framework to yield the graphs in Fig. 3.22.

3.5. Comparison of CFD and LPM

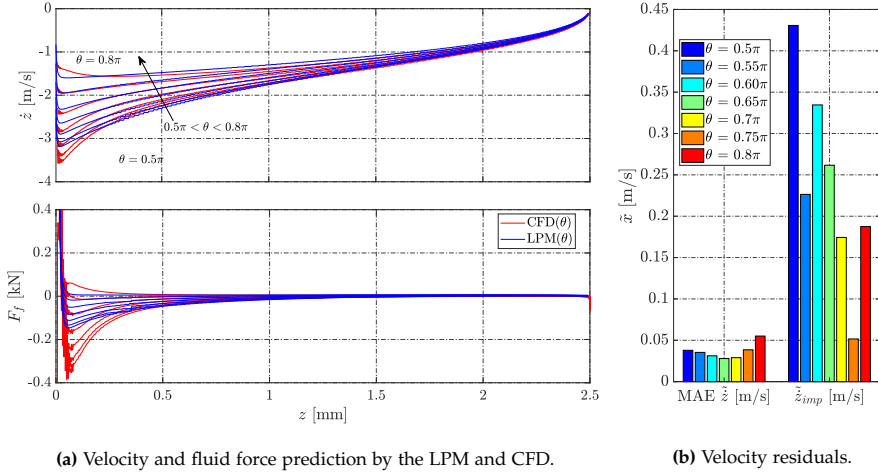


Fig. 3.23: Results for the baseline design of the plunger velocity and fluid force as function of plunger position in order to illustrate the differences between the CFD and LPM predictions. Seven increments of the DDU shaft position (θ) are simulated for both models in the interval given in the graph where θ rises along the direction of the arrow. The corresponding residuals by calculating the MAE of the position dependent velocity and the residual of the impact velocity (\dot{z}_{imp}).

The graphs show the transient response of the orifice, where the pressure forces accelerate the fluid until viscous forces and pressure forces are in balance and the fluid stops accelerating. As the flow is steady (at 20 ms) an actuating force is applied and the flow rises by Q_{MIF} and is reduced as the opening area is restricted, hence reducing Q . The combined fluid force of the CFD ($F_{f,CFD}$) and LPM ($F_{f,LPM}$) are similar, but the steady-state flow force (F_s) is affected too much by the flow causing the combined force of the LPM to be lower than the CFD. This difference is insignificant compared to the one occurring in the region at 21.5 ms. Excessive damping is predicted by the LPM and the consequence of a moving and locally accelerating fluid obviously does mean the simplifications of the LPM do introduce inaccuracy.

The velocities, forces and maximum pressure acting during closing were predicted by CFD and presented in Chapter 1. The velocities and forces from CFD are summarized here together with the corresponding LPM predictions and residuals (MAE of the velocity and the absolute difference in predicted impact speeds for each set of simulations) in Fig. 3.23.

Figure 3.23a illustrates closing movement of the valve by a constant actuating force, $F_a = -50$ N, i.e. $z = 2.5 \rightarrow 0$ mm over time. The fluid force (F_f) develops as a function of the plunger position (z) and velocity (\dot{z}). The closing force grows larger towards end-stop until the end-damping becomes dominating thus starting to decelerate the plunger. A clear discrepancy be-

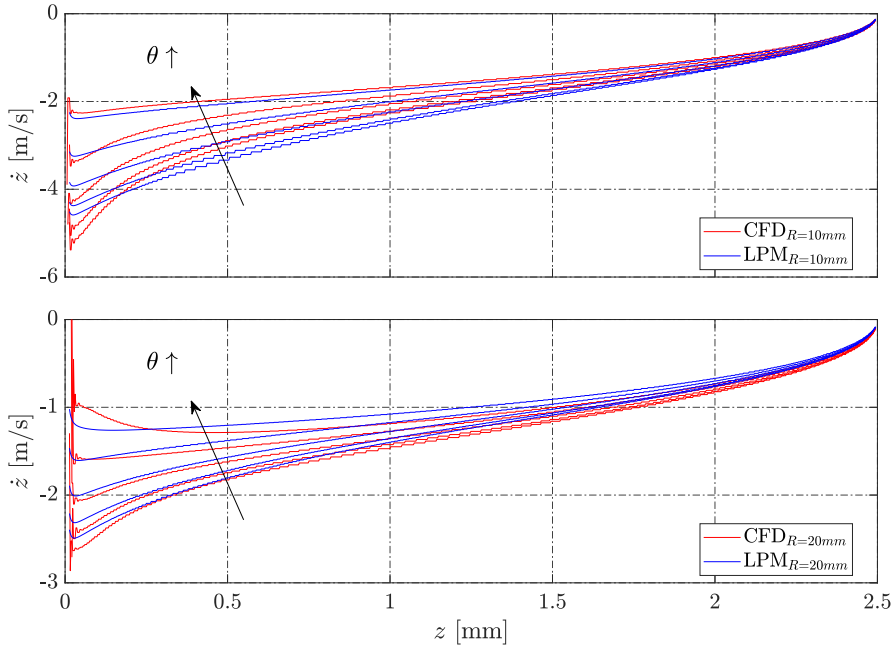


Fig. 3.24: The graphs show plunger velocity of two different designs with R at the boundary of the design space. θ is varied in the same range but only with 5 increments here compared to that of Fig. 3.23a.

tween the peak of F_f is observed, although the tendency is captured by the LPM when compared to the CFD model. The valve will be switched only near full stroke (around 0.8π). In this region the flow is low and the model residuals of the fluid force are sufficiently low. Furthermore, the residuals of impact speeds are relatively low and the magnitude of the MAE indicates that the total switching time is accurately predicted. The LPM is acceptable for the reference design point.

The LPM is parametrized by simple geometrical scaling factors and therefore the applied discharge coefficient, MI force coefficients and MIF area may be erroneous. This means that variations on l_s , R , w_{in} may cause the derived LPM to become inaccurate. To uncover this a series of simulations have been made at the limits of the design space. Initially only R is varied while θ is varied in a similar manner as in Fig. 3.23a (now only five increments). This yields Fig. 3.24.

The graphs indicate that the two new designs have a significant change in the velocity range upon reaching the seat. The wider design is heavier, has lower throttling loss (i.e. lower pressure force) and a larger MIF. The

3.5. Comparison of CFD and LPM

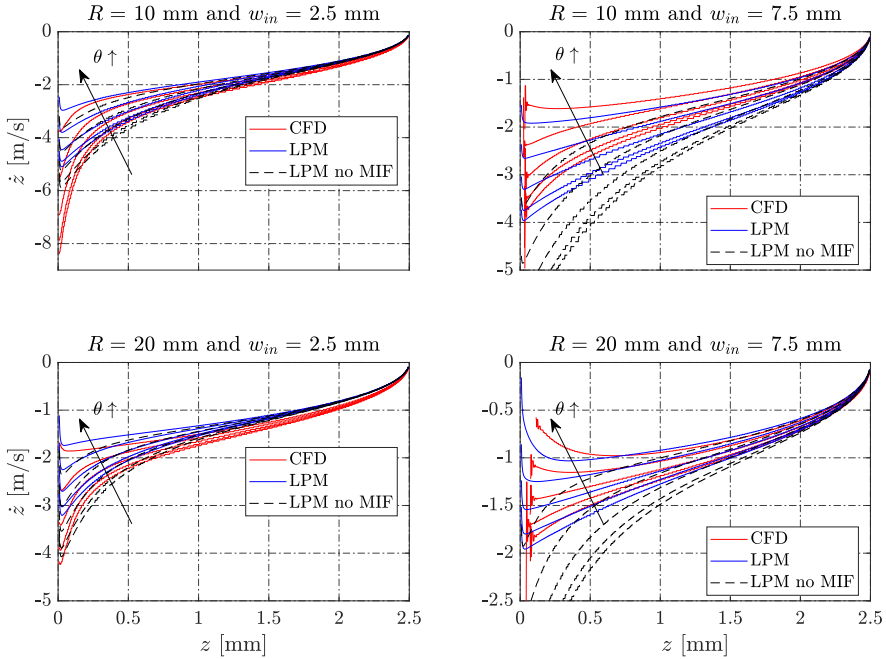


Fig. 3.25: Same approach as Fig. 3.24 but both R and w_{in} are varied.

larger plunger therefore has slower switching time, but more attractive impact speeds. The graphs illustrate a sufficient coherence between LPM and CFD, and therefore the analysis is expanded. Changes to both R and w_{in} are done for each simulation, where the LPM is tested with and without the MIF. This yields the results of Fig. 3.25, with the residuals in Fig. 3.26 showing the general tendency that predictions are more accurate when θ is high, i.e. when the flow is low. Furthermore, the parametric changes have clearly caused the residuals to grow larger compared to the baseline design.

The significance of using a MIF in the LPM is displayed by the differences of the blue and the dashed black lines in Fig. 3.25. The MIF is most relevant when the shadow area of the plunger is large. For the case of $R = 20$ mm and $w_{in} = 2.5$ mm the simulations show that removing the contribution from the MIF makes the CFD and LPM fit better, at least at high flow rates. This is an indication that the area does not scale entirely as expected from the simple expression of k_{MIF} .

The geometrical changes and variations in flow conditions definitely are cause of changes in the velocity profiles in general, both in the LPM and CFD analysis. The optimal design that balance; switching speed, throttling loss, switching energy and impact speed, are not analytically obvious. Therefore,

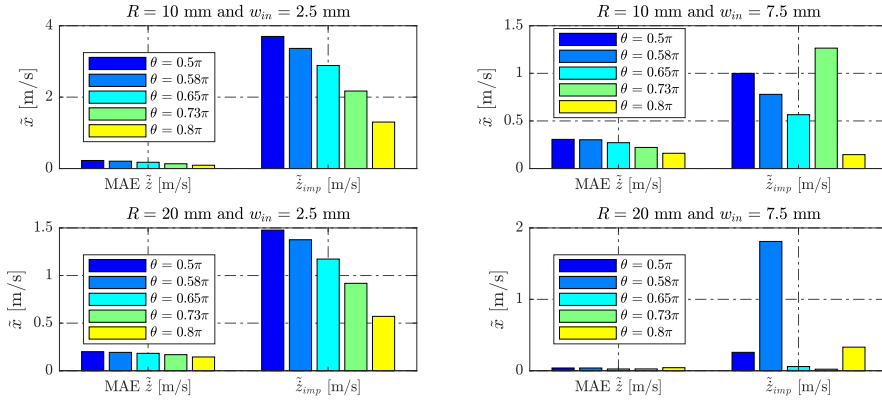


Fig. 3.26: Residuals corresponding to Fig. 3.25 with variations on both R and w .

model-based optimization is considered necessary. There are some obvious differences to the predictions and this emphasizes the need for validating the optimum found by the LPM to a CFD simulation. No other better and obvious approaches have been found compared to the one presented here.

3.5.1 LPM vs CFD of the Optimum Valve

The final step in the design framework before manufacturing is to compare the LPM used in optimization and the CFD model. The comparison is given in Fig. 3.27, where the only difference in the resulting force is the prediction of the fluid force, F_f .

The predicted fluid forces do have a bias error which at end-stop diverges more due to the high dependency on z and \dot{z} in this region. This does not result in a noticeable difference in switching time. The zoomed graph does show that the two predictions do not agree on the timing for reaching the end-stop. The CFD model gives a more rapid rise in fluid force than that of the LPM, and a bias error is clear from the predicted fluid force of the two models. The velocity magnitudes are comparable and the observed discrepancy of the fluid force (F_f) near end-stop are similar to the baseline model residuals presented in Fig. 3.23. However, if the impact speed is taken at $z = 10 \mu\text{m}$ the CFD and LPM estimates the value to be -1.2 and -0.6 m/s, respectively.

3.6. Mechanical End-stop and Spring Forces, $F_m + F_s$

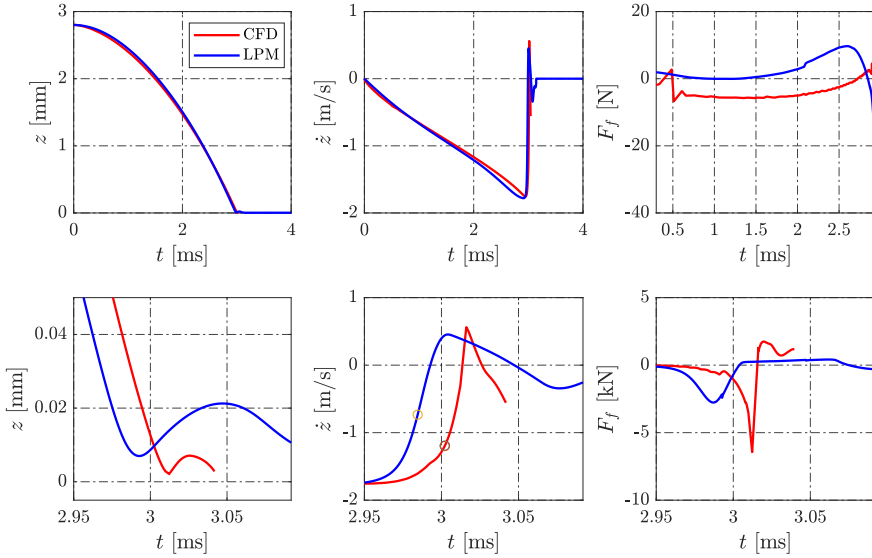


Fig. 3.27: Comparison of the high-fidelity CFD model with a compressible and piezo-viscous fluid, and the low-fidelity LPM using scaled coefficients as presented in this chapter. The lowest row of graphs are identical to the ones above but with another time-scale to visualize the deceleration situation. The LPM is used for optimization without consulting any CFD simulations, only when the optimum solution is found the above comparison is made and it is concluded whether or not the performance predicted by the LPM is similar to the dynamic CFD prediction.

3.6 Mechanical End-stop and Spring Forces, $F_m + F_s$

The valve design may include a regular linear spring and/or a Belleville spring washer. The latter is for end-damping purposes as was discussed in Chapter 2, and the force of a linear spring and a Belleville spring washer have been described by

$$F_s = F_i + k_s(l_s - z) + \text{End}_{on?} F_{Bs} \quad (3.37)$$

where $\text{End}_{on?}$ is an integer value of 0 or 1 describing whether or not a Belleville spring is included, k_s is the spring stiffness and F_i is the pre-compression of the spring.

The force (F_{Bs}) and critical stress concentrations of a Belleville spring washer are explained in [75]. The force resulting from a displacement of the spring is given by

$$F_{Bs} = \frac{4Ez}{K_1 D_o^2 (1 - \nu^2)} \left((h - z) \left(h - \frac{z}{2} \right) t + t^3 \right) \quad \text{for } z \leq h \quad (3.38)$$

where E and ν are Young's modulus and is Poisson's ratio of the material, D_i

and D_o are the inner and outer diameter of the spring, h is the un-deformed height, t is the thickness of the plate and y is the displacement of the spring. The parametrization is shown in Fig. 3.28. K_1 is given by

$$K_1 = \frac{6(R_d - 1)^2}{\pi \log(R_d) R_d^2} \quad \text{and} \quad R_d = \frac{D_o}{D_i} \quad (3.39)$$

The force profile can be shaped in various ways depending on the ratio h/t where D_i and h are chosen as design parameters. The inner diameter is chosen as $D_i = D_o f_1$, where D_o is fixed to the plunger size. The total height needs to be larger than the desired damping stroke length (z_{max}) and thus defined as: $h = y_{max} (1 + f_2)^{-1}$. The thickness is chosen based on the height: $t = f_3^{-1} h$.

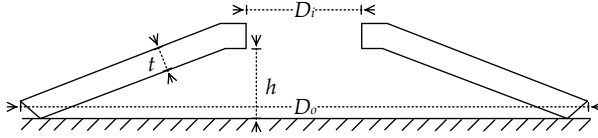


Fig. 3.28: Belleville spring washer parametrization.

The critical stress zones are functions of the above parameters that can be found in textbooks, e.g. [75]. These are evaluated before a dynamic simulation is carried out thus avoiding wasting time on evaluation of an infeasible design. Furthermore, the lower and upper bounds of the design space have been determined using knowledge about the kinetic energy expected to be absorbed, in order to limit the amount of infeasible designs.

Mathematically contact mechanics introduce non-smooth behavior as the mechanical end-stop force occurs suddenly. This may be considered as a high stiffness spring, which is valid in the elastic region of the material's deformation. The mechanical end-stop force is modelled as

$$F_m = \begin{cases} k_{s,end}(z - z_{asp}) & \text{if } z \leq z_{asp} \\ k_{s,end}(l_s - z - z_{asp}) & \text{if } z \geq l_s - z_{asp} \end{cases} \quad (3.40)$$

where $k_{s,end}$ is the stiffness of the contacting bodies, which is governed by Young's modulus of the materials and the area of contact, z_{asp} is the plunger height for which asperities may come into contact (approximated based on surface roughness) and thus creating a linearly increasing force resisting elastic deformation.

3.7 Valve Energy Losses in a DDU

The design framework needs to assess the energy loss in the valves. Therefore, the energy conservations not contributing to the output power, i.e. en-

3.7. Valve Energy Losses in a DDU

ergy losses, must be described. This includes the switching loss and valve throttling loss. This section builds on the ideas from [Paper D] about the possibilities of deriving analytic solutions describing the losses. Expressions of this sort serves as insight into the overall dependencies of the energy losses and may be applied as rough design rules.

3.7.1 Efficiency

The definition of a systems efficiency is

$$\eta \triangleq \frac{E_{out}}{E_{in}} \approx 1 - \frac{E_{loss}}{E_{in}} \quad (3.41)$$

where E_{loss} is the difference between input and output energy. It should be noted that E_{loss} is approximated. The energy losses may be solved numerically or analytically depending on the equations. The main difference being computational effort, and where the numerical integration approach allows more complex equations and couplings.

Regularly fluid power machines uses the notion of volumetric and mechanical efficiency. For a DDU the traditional translation of these is somewhat misleading due to so-called pump shrinkage as discussed in e.g. [61]. This shrinkage is included directly in the definition of input energy in the present work. Also, the efficiency of a DDU will be affected by the fraction of idling cycles. From (3.41) the volumetric efficiency of a DDU is established as

$$\eta_\psi = 1 - \frac{\psi(E_a + E_f) + (1 - \psi)E_{L,f}}{\psi E_{in} + (1 - \psi)E_{L,in}} \quad (3.42)$$

where $\psi \in (0 \ 1]$ is the displacement fraction of the DDU, E_a is work used to actuate the valve plunger, E_f and $E_{L,f}$ are the energies lost from viscous friction in the fluid when motoring and idling respectively, E_{in} is the motor input energy and $E_{L,in}$ is the input energy during idling (which is ≈ 0 if the energy required to maintain the level of the low pressure manifold and the mechanical losses are omitted). The input energy consists of a hydraulic term and a term considering energy required for compression and decompression from the hydraulic- and mechanical- power is defined for motoring and pumping as

$$E_{in} = \int_0^{2\pi} \underbrace{Q_H p_H - Q_L p_L}_{\text{hydraulic}} + \underbrace{p_C(Q_L - Q_H + A_p \dot{z}_p)}_{\text{compression}} d\theta \quad (3.43)$$

The hydraulic input energy considers the energy from high and low pressure manifold. The flow pumped to the LP manifold is in this regard considered to be regenerated, but this term may be omitted if that is not the case. When this is not regenerated it is relevant to lower p_L as much as possible without

causing cavitation. The energy conversion when compressing and decompressing the fluid in the piston chamber happens when Q_H and Q_L are zero. Then energy will either be added or removed to the system in order to change p_C .

The various sources of energy loss in the fluid can be divided as

$$E_f = \underbrace{E_{glid} + E_{ecc}}_{\text{mechanical}} + \underbrace{E_{leak} + E_{throt} + E_{man}}_{\text{volumetric}} \quad (3.44)$$

where E_{man} is the energy loss in the hydraulic manifold, E_{throt} is the throttling loss in the two valves, E_{glid} is the energy loss from friction in the gliding interfaces of the pistons, E_{ecc} is the energy loss from friction between piston and eccentric shaft and E_{leak} is the fluid leaking out of the pressure chamber (through valves or through gliding interfaces). Predicting the size of these losses accurately is difficult, especially when mixed friction problems are considered. Therefore, the problem is simplified to study the throttling loss and the actuating energy since these are the only contributions related directly to the valve design when the cross-port leakage is zero. The losses during idling ($E_{I,f}$) contains the throttling loss and manifold loss evaluated in the LPV.

The electric energy required to open and close the valve (E_a) depends upon the required mechanical work (W_{switch}) and the efficiency of the actuator (η_a). The required mechanical work can be described as the line integral of the force used to actuate the moving body from a to b . This force is not known directly, which is why the counteracting forces of (3.10) have been integrated instead.

$$E_a = \frac{W_{switch,H}}{\eta_{a,H}} + \frac{W_{switch,L}}{\eta_{a,L}} \quad (3.45)$$

$$W_{switch,i} = \int_{l_s}^0 \left(m\ddot{z}_i + F_{f,i} - F_{s,i} \right) dz_i \quad (3.46)$$

This holds under the condition where each valve closes actively once for each revolution. The work required to compress the spring is considered to be completely reversible, and the integration over one revolution thus adds up to zero energy lost. The remaining energy required to open the valve comes from the fluid force. This is associated with the fluid throttling loss (E_{throt}) to move fluid in and out of the chamber described as

$$E_{throt} = \int_{t_0}^{t_c} |Q_H(p_H - p_c)| + |Q_L(p_c - p_L)| dt \quad (3.47)$$

where t_0 is the initial time and t_c is the time until the DDU shaft has rotated 2π rad, i.e. it is a function of the rotation speed.

3.7. Valve Energy Losses in a DDU

The above energies may be computed by solving all the relevant coupled non-linear differential equations numerically. Alternatively, expressions may be derived by analytical integration and simple assumptions.

3.7.2 Analytical Integration

The time averaged work required to actuate the plunger is

$$\bar{E}_a = \frac{\overline{W_{switch,H}}}{\eta_{a,H}} + \frac{\overline{W_{switch,L}}}{\eta_{a,L}} \quad (3.48)$$

The equations are derived by assuming the steady-state solution of the plunger position to take the form: $z = \frac{l_s}{2} \sin(\omega t)$. The frequency, ω is defined as the inverse of the switching time (opening and closing). Furthermore, the friction coefficients (k_a, k_v, k_d) are assumed constant, and the flow force is omitted to consider the worst-case energy loss. This yields the expression

$$\overline{W_{switch,i}} = \left(\frac{k_d \omega l_s}{3} + \frac{\pi k_v}{4} + \frac{(m + k_a) \omega l_s}{48} \right) \omega l_s^2 \quad (3.49)$$

The dynamic and static computation of W_{switch} are compared later in this section.

The significance of the throttling loss is determined by evaluating the hydraulic power loss across the valve for one revolution as discussed in [Paper J].

$$P_{throt} = 2 \int_0^\pi Q \Delta p d\theta \quad (3.50)$$

The unit of this power is [W rad]. This is integrated over half a rotation and the factor of two accounts for both HPV and LPV. This means that compression and decompression periods are omitted, i.e. this is the worst case energy loss. The flow is assumed equal to the piston velocity multiplied by its cross sectional area ($A_P \dot{z}_P$). Ideally the piston movement is: $\dot{z}_P = -r_e \dot{\theta} \sin(\theta)$ and using (3.23) to replace Δp the expression of (3.50) becomes

$$P_{throt} = 2 \int_0^\pi (A_P \dot{z}_P)^2 (k_{f1} A_P \dot{z}_P + k_{f2}) d\theta \quad (3.51)$$

where the displaced volume is $V_d = 2r_e A_P$. The expression for the power loss over one cycle is divided by the rotation speed to convert from power to energy, thus arriving at the total throttling loss

$$\bar{E}_{throt} = \frac{P_{throt,cycle}}{\dot{\theta}} = \frac{\dot{\theta} V_d^2 (V_d \dot{\theta} k_{f1} + \frac{3}{4} \pi k_{f2})}{3} \quad (3.52)$$

normally $k_{f1} \gg k_{f2}$ and the magnitudes of remaining parameters causes the turbulent term to dominate, however, low displacement and low rotation speed machines will see a more significant contribution from the laminar part of the equation.

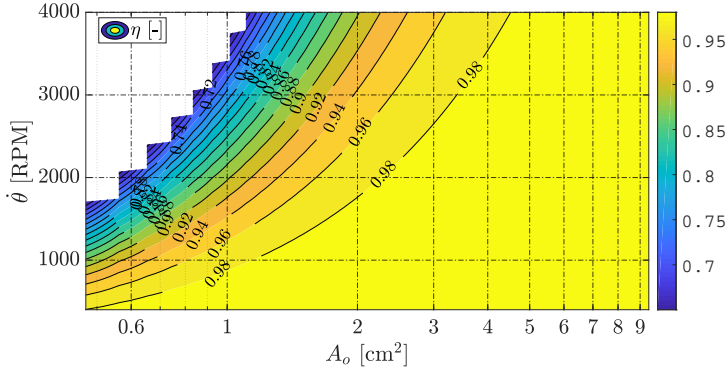


Fig. 3.29: Computation of the efficiency: $\eta = 1 - \frac{E_{thrott}}{E_{out,ideal}}$ as function of orifice area and rotation speed. The x-axis is logarithmic. The orifice area of the AAU prototype MCVi2.0 and the new MMVi1.1 are 4.7 and 4.15 cm², respectively.

3.7.3 Valve Dimensioning at Certain Operating Conditions

To illustrate when the throttling loss becomes significant it is computed for a range of values and then set relative to the ideal amount of output energy during one revolution [68]

$$E_{out,ideal} = V_{de}\bar{\beta} \left(2 - e^{-\frac{\Delta p_m}{\bar{\beta}}} - e^{\frac{\Delta p_m}{\bar{\beta}}} \right) + V_d\bar{\beta} \left(1 - e^{-\frac{\Delta p_m}{\bar{\beta}}} \right) \quad (3.53)$$

where $\bar{\beta}$ is the mean stiffness of the fluid. This expression is also a quick tool to determine the pressure difference suitable for a given DDU since the energy will start to deteriorate when the difference of high and low pressure (Δp_m) goes towards the effective stiffness causing the exponential function with positive exponent to grow as the two others approach zero. This analysis considers $\Delta p_m = 350$ bar and $V_d = 50$ cm³ for each chamber. The energies are computed at various rotational speeds (θ) and valve orifice areas (A_o). The efficiencies hereof are shown in Fig. 3.29.

The graph reveals a requirement of larger opening areas when the rotational speed is increased. The influence of the throttling loss when increasing the speed of the DDU is not significant when $A_o > 3$ cm². However, increasing the speed causes increase in flow force which should not exceed the force holding the valve open. This would cause the DDU to be dysfunctional and puts a natural constraint on the possible rotation speed of the DDU. According to theoretical results of the flow force, the speed limit with the proposed optimum design is around 3800 RPM.

A machine with low displacement and/or running at low speeds can be designed with correspondingly smaller orifice area and still maintain good

efficiency. The presented equations serves as a rapid method for estimating whether or not a proposed dimensioning of a valve is feasible considering the DDU requirements.

3.7.4 Energy Dissipated during Switching

The coefficients of (3.49) do vary as a function of the plunger position and to some extend velocity. The following analysis shows the computed energy and introduced error when considering these coefficients as being constant and approximating the work by assuming that the plunger moves as a harmonic oscillator. Evaluating the work for a range of stroke lengths and switching times yields the results in Fig. 3.30 and four points have been selected to illustrate the difference between CFD, dynamic and static model predictions. The graphs shows that the switching energy predicted by CFD corresponds

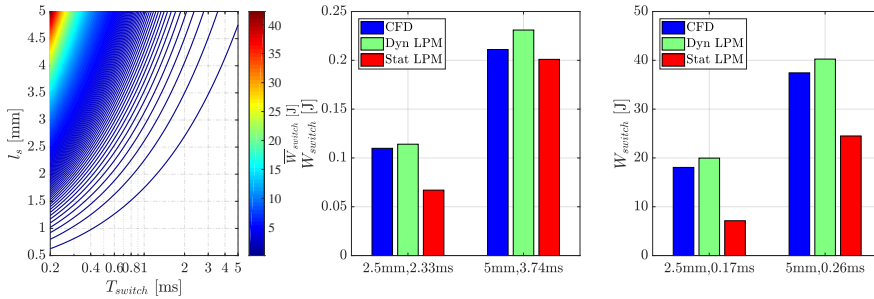


Fig. 3.30: To the left: The energy dissipated when switching the valve. The energies are found with (3.49). The bar plots: Shows the losses predicted by the various models at two different stroke lengths and two different switching speeds. These energies must be divided by the actuator's efficiency to estimate E_a . The dyn LPM means numerical integration is used and stat LPM is the analytic solution.

well to the ones found when solving the defined equations with numerical integration (dyn LPM). The additional assumptions made for the analytic solution (stat LPM) does introduce an inaccuracy causing the loss to be only half of the other predictions. However, the correct dependencies are captured where the change in order of magnitude of the switching time does give double the order of magnitude in energy loss. Doubling l_s gives approximately twice the energy loss, which means the quadratic dependency observed in (3.49) is compensated by the correspondingly longer switching period resulting hereof. A topological optimization study of the plunger to reduce the resisting forces of the fluid is not considered worth the effort as the dissipated energy is 0.1 J for this valve according to CFD.

The analysis shows that its contribution is marginal compared to the input energy and the throttling loss even if the actuators efficiency is only 10%.

Furthermore, the results can be used to determine the consequence of putting requirement on the switching time.

3.8 Stresses in the Plunger and Seat

It is best practice in most mechanical design approaches to perform a FEA to find the stresses in load holding parts before manufacturing. These parts are the plunger and seat, which have mechanical contact. Paper B presented solutions of various contact formulations, which did influence the peak stress significantly. The highest contact pressure was achieved by the bonded formulation, which is why this has been used for this analysis to be conservative. The von Mises stress in the plunger when a 350 bar pressure differential is across the valve seat is found by FEA and shown in Fig. 3.31.

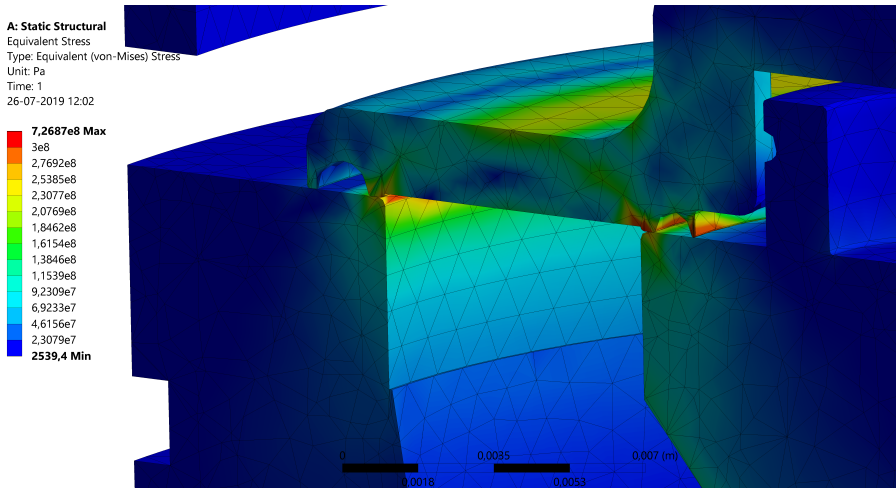


Fig. 3.31: FEA of the plunger and seat with a scale of 1:1 scale on the deformations caused by pressure differential of 350 bar. The von Mises stress in the zone of highest deformation ($10\ \mu\text{m}$) is around 150 MPa.

The von Mises stress in the material peaks around the contact zones which is as expected. The stresses associated with contact problems are normally compressive of nature and local singularities are typically difficult to avoid. The FEA is therefore a rough analysis where especially the stresses outside the contact zone are relevant to study and maintain low. Most regions of the geometry have von Mises stress of 200 MPa and below. The shear stress is below 350 MPa in the entire domain and does therefore not concern the long-term durability.

3.9 Hydraulic Circuit Design

When focusing all this effort on making efficient and reliable valves it is important that the efficiency does not suffer elsewhere, and that the predicted flow force is realistic. The switching components must be installed in an environment with flow passages to and from the torque generating chamber. The valve design couples to the possible designs of the remaining hydraulic circuit, where the viscous effects, recirculation and stagnation can result in a lower effective energy output and also to asymmetry causing change in fluid forces potentially making the valve design infeasible. The steady-state peak fluid forces were studied in [Paper J] showing that the proposed manifold design does not violate the symmetry assumption used to create the LPM.

The topic of optimizing and designing manifolds are not well documented in the literature, recently a CFD analysis with experimental data was published [125] to investigate the accuracy of predicting the frictional losses. Lately, the invention of metal printing has extended the possibilities in designing both compact and efficient manifolds, but yet only feasible in high-fidelity applications. It would be possible to construct large parts of the DDU in one mono-block and thereby limit the required threads, bolts and seals. Since the focus is on modification of another machine the approach taken is to construct a block for each cylinder chamber.

An efficient utilization of space (as shown by the mono-block design of Fig. 3.32) is achieved by placing the LPV after the chamber outlet (p_C). If this valve is closed the fluid will pass through and around the LPV to reach the HPV, where a $p_C > p_H$ opens the flow passage.

The construction must be designed so that the rated machine pressure does not result in mechanical stress above the fatigue limit of the material. The flow paths between high pressure and the piston chamber must be associated with low energy losses to ensure optimal power output. Optimization of this is outside the scope of this work.

3.9.1 Analysis of the Fluid Dynamics

The annular flow profile in the seat must be transformed into a circular flow profile in order to be useful for hydraulic circuit design. The idea in 2D is illustrated in Fig. 3.33 where the right part of the drawing shows how stagnation of the fluid can possibly be minimized by three different shapes (S_i). At stagnation the fluid is brought to rest isentropically and as a consequence local temperature rise will occur depending on the velocity reduction and local pressure changes.

To ensure that the mean flow velocity does not change significantly in this region the two areas are equalled, $A_1 = A_2$. This is done by simple geometrical considerations. The seat design is evaluated by enforcing a constant

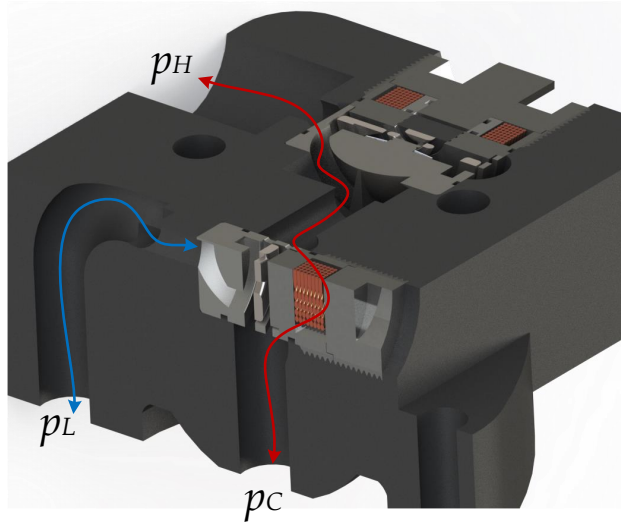


Fig. 3.32: Isometric cross-sectional view of the hydraulic circuit design II (two cross-sections). The viscous losses estimated by CFD with flow through the LPV or HPV are: 2.29 and 2.30 bar respectively.

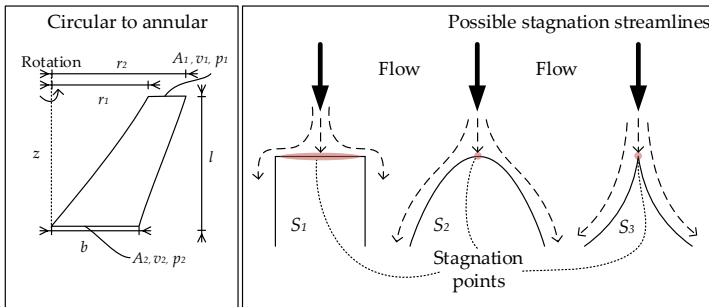


Fig. 3.33: Conversion of annular- to circular- flow and manipulation of stagnation streamlines.

boundary pressure (5 bar) on the outlet with flow normal to the boundary. A target mass flow rate is specified to match the peak flow of the DDU and a steady evaluation is performed with best practice convergence thresholds and turbulence settings where the SST $k-\omega$ model is solved. The analysis converges within the allowed iterations and the CFD results are visualized in Figs. 3.34 (surface pressure) and 3.35 (velocity magnitudes).

According to Bernoulli's principle, energy should be conserved as either

3.9. Hydraulic Circuit Design

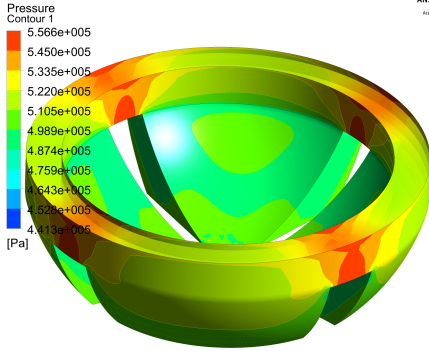


Fig. 3.34: Spatial pressure values in the seat geometry (S_1) found from CFD analysis.

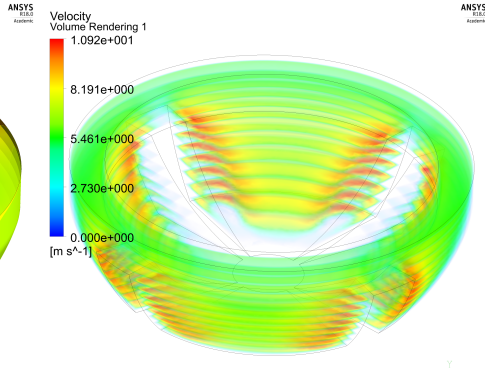


Fig. 3.35: Spatial velocities in the seat geometry (S_1) found from CFD analysis.

pressure, kinetic or potential energy. This is only valid for incompressible, steady and inviscid flows. The analysis is steady and incompressible, thus the only cause of error are viscous effects. The size of lost energy is

$$p_{loss} = p_1 + v_1^2 \rho - (p_2 + v_2^2 \rho) \quad (3.54)$$

Where the notations of pressure (p) and velocity (v) are shown in Fig. 3.33. Gravity is ignored in the CFD and thus also in the energy conservation.

Taking the area weighted average of the pressure on the inlet and outlet boundary gives a p_{loss} of 0.3 bar. The pressure results of Fig. 3.34 show that high pressures occur at the inlet near the boundaries of the fluid domain indicating stagnation. It was assumed that this effect could be reduced by smoothing the edges to guide the flow around these corners, i.e. switching from S_1 to S_2 of Fig. 3.33 (S_3 is not considered due to manufacturing complications). The rounded corners results in a p_{loss} of 0.2 bar, i.e. a reduction of 33%. The min and max pressures in the entire domain are 4.71 and 5.41 bar for S_2 compared to 4.41 and 5.56 bar for S_1 .

Implementing the Valve in the Mono-Block

The flow field for the mono-block in Fig. 3.32 has been solved by ANSYS Fluent to approximate the losses that can be expected and visualize if there are any obvious zones with circulating flow. The results of velocity and pressure when the LPV is open are shown in Fig. 3.36 and 3.37.

The flow runs from the high pressure tube down to the low pressure tube. The fluid swirls around the torus surrounding the valve and the velocity magnitude peaks near the plunger. The flow-induced force was presented in [Paper I] for various openings both from CFD and experiments where a sufficient correlation exists meaning the valve is not spontaneously closed

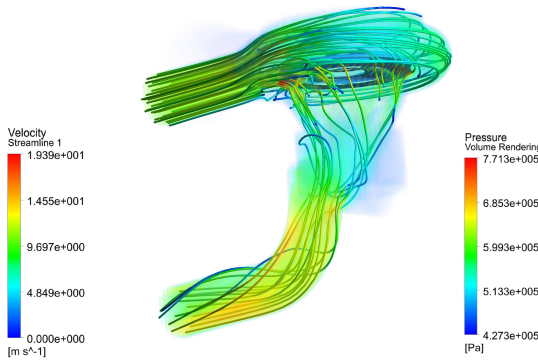


Fig. 3.36: 3D CFD solution of the velocity field and streamlines showing direction where the color of each line indicates magnitude.

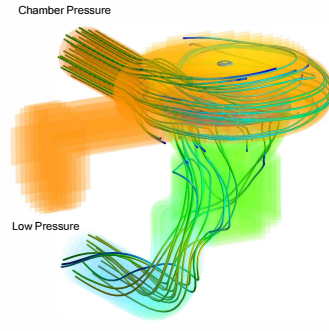


Fig. 3.37: 3D CFD solution of the pressure field corresponding to Fig. 3.36. $d_{pipe} = 15$ mm.

at peak flow rate. The associated viscous loss when either the LPV or HPV is fully open is around 2.3 bar. This indicates that manifold design is more relevant than fine-tuning the discharge coefficient of the valve where only 0.2 bar is predicted to be lost.

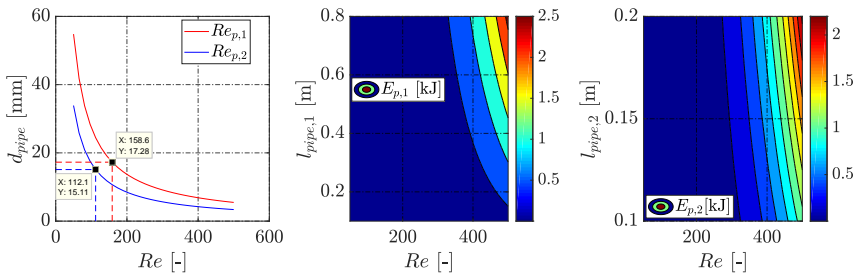


Fig. 3.38: The required pipe diameter to achieve specific Reynolds numbers at peak flow of the current machine size. Estimates of the energy losses when changing diameter and length of a pipe with laminar flow are given in the contour plots.

A given Re in the pipe can be realized by a certain pipe diameter based on the flow magnitude. From this a loss coefficient may be calculated, which when multiplied by the length of the tube gives the total friction loss in the pipe. The left most graph of Fig. 3.38 reveals a trade-off between d_{pipe} and Re and for this specific problem it is realistic to dimension the pipe as marked on the graph. The length of pipe 1 and 2 must be maintained as short as possible to limit losses. The pipe length and diameter affect the systems hydraulic inductance and a low diameter makes it possible to create a more compact DDU.

3.10 Summary

The first phase of the framework included identifying ways of describing the system mathematically. This has resulted in an un-steady CFD model with a moveable plunger, a steady CFD model with a static plunger, a Lumped Parameter Model (LPM) and analytic solutions to this LPM (cyclic throttling loss and switching energy) to arrive at simple design equations. Depending on the time available and system requirements the designer chooses the most suitable models.

The approach taken here is to filter out infeasible designs by finding: the peak flow force versus opening force, the cyclic throttling loss and the peak stresses in the end-damping spring. This speeds up the optimization. The LPM consists of coupled ODEs, which are solved numerically to investigate the entire system. Compared to earlier work contributions have been made concerning; Movement-Induced (MI) flow and forces, transient response of the orifice and the flow force.

The LPM is constructed with three dynamic CFD simulations of a baseline design. One low constant velocity-, one high velocity-, and one constant acceleration- test case. This gives damping coefficients and MIF area, these are scaled according to simple geometrical relations. The LPM does itself introduce inaccuracy and the scaling factors will as well. The residuals of the baseline design and designs lying on the boundaries of the design space were used to assess the model accuracy, where the impact velocity was difficult to verify. However, the LPM makes it possible to search for candidate design points and comparing end-damping profiles of the proposed optimum in retrospect. This retrospect analysis showed coherence between LPM and CFD models for the optimal design considered.

The hydraulic design was analysed to show how a valve design decision propagates into other design choices, i.e. of the manifold. The manifold size and shape must be adapted to the valve design, and doing so without introducing unexpected fluid forces on the valve plunger. The flow forces acting on the plunger predicted from 3D CFD and 2D axisymmetric were similar.

The model of valve fluid inertia, hose dynamics and accumulator may be included also for the optimization, but in this work solely applied for validation of the piston chamber pressure.

Chapter 3. The Design Framework

Chapter 4

Validation of the Framework

“Religion is a culture of faith; science is a culture of doubt.”

– Richard P. Feynman (1918 – 1988)

The design framework is based on known physics and well-proven computational methods, however, assumptions and geometrical simplifications have been made which are sought validated to increase the confidence of the established framework. This is realized by testing a few prototypes and comparing results to the ones predicted from the model. The validation mainly concerns the switching dynamics of the valve and flow properties when inserted into a DDU.

4.1 Purpose of the Experiments

In [Paper C] a relation between impact velocity and durability was identified for different valves. Prediction of this velocity is therefore relevant to create durable designs. Furthermore, a MI flow from plunger movement has been observed in simulation. Experimental evidence of this flow in digital valves was desired, since it alters the fluid force acting on the plunger during switching as presented in the previous chapter. This also influences the throttling loss while switching.

In summary the following points have been investigated:

- The accuracy of the predicted fluid force for a simple test situation, compared to when the fluid is pressurized and boundary conditions are similar to the ones in a DDU.
- Movement-Induced Flow (MIF) discovered in [Paper E] and experimentally investigated in [Paper H].

- The pressure dynamics of the fluid volume in the cushioning groove of the proposed plunger concept.
- The experimental fluid compressibility and pressure dynamics in the piston chamber.
- The severity of the run-in wear on the sealing surfaces and actuator in the digital valves.

The above have been addressed in [Paper A, G & H], with exception of the last point where no results have been published. These points support the focus areas of the proposed simulation framework, and have given insight into possible design complications of the current valve design. The methods plus results are summarized in the following.

4.2 Experimental Test-rigs

Three different test-rigs have been applied for validation of the proposed simulation models. They differ w.r.t. the possible testing cases, cost and measurement possibilities as discussed below.

4.2.1 Test-rig Concept I

The first and most simple test-rig was proposed during a PhD study at AAU focusing on valve actuator design [68]. The concept and the actual test-rig are shown in Fig. 4.1.

The test-rig focusses mainly on a quick assessment of the valve's switching performance where the plunger and actuating current are observed. This is done by either reflection of a laser as illustrated by Fig. 4.1 or with a high-speed camera where the opening sequence is shown at three time-instants in Fig. 4.2. The fluid can move freely around the seat and housing as illustrated by solid red lines in Fig. 4.1a thereby ensuring a connection of the two valve ports even though the valve is actually closed. In a DDU this connection is not possible.

The approach of this experiment is to validate the dynamics when the fluid medium is air, and by changing the fluid to oil, the difference between the measurements equals the MI force. This has been used to validate the integrated quantity from CFD that was used to construct a LPM. The results have increased the confidence in the values predicted by the dynamic CFD framework.

A part of the fluid domain is visible and is recorded with a high-speed camera. This shows plunger movement and reveals if the reflecting pin is moving as intended. Furthermore, the behavior of the fluid can be observed directly through the oil reservoir during switching.

4.2. Experimental Test-rigs

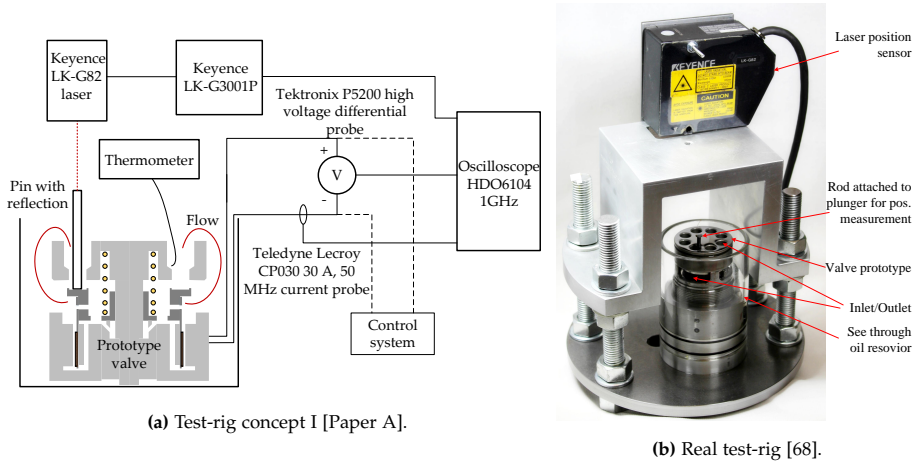


Fig. 4.1: Switching at atmospheric pressure, with or without oil. The solid red lines in Fig. 4.1a indicate that the fluid can travel around the valve seat and housing, which is not the case in a DDU. The dotted red line indicates the laser beam.

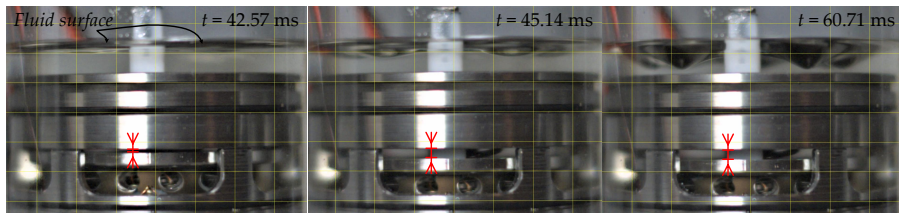


Fig. 4.2: Opening sequence, movement is initiated around 42.57 ms where no clear change is visible on the fluid surface. After 45.14 ms the valve is fully open and a small change in the fluid surface is observed. Finally, at $t = 60.71$ ms the fluid surface attains maximum peaks due to the MIF. The switching is done at atmospheric pressure and the experiment repeated several times.

This test-rig has the main drawback that the fluid cannot be pressurized. In addition, observations have shown that when at end-stop the reflecting pin is vibrating due to the mechanical impact. This causes noise to the position measurement. Furthermore, validating the pressure dynamics inside a cushioning groove is not realistic to do in this test-rig.

4.2.2 Test-rig Concept II

Measurements of the cushioning pressure, MIF and plunger position in a pressurized fluid have been performed with the test-rig concept II shown in Fig. 4.3.

This test-rig is dimensioned for 5 bar and comprises two transparent hose connections separated by the digital valve. The fluid level in port 1 (p_1) is

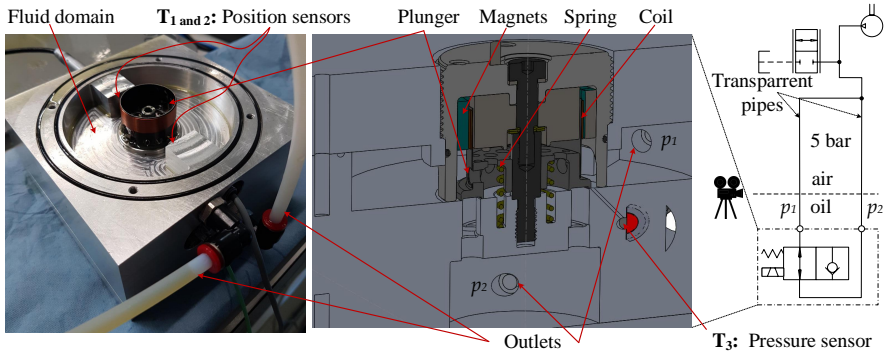


Fig. 4.3: "Actual test-rig and cropped CAD model of the designed test-rig, where the location of the three implemented sensors ($T_1 - T_3$) are denoted along with the two pressure outlets. The hydraulic layout is given to the right." [Paper H].

expected to decrease as the valve closes and this fluid is directed to port 2 (p_2). A difference in the fluid level should therefore be visible through the hoses. The system is pressurized with pneumatics.

A bore is connecting the pressure sensor, T_3 with the surface of the seat where the groove of the plunger will contact. It is not possible to predict the exact pressure loss and transients through this bore with simple analytic expressions. The bore has therefore been designed based on what is possible to drill while making it as short as possible to limit this effect. It is however a source of uncertainty.

The various valves that have been tested includes three different cushion designs where the difference lies in the shape and amount of notches (from the groove to pressure lines, see [Paper H]). After the tests some of the specimens had their groove widened, thereby reducing the metal-to-metal contact surface.

The pneumatic pressurization proved to be a problematic constellation, due to problems with refilling of oil, de-pressurization and flushing air out of the system. The air contamination level is therefore potentially very different from normal levels, which may have affected the MIF and the damping pressure. However, this should not disturb the MI force significantly. The fact that p_1 and p_2 are not directly connected to each other means that the fluid resistance is expected to be higher than that of test-rig I due to MIF.

4.2.3 Test-rig Concept III

The highest level of test environment is implementation of the valves in a DDU. This allows validation of the valves functionality in the intended environment. Furthermore, the risk of infant mortality failure can be tested.

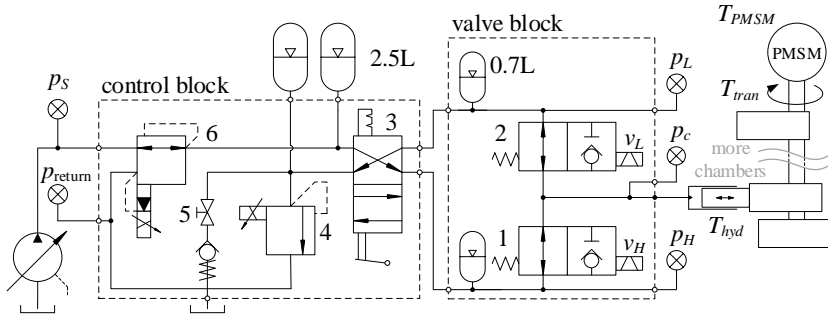


Fig. 4.4: Simplified hydraulic circuit of test-rig III. Illustration from [Paper G] where additional details are included.

Pressure measurements are enough to reveal if the duration from the switching signal is sent to the pressure in the piston chamber has changed. Measurement of the throttling loss in the valve is problematic since the pressure range of the sensors is 0-400 bar and the uncertainty is therefore above the magnitude of the expected pressure loss. This loss has already been validated in [69] by other sensors and therefore not necessary to do again. However, [Paper G] presented estimates of the throttling loss as function of rotation speed, which is not exact, but did show the expected tendency with faster rotation resulting in relative higher losses.

Prototyping of an entire machine is costly and a test environment can be established faster by modifying an existing machine as discussed in Chapter 2. This allows several pressure measurements with the measurement locations illustrated in Fig. 4.4.

4.3 Results

Several series of measurements have been collected throughout this work and the most relevant are presented here.

4.3.1 Valve Switching Results

The position measurement of test-rig I was associated with significant measurement noise during end-stop. The filtered signal results in a varying plunger position, while the simulation predicts a steady closed valve ($z = 0$) as shown in Fig. 4.5. This means either inaccurate model or uncertainty of the measurement of plunger position near end-stop.

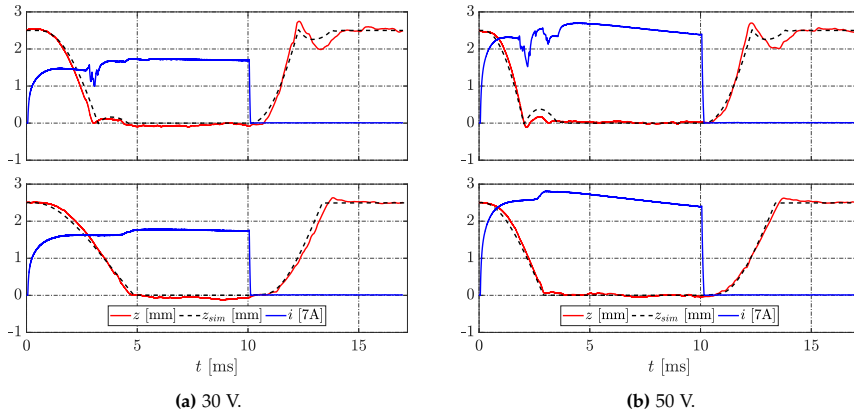


Fig. 4.5: Experimental results of dry (top plots) and oil tests (bottom plots) with two different voltage inputs (yielding peak currents of $1.7 \cdot 7$ and $2.8 \cdot 7$ A respectively). The measured current and plunger position are displayed. The dotted lines are simulation from the LPM, the data are from [Paper A] but graphs have slight modifications. Also, 40 V was tested yielding similar coherence.

The overall fit of the model is accurate for the chosen voltage inputs. A test without oil has been used to verify the spring force while the valve is opening. Hereafter the actuator force is verified while the valve is closing. With these two forces isolated and verified an oil can be added. A significant delay is observed on the switching time when including the fluid force predicted by (3.28) also, the end-stop profile is affected. This serves as a strong indicator that the MI force is captured by both CFD and LPM and that the measurement uncertainty is not a problem for the majority of the switching time. The dominating term of the simulated fluid force is the added mass, i.e. to predict the switching time sufficiently the remaining terms are not essential.

The raw data of test-rig I and II with the same valve design implemented are shown in Fig. 4.6 for comparison of the two test-rig's uncertainty and filtering influence. Due to measurement oscillation from test-rig I, the valve is maintained closed for a longer period to observe the attenuation of this.

The measurement noise from test-rig I is clearly more dominating than in test-rig II. In addition, the filtered value is oscillating until around 60 ms where the oscillation of the filtered signal is attenuated and a steady-state near zero is reached. The primary cause of this is vibration of the reflecting surface, which has been verified by high-speed film. This makes validation of the impact situation in test-rig I flawed and a more rigid construction is necessary. The signal is smoother when using an Eddy-current transducer and the measured end-damping profile shows that the desired damping is introduced. The potential causes of this damping are discussed in the follow-

4.3. Results

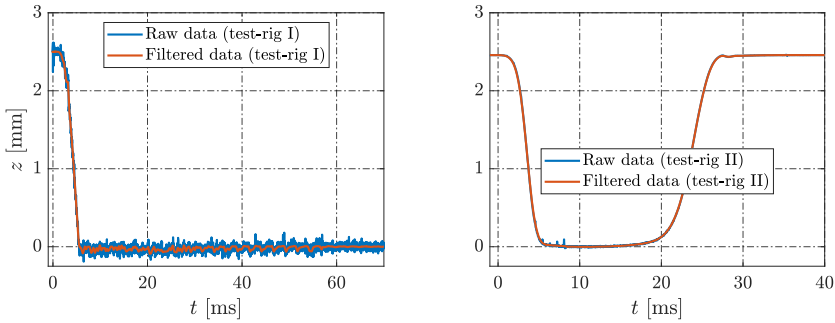


Fig. 4.6: Raw data compared with the filtered ones of the laser transducer (test-rig I) and the Eddy-current transducer (test-rig II). The plunger is with a cushioning groove (C_2) as presented in [Paper H].

ing.

4.3.2 Valve Switching Results - With a Cushion Groove

The simulation and measured results of plunger position (velocity derived hereof), current and cushion pressure during switching in test-rig II are shown in Fig. 4.7. The valve is actively closed by the moving-coil and hereafter opened passively by the spring. The measurement resolution is three times denser than the data points displayed in the graphs.

Prediction of z fits worse than in test-rig I. Although the switching time is predicted accurately there is a noticeable difference in the shape of the velocity. The cushioning pressure is very sensitive to the plunger's position and velocity, and the pressure characteristics looks quite different although similar peak values are reached. In order to remedy this, both the measured position and velocity have been used in simulation case 2 (sim_2) to reveal the consequence on the cushion pressure. This is shown in the lowest plots of Fig. 4.7 where the cushion pressures fits better in magnitude and duration, although the transient after closure is not accurate.

The observed difference between the measured plunger position of test-rig I and II definitely plays a role for the damping and sticking force. The exact same plunger has been tested in both test-rigs resulting in different tendencies, i.e. the environment affects the switching behavior. Test-rig II is very similar to that of a DDU and will inherently add damping since the MIF must go around the plunger or be compressed in the piston chamber. CFD simulation of valve switching when the flows across the inlet/outlet boundaries are zero was presented in Fig. 3.7. This analysis showed that the zero flow boundary resulted in a more gradual deceleration of the plunger than when the fluid could move freely. This is the same tendency that has

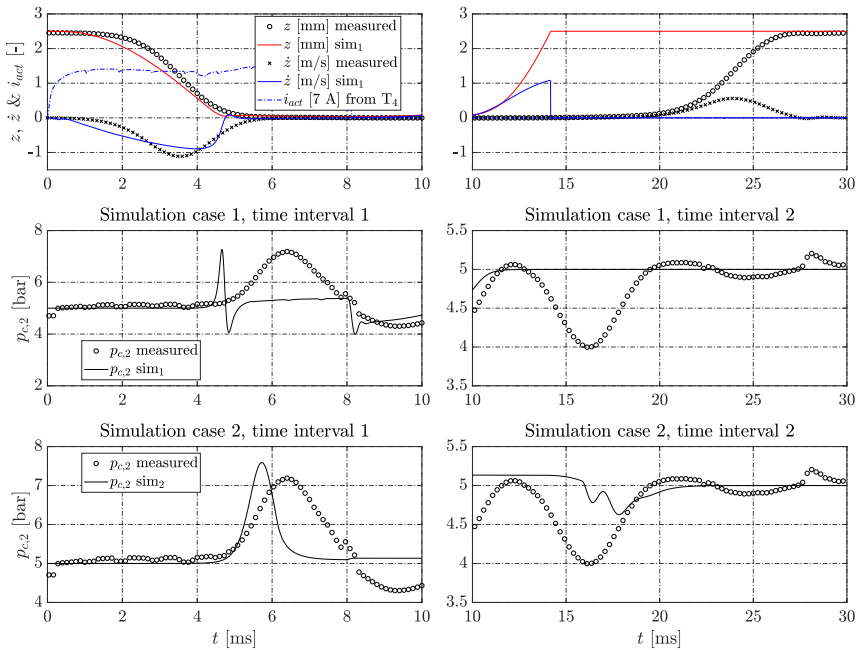


Fig. 4.7: "Comparison of measurements versus simulated values for C_2 . The valve is initially being closed, hereafter the mechanical spring passively returns the plunger to its initial position. Sim_1 only uses the measured current in simulation and sim_2 refers to the case where the measured z and \dot{z} are used directly in the simulation." [Paper H]

been observed experimentally.

The poor prediction of the stiction period in test-rig II has been remedied by performing additional experiments in test-rig I. Three specimens were manufactured with incremental changes of the cushioning groove width where $l_{t,i} = 2l + 2r_i$, the total length $l_{t,i} = 1.7$ mm being constant and $l = l_1 = l_2 = l_3 = l_4$ being varied. See the parameters on the geometry in Fig. 3.20. The stiction periods from varying l are presented in Fig. 4.8a, where the CFD simulation was carried out with initial plunger position of $z_i = 20$ μm . The two different LPM formulations, LPM1 and LPM2, which use two different flow formulations as described in [Paper H], have been simulated with four different starting positions. The reason for doing so is that the contacting surfaces are rough and therefore a fluid will always be present between the two surfaces. However, the amount is unknown and not possible to measure directly. Furthermore, a position of zero creates a singularity in the model and 1 μm is therefore chosen as the lowest initial position. Three corresponding measurements of the plunger position are given in Fig. 4.8b where the valve closes initially and after some time is opened (the corresponding

4.3. Results

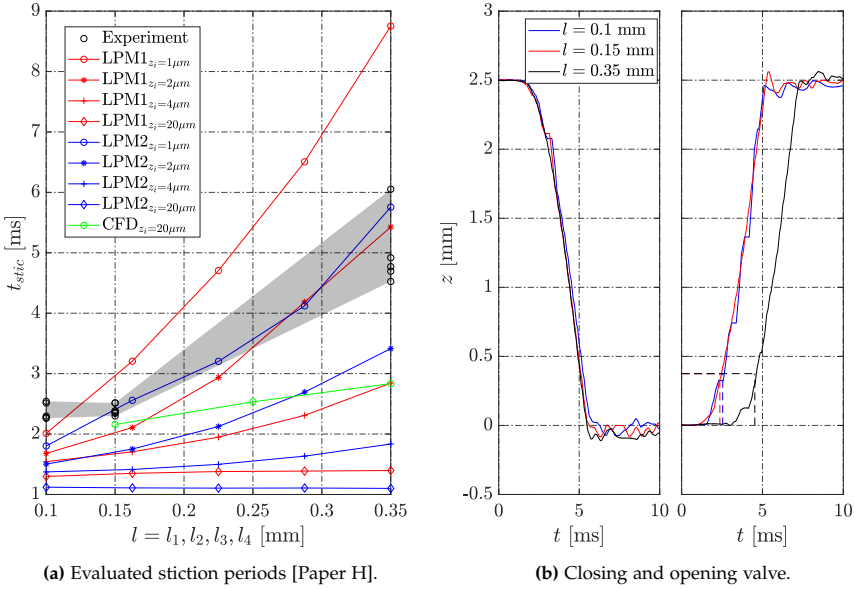


Fig. 4.8: Stiction periods (time from 0 to 15% of full stroke) calculated from several experiments of the three different increments in contact- and cushion- widths. The dotted lines shows examples of stiction period calculations. The LPM uses Poiseuille flow and the LPM2 uses a turbulent flow model to model the flow from the cushion groove. The index with z_i gives the plunger position relative to the seat when the simulation is initialized.

stiction periods are marked by dotted lines).

The measurements of Fig. 4.8b show that the two lowest increments of l give almost identical responses whereas the widest contact area gives a significantly longer stiction period shown with the black lines.

The plunger surface finishing is done by polishing after best practice and normally produces R_a values between 0.1-0.4 μm . This means that on average there will be a minimum fluid gap corresponding to this range since local asperities will contact thus leaving fluid gaps and pockets locally on the surface geometry. The results of Fig. 4.8a indicates that the stiction force is sufficiently represented by the LPM1 when $z_i = 2 \mu m$. Besides, there is no measurable difference in stiction when $l = 0.1$ mm and $l = 0.15$ mm. Microscope inspection has later shown that the exact length of the contacting surface does involve uncertainty which may be part of the explanation. Simulation using LPM2 is most accurate when $z_i = 1 \mu m$ but is computationally expensive compared to LPM1. This range is realistic and since LPM1 is much more rapid to solve, a limit of the gap height has been set to $2 \mu m$ and the LPM1 has been used. The presented results from CFD shows longer stiction periods than what is predicted by both LPM1 and LPM2 at the same initial plunger position. The primary difference of the CFD and LPM is fluid inertia

and intake loss being omitted in the LPM.

Switching Repeatability

To verify the reproducibility of the results, the standard deviation and mean value of the closing, opening and stiction periods were calculated for 30 switching cycles. The definition of a closing, opening and stiction period are given in [Paper H] where the results also can be found.

In short the results showed that the closing time (t_{cl}) has a low standard deviation and is thus repeatable. No significant difference of the standard deviation is observed between dry and oil tests. Contrary, the opening time has a larger standard deviation. When oil is present a standard deviation of 0.2 ms is measured on the stiction period assuming a standard distribution. This means that the stiction force is to some degree stochastic due to the roughness of contacting surfaces and alignment of these.

Movement-Induced Flow

The theory predicts that closing the valve will displace a total of 0.9 mL. Only a third, 0.3 mL, of this was measured in test-rig II, but also a significantly higher damping than anticipated was measured. A plausible explanation for this is, that the compressed fluid volume causes a resisting force as p_2 rises and p_1 either remains constant or decreases due to the expanded volume. This would mean that the MIF is travelling around the plunger instead of into the outlet tube where it was supposed to be measured. In addition, the system may contain unwanted air in the oil, which however does not explain the excessive damping force.

The pictures presented in Fig. 4.2 clearly shows a variation on the fluid surface over time. A total of 8 bores are present in the valve seat where these 'mountain shaped notches' occur (one of these is filled with the laser reflecting pin and no fluid is displaced in this bore). These indicate that the fast switching creates local suction zones causing the fluid to move. The exact volume of this MI fluid is difficult to quantify based on the pictures directly. However, when studying the pictures in detail the shape is similar to a Gaussian distribution, where a standard deviation, $\sigma = r_b = 2$ mm, corresponding the bore radius is a reasonable estimate.

$$h(x, y) = \sum_{i=1}^7 h \exp \left(-\frac{(x - x_i)^2 + (y - y_i)^2}{2\sigma^2} \right) \quad (4.1)$$

where h is the peak value/height of the "mountain", x_i and y_i are the coordinates of the peak h and the function $h(x, y)$ thus describes the 2D fluid height with zero reference being the fluid surface height at $t = 0$. The function is given in Fig. 4.9b, and Fig. 4.9c shows the function as a contour.

4.3. Results

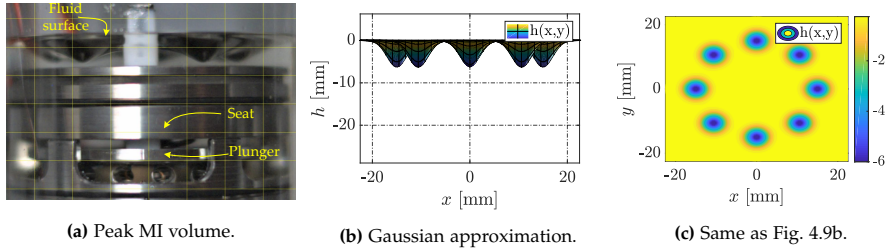


Fig. 4.9: Peak MIF after opening the MCVi2.1 with corresponding approximation of surface texture change by Gaussian distributions.

These results were presented in [Paper H] where a total MI volume of 1.12 mL was found by CFD during opening and 1.1 mL is calculated by double integration of (4.1) when the experimental value of h is -6.26 mm. This value of h has been measured on the images through the high-speed camera software.

4.3.3 Valves Tested in a DDU

The experimental study in [Paper G] was aimed at testing the valve design with a cushioning groove when inserted in a DDU. The pressure over time (both measurement and simulation) and as function of the chamber volume are given in Fig. 4.10.

The supply-, high-, low- and chamber- pressures are measured at the locations illustrated by Fig. 4.4. The simulation results are obtained by using the measured supply pressure (p_S) along with the DDU shaft angle (θ). The results clearly show two dominating pressure frequencies where the slowest (≈ 0.1 kHz) is affected by increase in rotation speed, and in fact non-existent as the rotation is 200 RPM (see results in [Paper G]). The second faster frequency is assumed to be a result of the fluid inertia between the piston chamber and the 0.7 L accumulator placed next to the HPV. The proposed model does give piston chamber pressure oscillations, although at a frequency twice higher than the experimental one. The actual test-rig includes fittings between block and hose along with curved flow paths in the valve block, which may act to decrease the pressure dissipation rate. These pressure cycles are relevant to predict the fatigue of the machine, also they introduce torque ripples on the shaft. Ideally, the chamber pressure should be constant and as close to the high pressure (p_H) as possible.

These results show that there may exist a correlation between increasing the valve size and increasing the hydraulic inductance of the system, hence contributing to the piston chamber pressure dynamics. Further investigation would require additional pressure measurement just after valve number 3 in

Chapter 4. Validation of the Framework

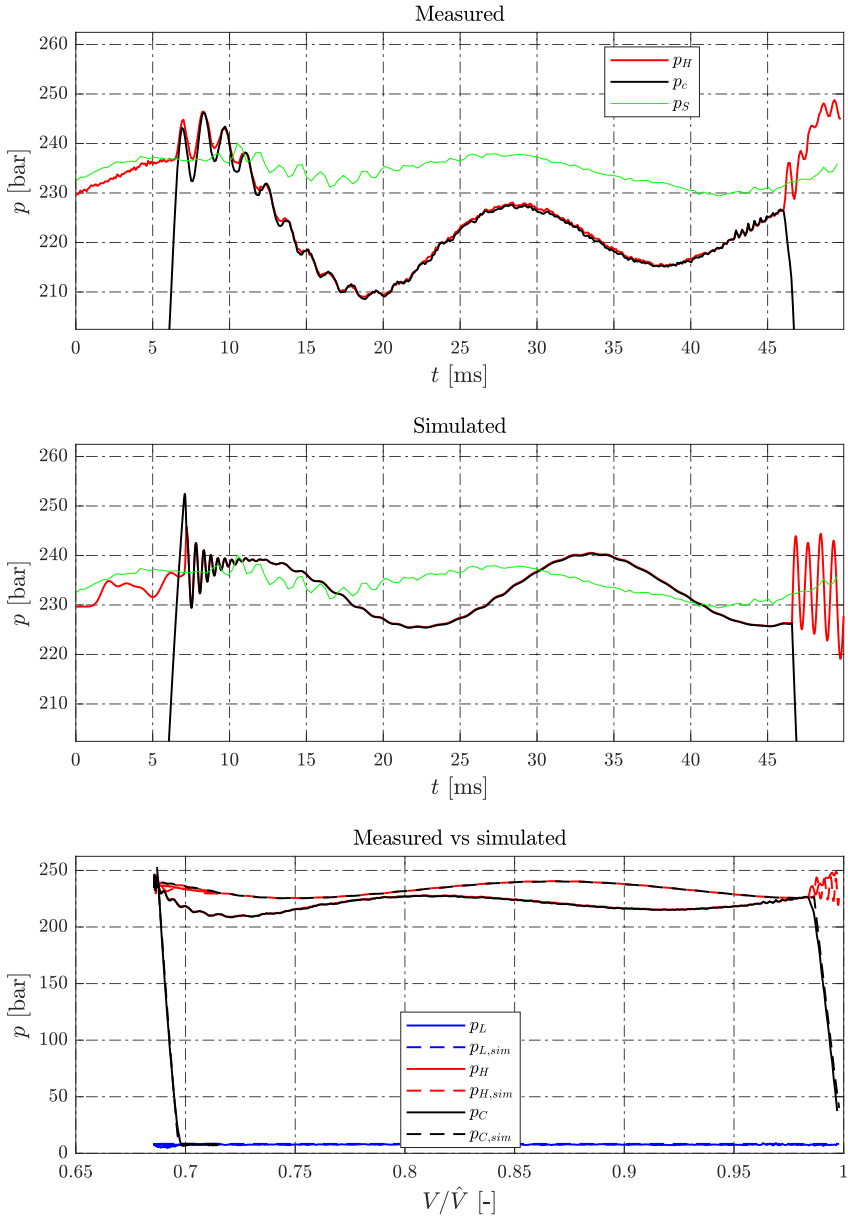


Fig. 4.10: Comparison of the simulated pressures and the measured ones. Experimental results are from [Paper G] and displayed in the first and last plot (the PV-diagram is relative to the maximum volume, \hat{V}). The plot in the middle contains simulation results of the pressures, p_H , p_L and p_C where the measured supply pressure (p_s) is used in the simulation.

Fig. 4.4 and test of different sized valves. Furthermore, the measured pressure has in general shown that stiction periods does not cause cavitation nor pressure peaks as excessive as the ones from simulation. These conclusions have been common for all the tested valve concepts.

4.3.4 Run-in Wear

Four different valve plungers have been tested within the DDU, where microscope images have been taken after these tests were performed to identify if it was relevant to do before and after studies of the wearing surfaces. One specimen has a titanium valve plunger with a flat contact surface, i.e. MCVi2.0 or just C_1 (notation of [Paper H]). The other specimens are MCVi2.1 with stainless steel plungers and cushioning grooves. The three increments of l used for the stiction experiments (Fig. 4.8) have all been tested and the mechanical constructions have been able to withstand the pressure force. The procedure is to run the DDU for some amount of switching cycles at constant; differential pressure (190 bar), rotation speed (400 RPM) and fluid temperature (40 °C) where a data sample of both the HPV and LPV switching is saved every minute. Three consecutive samples with 1 min intervals are given in Fig. 4.11.

The results show that the repeatability is good. This means; the switching times of the valves are similar for each cycle, the measured pressure oscillations are repeatable, i.e. that each load cycle is similar.

The pre- and post- DDU test procedure is to scan a given plunger with a Zeiss Axio Scope A1 and an Axiocam 503 color camera. Two different EC EPIPLAN lenses are used (5x and 20x) for either coarse- or fine- inspection.

This preliminary study showed that the moving-coil of the actuator did have a visible abrasive wear formation, and as the DDU was tested for longer periods (one lasting 10e3, one for 20e3, and the last one for 27e3 cycles) the moving-coil either open-circuited or short-circuited from mechanical rupture. The case of a short-circuit happened once and is clearly visible in Fig. 4.12. Metal debris has been identified near the magnets of the valve, which is a plausible cause to this type of wear. The open-circuit failure occurred due to fatigue of the bobbin mounted on the plunger. This must be re-dimensioned if longer periods of testing are desired with this concept or the loads reduced. No significant stresses are intended to be applied to the moving-coil part, but impact forces during opening of the valve may be a cause of the observed failure, i.e. end-damping after opening the valve may be beneficial. All the valves were functional and undamaged before testing, i.e. all failures are caused by operation in the DDU.

The infant mortality failure modes of the sealing surfaces are either excessive loss of material (becoming problematic debris) or plastically deformed surfaces. Long-term wear such as exchange of materials between seat and plunger or eroded flow edges may contribute to a change in DDU perfor-

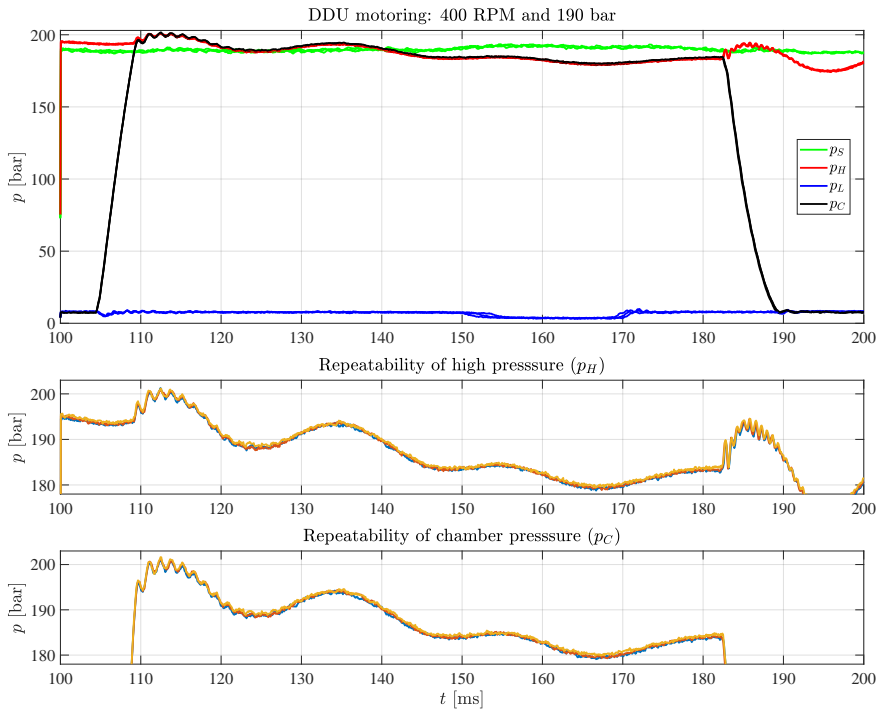


Fig. 4.11: Three samples of various pressure measurements of the DDU with C_1 in the LPV and C_3 in the HPV both with a moving-coil actuator.

mance. The experience from the run-in tests has not given reason for concerns about infant mortality failures of the contacting surfaces. However, local tribo-oxidative wear formations and possible abrasive wear marks have been found by microscope as seen in Fig. 4.13 on the cushioning design. Furthermore, a titanium plunger has been tested for around 100e3 cycles and the most distinct wear marks are shown in Fig. 4.15. Two different wear mechanisms have been found, the first indicates that only around half of the surface is worn and the second is surface fatigue similar to delamination wear, where small laminates of the surface have been worn off. In [Paper C] a list of possible wear processes was established, where surface fatigue like pitting or delamination were among the concerns.

These images lack a before and after view of the same location, which is why a series of surface images have been taken of a new specimen before test. This is done by rotating the specimen in known increments. This corresponds to each yellow box in Fig. 4.14. The images for C_2 before test are given in Appendix II along with ultrasound inspection of the other plunger surfaces to validate that these surfaces have the expected shape.

4.3. Results

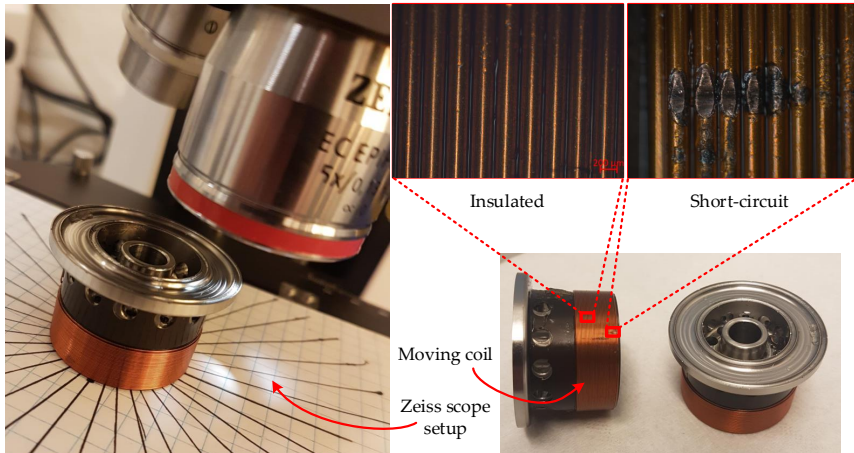
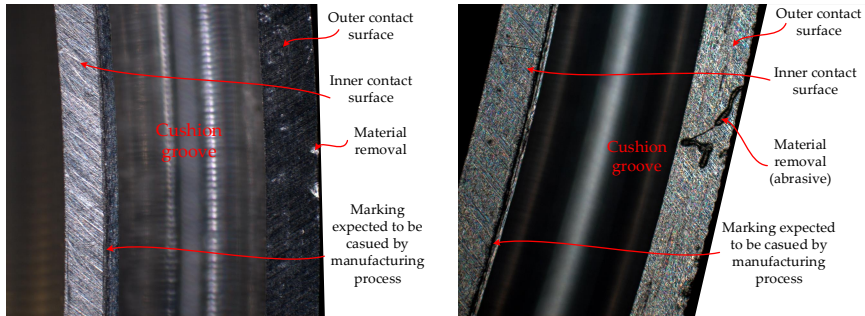


Fig. 4.12: Zeiss microscope setup.

Examples of a surface evaluation plot of plunger concept C_2 are illustrated in Figs. 4.14 and 4.15 along with a view of a potential wear mechanism for the cushioning design. The amount of cycles before actuator failure was around $10e3$ for C_2 with $l = 0.15$ mm, C_2 with $l = 0.1$ mm lasted for $27e3$ cycles. Also, C_3 with $l = 0.15$ mm has been tested where the actuator lasted for $20e3$ cycles. Furthermore, scans of the worn titanium C_1 plunger are given to illustrate possible wear mechanisms. This design has so far lasted for around $100e3$ cycles and has a visible difference between the inner and outer part of the outer ring. The images suggest that only half of the sealing surfaces are actually in contact, at least a sudden jump in surface topography is observed. This also utilizes a moving-coil actuator, which has lasted for substantially longer than the other tested specimens have. This may be purely statistical that some specimens are assembled better and last longer. Otherwise, it may be caused by fewer wear particles from the titanium plunger, or due to the lower mass of the plunger, which means the impact energy during opening of the valve is lower.

The length of the contact surface, l should have been 0.15 mm in both Fig. 4.15 and 4.16, but manufacturing has resulted in some variations of this contact length. This may be an explanation for the difference in stiction period observed earlier in Fig. 4.8, where the difference between the contact zones may be different than the one used in simulation.

During the above testing a total of two valve seats have been used, one only used with the titanium plunger, the other tested with a total of four different cushioning groove plungers, where the actuator of plunger: C_2 with



(a) Visible surface imperfections (Dark-Field filter). (b) Other visible surface imperfections (C-DIC filter).

Fig. 4.13: Zeiss microscope images showing 2.65 mm x 2.0 mm (width x height) of the plunger surface. Two different light filters have been used to locate interesting areas. Around 20e3 cycles were performed.

$l = 0.1$, C_2 with $l = 0.15$ mm and C_3 with $l = 0.15$ mm, all have failed.

The two seats have experienced approximately an equal amount of switching cycles where one is with end-damping, the other with flat surfaces, i.e. the titanium plunger. The contacting surfaces of both parts have been examined and an example of the wear zones is given in Fig. 4.16 along with a before and after image of plunger concept C_2 .

There are clear marks on both the seat and plunger for C_1 and C_2 . But it is unclear whether or not this type of wear will become critical after billions of cycles at full load. The flat design has had more load repetitions and no impact damping, which may be the explanation for a slightly more severe wear zone where material removal has occurred along with more visible wear on the seat. The seat in MCVi2.1 has been assembled with all the three different increments of C_2 with varying land width (l) as discussed earlier. The images of C_2 does not reveal three distinctly different wear zones on the seat. However, upon close inspection it could be argued that the outer parts of the seat wear marks are slightly more severe. This is the region where the plungers with short contact lengths have been impacting. In total it is again difficult to determine the severity with the low amount of switching cycles. Since no significant material removal has been observed on the tested cushioning designs seat wear is currently not considered as critical. Reducing noise of the machine is however still of priority. Generally the before and after images show no visible wear zones which is why many of these are left out.

4.4. Summary

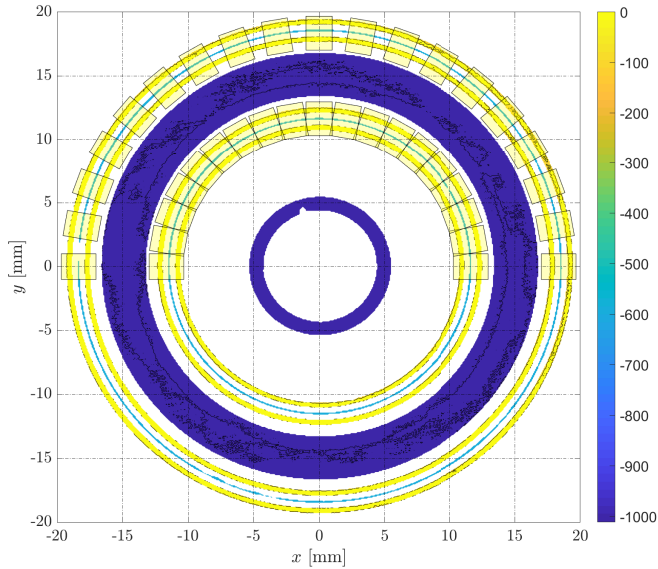


Fig. 4.14: Distance to the plunger surface of concept 2 (C_2 where $l = 0.35$ mm) examined by ultrasound. Each yellow box indicates an area that has been scanned in the microscope before and after testing.

4.4 Summary

The switching dynamics have been measured and compared to the response obtained by the mathematical representation of the actuator force, spring force and fluid force. The correlations of these results are sufficient to apply the model for optimization.

Stiction periods for a flat contact area are sufficiently predicted by simulation. Introducing a cushioning groove means that the initial plunger position plays an important role along with the choice of model to describe the flow in and out of the groove. Experimental data of the cushioning groove pressure during valve closing agrees with a Poiseuille flow model, the model is also appropriate to predict the stiction force for the situation considered.

A movement-induced flow has been observed as a consequence of a moving plunger. This observation is done in two distinctly different test-rigs resulting in different magnitudes, but both agreeing that the movement causes a displacement of fluid as the theory predicts. The sizing of the plunger therefore plays a role in determining the flow conditions during fast valve switching.

The measured and simulated pressure gradient in the DDU chamber dur-

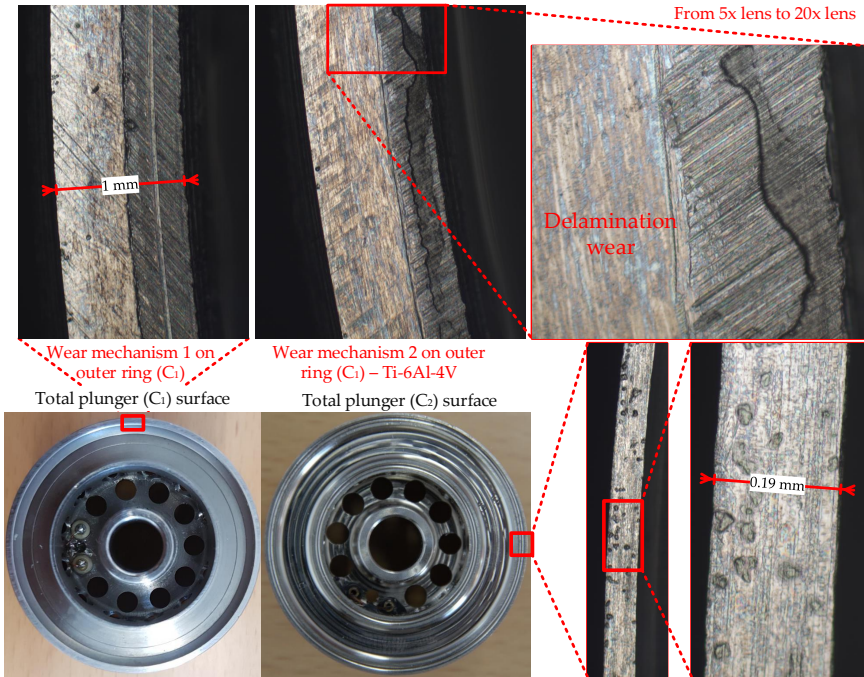


Fig. 4.15: The three images in the upper part of the figure shows the outer contact surface of plunger concept 1 (C_1). The lowest images show the surfaces of plunger C_1 and C_2 , a zoomed image (5x lens) of the largest circle, and a further zoom (20x lens). The chosen section shows the typical observed surface change, i.e. the dark spots.

ing compression and decompression are similar, i.e. the applied fluid compressibility model is sufficient. The loss from supply to high pressure is under-estimated by simulation, i.e. the actual hydraulic resistance is greater than the theoretical one. The oscillation frequency plus amplitude of the pressure in the piston chamber also shows a discrepancy which may be correlated to the difference in hydraulic resistance. The experiments showed that the throttling loss is low, however the measurement is not accurate enough to determine the exact magnitude of this loss.

The run-in wear on the moving-coil actuator was more severe than anticipated. Longer periods of continuous operation were expected. However, this preliminary wear study has found no significant issues on the sealing surfaces. It is clear that this is no guarantee for the long-term effects. To do lifetime testing of valves an entirely different test-rig is considered necessary. Furthermore, reducing the noise from the switching valves is considered relevant.

4.4. Summary

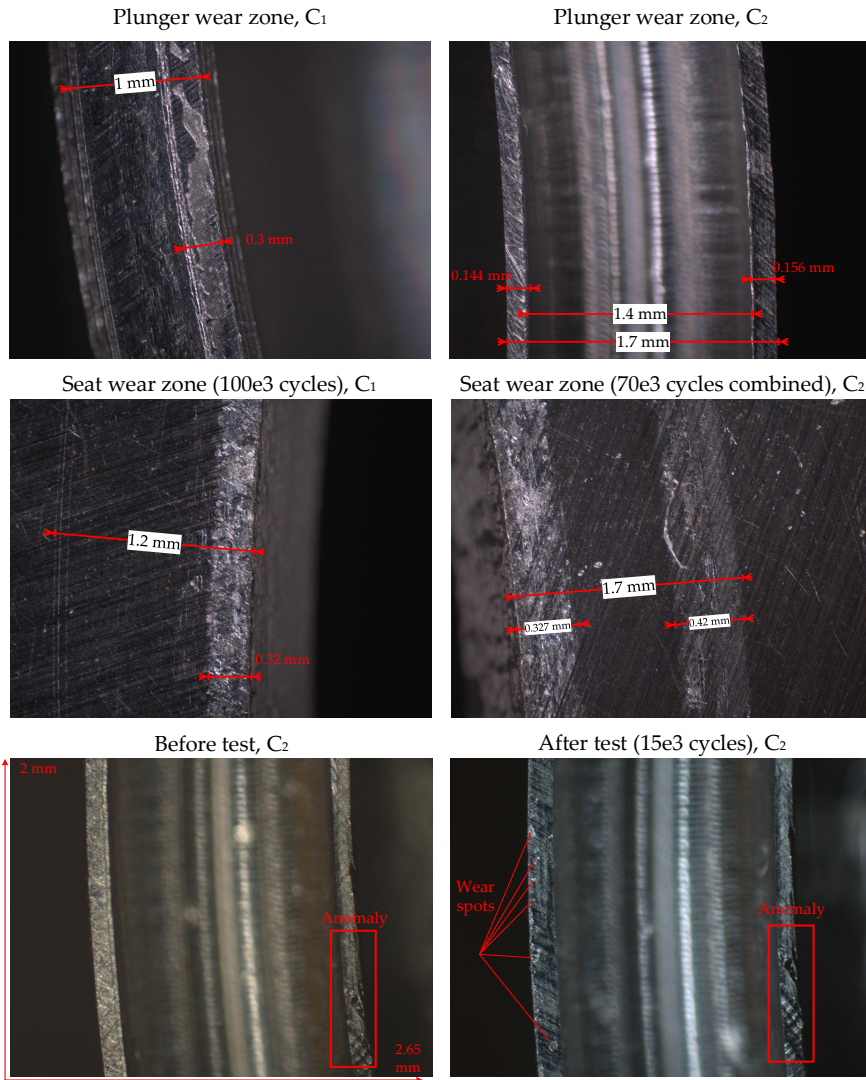


Fig. 4.16: Zeiss microscope images of plunger and seat wear zones with the relevant lengths denoted. There is a difference of scale between seat and plunger images due to the focus of the microscope. The images at the bottom show before and after views of the exact same location of C₂. A distinct surface anomaly was observed both before and after as denoted in the figure. The differences are minor, but small 'spots' as indicated are only visible on the after image.

Chapter 4. Validation of the Framework

Chapter 5

Closing Remarks

Based on the hypothesis of this work: "*It is possible to advance and validate the current state-of-the-art modelling framework describing the relevant fluid dynamics of digital valves and reduce the impact loads.*" some closing remarks may be made.

5.1 Conclusions

A general design framework for digital valves was established based on the state-of-the-art established in [Paper C]. Missing links to realize this framework included knowledge about the fluid dynamical aspects during switching, as well as predicting long-term lifetime and wear. This work has in total been advancing and validating models describing the fluid dynamics in digital valves in order to predict the plunger speed near end-stop, and to elaborate on the possibilities of applying models with different levels of fidelity.

A dynamic 2D axisymmetric CFD simulation model was developed and especially the stability of the solution near end-stop required customized meshing techniques and dynamic constraint of the time step-size as briefly discussed in [Paper E] and further elaborated in this dissertation. In [Paper A & H] the models were sought validated by looking at the integrated quantities; fluid force and boundary mass flow rate. This concerns the Movement-Induced (MI) force and the MI Flow (MIF) where measurements of the plunger position served as in-direct validation of the fluid force.

The transient response of the orifice in a digital valve evaluated by CFD simulation revealed a fluid inertia, which could be approximated by a simple parametric expression [Paper E]. The effect of this transient response when used in a DDU environment, i.e. describing the flow between accumulator and pressure chamber gave rise to pressure chamber oscillations similar to

the ones observed experimentally in [Paper G].

The computationally heavy simulation tool has been decomposed to a lower fidelity parametric Lumped Parameter Model (LPM) aided by prior proposals from the literature and from the observations done by CFD simulation. These contributions have been presented loosely in [Paper A, D, E, H, I, J] and summarized in this dissertation. The model adjustments concerns: determination and scaling of MI forces and flow by considering a baseline design; a novel flow-induced force model; transient response of the orifice (fluid inertia) and a model for a cushioning groove with stiction and damping effects.

Available models to quantify the reliability of seat valves were studied in [Paper B]. The analysis showed a risk of internal leakage developing, but the uncertainty related to this prediction essentially makes the approach unfit to actually quantify the risk. A relationship between switching cycles and internal leakage was used to assess the influence of such leaking valves on the efficiency of a DDU in [Paper D]. This suggested that the valve losses would be lowest when not utilizing the full displacement of the DDU.

A series of motor tests was presented in [Paper G], where two different plunger concepts were tested. The tendencies of valve switching speed, energy loss and chamber pressure when varying the rotation speed revealed a quicker plunger motion as rotation speed increased. In addition, the actuator requirement lowered and the chamber pressure started diverging more from the supply pressure.

The voltage shaping approach of [Paper F] did show theoretical potential to improve the DDU performance. However, implementation of the presented algorithm was not prioritized from a research perspective because the plunger impact profile was not possible to measure or estimate properly by the observer as discussed in [Paper G].

An example of the optimization problem was formulated with the revised models describing the fluid dynamics. This means impact speeds of the two valves could be constrained and/or minimized along with the energy losses. The example resulted in a design with significantly smoother deceleration profile near end-stop, while maintaining the valve energy losses low compared to the previous iterations. The plunger material was chosen to be stainless steel to ensure a cheap design, and due to a lower plunger volume, the mass of the plunger was approximately unchanged compared to the prior titanium equivalent.

A preliminary study of the wear and failure modes of the plunger showed high risk of failure in the moving-coil. Regarding the mechanical contact surfaces no infant failures have been observed, however, visible wear zones have been documented. These are relevant to study over longer periods of operation to be able to conclude if a cushioning design is in fact more durable.

5.2 Future Work

The experience from this work has resulted in the following proposals for further research topics in prioritized order.

- Manufacturing of the new prototype with possibility of measuring the velocity profile near impact.
- The long-term durability remains to be validated by experiments. This type of accelerated tests is a complicated discipline for hydraulic systems and no rigid methodology exists at the present of writing.
- Validation of the CFD framework during valve switching while a known flow is flowing across the valve orifice.
- Additional experimental insight about the observed pressure oscillations.
- The CFD framework has its limitation in the elastohydrodynamic lubrication regime where the fluid gap height goes to an order of magnitude similar to that of the surface roughness. This may be resolved by using the presented CFD framework in combination with methods of tribology. This may become computationally expensive and not necessarily realistic for optimization routines. However, it may give more accurate fluid and contact pressures between the two bodies.
- The proposed models have some documented disagreements on the magnitude of plunger velocity near end-stop. This may be remedied by other modelling techniques.

References

- [1] P. Achten, M. Linjama, R. Scheidl, and S. Schmidt, "Discussion: Is the future of fluid power digital?" *Proc. Inst. Mech. Eng. Part I J. Syst. Control Eng.*, vol. 226, no. 6, pp. 724–726, 2012.
- [2] R. Aghababaei, D. Warner, and J. Molinari, "Critical length scale controls adhesive wear mechanisms," *Nat. Commun.*, vol. 7, no. 11816, pp. 1–8, 2016.
- [3] R. Amirante, P. G. Moscatelli, and L. A. Catalano, "Evaluation of the flow forces on a direct (single stage) proportional valve by means of a computational fluid dynamic analysis," *Energy Convers. Manag.*, vol. 48, no. 3, pp. 942–953, 2007.
- [4] R. Amirante, L. A. Catalano, C. Poloni, and P. Tamburrano, "Fluid-dynamic design optimization of hydraulic proportional directional valves," *Eng. Optim.*, vol. 46, no. 10, pp. 1295–1314, 2014. [Online]. Available: <https://doi.org/10.1080/0305215X.2013.836638>
- [5] M. M. Bech, C. Noergaard, and D. B. Roemer, "A Global Multi-Objective Optimization Tool for Design of Mechatronic Components using Generalized Differential Evolution," in *42nd Annu. Conf. IEEE Ind. Electron. Soc.* Florence, Italy: IEEE Press, 2016, pp. 475 – 481.
- [6] N. C. Bender, T. O. Andersen, and H. C. Pedersen, "Parameter Correlation by Static and Dynamic Evaluations Utilizing a Mechatronic Design Procedure for a Digital Displacement Unit," *IEEE/ASME Trans. Mechatronics*, pp. 1–11, 2019.
- [7] —, "Feasibility of Deep Neural Network Surrogate Models in Fluid Dynamics," *Model. Identif. Control A Nor. Res. Bull.*, vol. 40, no. 2, pp. 71–87, 2019. [Online]. Available: <http://www.mic-journal.no/ABS/MIC-2019-2-1.asp>
- [8] N. C. Bender, J. H. Christensen, M. M. Bech, and H. C. Pedersen, "Experimental Study of a Digital Displacement Machine Utilizing a Cushion Valve Topology," in *Tenth Work. Digit. Fluid Power*, Linz, Austria, 2019.
- [9] N. C. Bender, H. C. Pedersen, M. M. Bech, and T. O. Andersen, "A Multi-Agent Evolution Algorithm Used for Input Shaping of a Repetitive Non-Linear Dynamic System," in *Proc. ASME/BATH Symp. Fluid Power Motion Control*, Bath, 2018, pp. 1–10.
- [10] N. C. Bender, H. C. Pedersen, and C. Nørgård, "Experimental Validation of Flow Force Models for Fast Switching Valves," in *Proc. ASME/BATH 2017 Symp. Fluid Power Motion Control*. Sarasota: ASME, 2017.
- [11] N. C. Bender, H. C. Pedersen, A. Plöckinger, and B. Winkler, "Reliability Analysis of a Hydraulic On/Off Fast Switching Valve," in *Ninth Work. Digit. Fluid Power*, Aalborg, 2017, pp. 1–18.
- [12] —, "Towards a modelling framework for designing active check valves – a review of state-of-the-art," *Int. J. Fluid Power*, vol. 19, no. 1, pp. 49 – 64, 2017.
- [13] —, "Evaluating the Influence of Leaking Active Check Valves in Digital Displacement Units," in *IEEE Glob. Fluid Power Soc. PhD Symp.* Samara: IEEE, 2018, pp. 1–9. [Online]. Available: <https://ieeexplore.ieee.org/document/8472399>

References

- [14] N. C. Bender, H. C. Pedersen, B. Winkler, and A. Plöckinger, "Numerical Investigation of Switching Features of a Hydraulic Seat Valve with Annular Flow Geometry," *Int. J. Fluid Power*, vol. 19, no. 3, pp. 152–164, 2018.
- [15] N. C. Bender, A. Plöckinger, P. Foschum, B. Winkler, and H. C. Pedersen, "Measurements of a Novel Digital Hydraulic Valve Comprising a Cushioning Feature," *J. Dyn. Syst. Meas. Control*, vol. under revi, 2019.
- [16] W. Borutzky, B. Barnard, and J. Thoma, "An orifice flow model for laminar and turbulent conditions," *Simul. Model. Pract. Theory*, vol. 10, no. 3-4, pp. 141 – 152, 2002.
- [17] C. E. Brennen, "A Review of Added Mass and Fluid Interial Forces," Naval Civil Engineering Laboratory, California, Tech. Rep. January, 1982.
- [18] N. Caldwell, "Review of Early Work on Digital Displacement ® Hydrostatic Transmission Systems," in *Proc. BATH/ASME 2018 Symp. Fluid Power Motion Control*, Bath, 2018, pp. 1–13.
- [19] —, "Digital displacement hydrostatic transmission systems," Ph.D. dissertation, University of Edinburgh, 2007.
- [20] F. J. Cavalieri, F. Zenklusen, and A. Cardona, "Determination of wear in internal combustion engine valves using the finite element method and experimental tests," *Mech. Mach. Theory*, vol. 104, no. 1, pp. 81–99, 2015.
- [21] P. Chapple, P. N. Lindholdt, and H. B. Larsen, "An Approach to Digital Distributor Valves in Low Speed Pumps and Motors," p. V001T01A041, 2014.
- [22] S. Chekurov and T. Lantela, "Selective Laser Melted Digital Hydraulic Valve System," *3D Print. Addit. Manuf.*, vol. 4, no. 4, 2017.
- [23] P. Cui, R. T. Burton, and P. R. Ukrainetz, "Development of a High Speed On / Off Valve," *SAE Tech. Pap.*, vol. 100, no. 911815, pp. 312–316, 1991.
- [24] S. Das and P. N. Suganthan, "Differential evolution: A survey of the state-of-the-art," *IEEE Trans. Evol. Comput.*, vol. 15, no. 1, pp. 4–31, 2011.
- [25] V. Delli Colli, F. Marignetti, and C. Attaianese, "Analytical and multiphysics approach to the optimal design of a 10-MW DFIG for direct-drive wind turbines," *IEEE Trans. Ind. Electron.*, vol. 59, no. 7, pp. 2791–2799, 2012.
- [26] M. Domaga, "Cfd Analysis of Pilot Operated Relief Valve," 2015.
- [27] M. Elgamil, M. Amin, and S. Kassem, "Development of High Performance High Flow Fast Switching Hydraulic Directional Control Valves," 2015.
- [28] P. Forsberg, R. Elo, and S. Jacobson, "The importance of oil and particle flow for exhaust valve wear - An experimental study," *Tribol. Int.*, vol. 69, no. 1, pp. 176–183, 2014.
- [29] J. E. Funk, D. J. Wood, and S. P. Chao, "The Transient Response of Orifices and Very Short Lines," *J. Basic Eng.*, vol. 94, no. 2, pp. 483–489, 1972.
- [30] M. Green, N. Caldwell, J. Macpherson, and W. H. S. Rampen, "DEXTER - The Application of a Digital Displacement ® Pump to a 16 Tonne Excavator," in *Proc. BATH/ASME 2018 Symp. Fluid Power Motion Control*, 2018, pp. 1–9.

References

- [31] A. H. Hansen, H. C. Pedersen, and R. H. Hansen, "Validation of Simulation Model for Full Scale Wave Simulator and Discrete Fluid Power PTO System," in *Proc. 9th JFPS Int. Symp. Fluid Power*, Matsue, 2014, pp. 231–238.
- [32] M. Heikkilä, J. Tammisto, M. Huova, K. Huhtala, and M. Linjama, "Experimental Evaluation of a Piston-Type Digital Pump-Motor-Transformer with Two Independent Outlets," pp. 83–97, 2010.
- [33] I. M. Hutchings, R. E. Winter, and J. E. Field, "Solid particle erosion of metals: the removal of surface material by spherical objects," *Proc. R. Soc. London. Ser. A*, vol. 348, no. 1654, pp. 379–392, 1976.
- [34] Hydac, "Solenoid Directional Valve Poppet Type - Pilot Operated 2 / 2 Normally Open UNF Cartridge – 350 bar WS16YR-01," pp. 1–2, 2018. [Online]. Available: www.hydac.com
- [35] T. A. Jankowski, E. N. Schmierer, F. C. Prenger, and S. P. Ashworth, "A Series Pressure Drop Representation for Flow Through Orifice Tubes," *J. Fluids Eng.*, vol. 130, no. 5, p. 051204, 2008. [Online]. Available: <http://fluidsengineering.asmedigitalcollection.asme.org/article.aspx?articleid=1478129>
- [36] X. Jannot, J.-C. Vannier, C. Marchand, M. Gabsi, J. Saint-Michel, and D. Sadarnac, "Multiphysic Modeling of a High-Speed Interior Permanent-Magnet Synchronous Machine for a Multiobjective Optimal Design," *IEEE Trans. ENERGY Convers.*, vol. 26, no. 2, pp. 457–467, 2011.
- [37] P. Johansen, "Tribodynamic Modeling of Digital Fluid Power Motors," Ph.D. dissertation, Aalborg University, 2014.
- [38] P. Johansen, N. C. Bender, A. H. Hansen, and L. Schmidt, "Investigation of squeeze film damping and associated loads," in *Fluid Power Motion Control*, Sarasota, Florida, 2017, pp. 1–9.
- [39] T. L. Jones, *Handbook of reliability prediction procedures for mechanical equipment*. West Bethesda, Maryland 20817-5700: NSWC, 2011, no. May.
- [40] S. Kim and H. Murrenhoff, "Measurement of Effective Bulk Modulus for Hydraulic Oil at Low Pressure," *J Fluids Eng.*, vol. 134, no. 2, p. 021201, 2012.
- [41] A. L. Knutson and J. D. Van de Ven, "Modelling and experimental validation of the displacement of a check valve in a hydraulic piston pump," *Int. J. Fluid Power*, vol. 17, no. 2, pp. 114–124, 2016.
- [42] H. Kogler, "The Hydraulic Buck Converter - Conceptual Study and Experiments The Hydraulic Buck Converter - Conceptual Study and Experiments," Ph.D dissertation, Johannes Kepler University, 2012.
- [43] S. Kukkonen, "Generalized Differential Evolution for Global Multi-Objective Optimization with Constraints," Ph.D. dissertation, Lappeenranta University of Technology, 2012.
- [44] R. Y. S. Lai, "Translatory Accelerating Motion of a Circular Disk in a Viscous Fluid," *Appl. Sci. Res*, vol. 27, no. 1, pp. 440–450, 1973.
- [45] L. D. Landau and E. M. Lifshitz, *Fluid Mechanics*, 2nd ed. Elsevir, 1956.

References

- [46] J. Lang, R. Nathan, and Q. Wu, "Experimental Study of Transient Squeezing Film Flow," *J. Fluids Eng.*, vol. 141, no. August, pp. 1–7, 2019.
- [47] J. Lang, S. Santhanam, and Q. Wu, "Exact and approximate solutions for transient squeezing flow," *Phys. Fluids*, vol. 29, no. 103606, 2017.
- [48] T. Lantela and M. Pietola, "High-flow rate miniature digital valve system," *Int. J. Fluid Power*, vol. 18, no. 3, pp. 188–195, 2017. [Online]. Available: <http://doi.org/10.1080/14399776.2017.1358025>
- [49] H. B. Larsen, M. Kjelland, A. Holland, and P. N. Lindholdt, "Digital Hydraulic Winch Drives," in *Proc. BATH/ASME 2018 Symp. Fluid Power Motion Control*, Bath, UK, 2018, pp. 1–9.
- [50] S. Y. Lee and J. F. Blackburn, "Contributions to Hydraulic Control, part I, Steady-State Axial forces on Control-Valve Pistons," *ASME*, vol. 74, no. 8, pp. 1005–111, 1952.
- [51] M. Leijon, H. Bernhoff, O. Ågren, J. Isberg, J. Sundberg, M. Berg, K. E. Karlsson, and A. Wolfbrandt, "Multiphysics simulation of wave energy to electric energy conversion by permanent magnet linear generator," *IEEE Trans. Energy Convers.*, vol. 20, no. 1, pp. 219–224, 2005.
- [52] R. Lewis and R. Dwyer-Joyce, "An Experimental Approach to Solving Combustion Engine Valve and Seat Wear Problems," *Tribol. Res. From Model Exp. to Ind. Probl.*, vol. 39, no. 1, pp. 629–640, 2001.
- [53] ———, "Wear of diesel engine inlet valves and seat inserts," *Proc Instn Mech Engrs, Part D J Automob. Eng.*, vol. 216, no. 3, pp. 205–216, 2002.
- [54] J. Liniger, "Design of Reliable Fluid Power Pitch Systems for Wind Turbines," PhD dissertation, Aalborg Universitet, 2018.
- [55] J. Liniger, H. C. Pedersen, and M. Soltani, "Reliable Fluid Power Pitch Systems: A Review of State of the Art for Design and Reliability Evaluation of Fluid Power Systems," *ASME/BATH 2015 Symp. Fluid Power Motion Control*, no. November, p. V001T01A026, 2015. [Online]. Available: <http://proceedings.asmedigitalcollection.asme.org/proceeding.aspx?doi=10.1115/FPMC2015-9541>
- [56] M. Linjama, M. Paloniitty, L. Tiainen, and K. Huhtala, "Mechatronic Design of Digital Hydraulic Micro Valve Package," *PROCEDIA Eng.*, 2015.
- [57] E. Lisowski, W. Czyzycki, and J. Rajda, "Three dimensional CFD analysis and experimental test of flow force acting on the spool of solenoid operated directional control valve," *Energy Convers. Manag.*, vol. 70, pp. 220–229, 2013.
- [58] Y. Liu, B. Ma, C. Zheng, and S. Zhang, "Degradation modeling and experiment of electro-hydraulic shift valve in contamination circumstances," *Adv. Mech. Eng.*, vol. 7, no. 5, pp. 1–9, 2015.
- [59] R. W. Lyczkowskia and J. X. Bouillard, "State-of-the-art review of erosion modeling in fluid/solids systems," *Prog. Energy Combust. Sci.*, vol. 28, pp. 543–602, 2002.
- [60] D. Malmquist, D. Frede, and J. Wikander, "Holistic design methodology for mechatronic systems," *Proc. Inst. Mech. Eng. Part I J. Syst. Control Eng.*, vol. 228, no. 10, pp. 741–757, 2014.

References

- [61] N. Manring and C. Williamson, "The Theoretical Volumetric Displacement of a Check-Valve Type, Digital Displacement Pump," *J. Dyn. Syst. Meas. Control*, vol. 141, no. 3, pp. 1–8, 2019.
- [62] F. McIntyre and U. Stein, "Electronically controlled valves," Patent US 2012 0000 554 A1, 2012. [Online]. Available: <https://patents.google.com/patent/US20120000554A1/en>
- [63] K. J. Merrill, "Modeling and Analysis of Active Valve Control of a Digital Pump-Motor," Ph.D. dissertation, Purdue University, 2013.
- [64] H. E. Merritt, *Hydraulic control systems*. New York: John Wiley & Sons, Inc., 1967.
- [65] C. Noergaard, M. M. Bech, D. B. Roemer, and L. Schmidt, "Experimental Validation of Modelled Fluid Forces in Fast Switching Hydraulic On/Off Valves," *Int Conf Fluid Power Mechatronics*, pp. 68–73, 2015.
- [66] C. Noergaard, M. M. Beck, D. B. Roemer, and H. C. Pedersen, "Optimization of Moving Coil Actuators for Digital Displacement Machines," in *Eighth Work. Digit. Fluid Power*. Tampere, Finland: Tampere University of Technology, 2016.
- [67] C. Noergaard, D. B. Roemer, and M. M. Bech, "MODELLING OF MOVING COIL ACTUATORS IN FAST SWITCHING VALVES SUITABLE FOR DIGITAL HYDRAULIC MACHINES," in *ASME/BATH Symp. Fluid Power Motion Control*, Chicago, 2015, pp. 1–10.
- [68] C. Noergaard, "Design, Optimization and Testing of Valves for Digital Displacement Machines," Ph.D. dissertation, Aalborg University, 2017.
- [69] C. Noergaard, M. M. Bech, T. O. Andersen, and J. Christensen, "Flow Characteristics and Sizing of Annular Seat Valves for Digital Displacement Machines," *Model. Identif. Control A Nor. Res. Bull.*, vol. 39, no. 1, pp. 23–35, 2018.
- [70] C. Noergaard, M. M. Bech, J. H. Christensen, and T. O. Andersen, "Modeling and Validation of Moving Coil Actuated Valve for Digital Displacement Machines," *IEEE Trans. Ind. Electron.*, vol. 65, no. 11, pp. 8749–8757, 2018.
- [71] C. Noergaard, J. H. Christensen, M. M. Bech, A. H. Hansen, and T. O. Andersen, "Test Rig for Valves of Digital Displacement Machines," in *Ninth Work. Digit. Fluid Power*, Aalborg, 2017, pp. 1–13.
- [72] C. Noergaard, E. L. Madsen, J. M. T. Joergensen, J. H. Christensen, and M. M. Bech, "Test of a Novel Moving Magnet Actuated Seat Valve for Digital Displacement Machines," *IEEE/ASME Trans. Mechatronics*, vol. 23, no. 5, pp. 2229–2239, 2018. [Online]. Available: <https://ieeexplore.ieee.org/document/8445616/>
- [73] C. Noergaard, D. B. Roemer, M. M. Bech, and T. O. Andersen, "Experimental Validation of Mathematical Framework for Fast Switching Valves Used in Digital Hydraulic Machines," in *FPMC*. ASME, 2015, pp. 1–9.
- [74] S. Nordås, M. M. Beck, M. K. Ebbesen, and T. O. Andersen, "Dynamic Response of a Digital Displacement Motor Operating with Various Displacement Strategies," *Energies*, pp. 1–25, 2019.

References

- [75] R. L. Norton, *Machine Design An Integrated Approach*, third edit ed. Pearson Prentice Hall, 2005.
- [76] M. Paloniitty, L. Matti, and K. Huhtala, "Durability Study on High Speed Water Hydraulic Minitaure on/off Valve," in *Fifth Work. Digit. Fluid Power*, Tampere, Finland, 2016, pp. 201–212.
- [77] Parker, "Directional Control Valve Series D3W," Kaarst, Germany, 2008. [Online]. Available: parker.com
- [78] —, "Poppet Type, 2-Way Valve Series DSH161," pp. 385–386, 2018. [Online]. Available: parker.com
- [79] G. S. Payne, A. E. Kiprakis, M. Ehsan, W. H. S. Rampen, J. P. Chick, and A. R. Wallace, "Efficiency and dynamic performance of Digital Displacement hydraulic transmission in tidal current energy converters," *J. Power Energy*, vol. 221, no. A, pp. 207–218, 2007.
- [80] N. H. Pedersen, P. Johansen, and T. O. Andersen, "Challenges with Respect to Control of Digital Displacement Hydraulic Units," *Model. Identif. Control*, vol. 39, no. 2, pp. 91–105, 2018.
- [81] N. H. Pedersen, "Development of Control Strategies for Digital Displacement Units," PhD dissertation, Aalborg University, 2018.
- [82] M. Penalba and J. V. Ringwood, "A review of wave-to-wire models for wave energy converters," *Energies*, vol. 9, no. 7, 2016.
- [83] R. A. Pizarro-Recabarren, J. R. Barbosa, and C. J. Deschamps, "Modeling the stiction effect in automatic compressor valves," *Int. J. Refrig.*, vol. 36, no. 7, pp. 1916–1924, 2013. [Online]. Available: <http://dx.doi.org/10.1016/j.ijrefrig.2013.09.042>
- [84] F. Rahimi, L. Feng, J. Wikander, and D. Frede, "Early Phase Design-Optimization of Mechatronic Systems," *Proc. 2017 5th Int. Conf. Control. Mechatronics Autom.*, pp. 42–49, 2017. [Online]. Available: <http://doi.acm.org/10.1145/3149827.3149838>
- [85] W. Rampen, "The Development of Digital Displacement Technology," 2010.
- [86] W. Rampen, N. Caldwell, and U. Stein, "Annular Valve," Patent US7 077 378 B2, 2006. [Online]. Available: <https://patents.google.com/patent/US7077378B2/en>
- [87] W. H. S. Rampen, "The Digital Displacement Hydraulic Piston Pump," Ph.D. dissertation, University of Edinburgh, 1992.
- [88] M. Resch and R. Scheidl, "A model for fluid stiction of quickly separating circular plates," *Proc. Inst. Mech. Eng. Part C J. Mech. Eng. Sci.*, vol. 228, no. 9, pp. 1540–1556, 2013. [Online]. Available: <http://pic.sagepub.com/lookup/doi/10.1177/0954406213509613>
- [89] B. Rexroth, "Directional spool valves, direct operated, with solenoid actuation, fast switching, WES," 2014. [Online]. Available: www.boschrexroth.com
- [90] D. B. Roemer, P. Johansen, M. M. Bech, and H. C. Pedersen, "Optimum design of a moving coil actuator for fast switching valves in digital hydraulic pumps and motors," *IEEE/ASME Trans. Mechatronics*, vol. 20, no. 6, pp. 2761–2770, 2015.

References

- [91] D. B. Roemer, P. Johansen, H. C. Pedersen, and T. O. Andersen, "Method for Lumped Parameter Simulation of Digital Displacement Pumps/Motors Based on CFD," *Appl. Mech. Mater.*, vol. 397-400, pp. 615–620, 2013.
- [92] —, "SIMULATION OF DYNAMIC BEHAVIOUR OF A DIGITAL DISPLACEMENT MOTOR USING 3D COMPUTATIONAL FLUID DYNAMICS ANALYSIS," *Proc. ASME/BATH Symp. Fluid Power Motion Control*, 2013.
- [93] —, "Optimum design of seat region in valves suitable for digital displacement machines," *Int. J. Mechatronics Autom.*, vol. 4, no. 2, pp. 116–126, 2014.
- [94] —, "Fluid Stiction Modeling for Quickly Separating Plates Considering the Liquid Tensile Strength," *ASME Fluids Eng.*, vol. 137, no. 6, pp. 61 205–61 208, 2015.
- [95] D. B. Roemer, P. Johansen, L. Schmidt, and T. O. Andersen, "Modeling of Movement-Induced and Flow-Induced Fluid Forces in Fast Switching Valves," *Inter. Conf. Fluid Power and Mechatronics*, pp. 978–983, 2015.
- [96] D. B. Roemer, H. C. Pedersen, and T. O. Andersen, "Modeling of Dynamic Fluid Forces in Fast Switching Valves," in *ASME/BATH Symp. Fluid Power Motion Control*, Chicago, 2015, pp. 1–10.
- [97] D. B. Roemer, C. Noergaard, M. M. Bech, and P. Johansen, "Valve and Manifold considerations for Efficient Digital Hydraulic Machines," in *Eighth Work. Digit. Fluid Power*. Tampere, Finland: Tampere University of Technology, 2016, pp. 213–227.
- [98] D. B. Roemer, "Design and Optimization of Fast Switching Valves for Large Scale Digital Hydraulic Motors," Ph.D. dissertation, Aalborg University, 2014.
- [99] S. Salter and W. Rampen, "Pump control method and poppet valve therefor," Patent EP0 361 927 A1, 1994. [Online]. Available: <https://patents.google.com/patent/EP0361927B1/en>
- [100] —, "Improved Fluid-Working Machine," 1995.
- [101] M. Sasaki, A. Yuge, T. Hayashi, H. Nishino, M. Uchida, and T. Noguchi, "Large Capacity Hydrostatic Transmission with Variable Displacement," in *9th Int. Fluid Power Conf.*, Aachen, Germany, 2014.
- [102] R. Scheidl and C. Gradl, "An Oil Stiction Model for Flat Armature Solenoid Switching Valves," *ASME/BATH 2013 Symp. Fluid Power Motion Control*, no. FPMC2013-4467, 2013.
- [103] —, "An Approximate Computational Method for the Fluid Stiction Problem of Two Separating Parallel Plates With Cavitation," *ASME J. Fluids Eng.*, vol. 138, no. 6, pp. 61 301–61 312, 2016.
- [104] R. Scheidl, C. Gradl, and A. Plöckinger, "The Cushioning Groove for Solenoid Switching Valves Concept and Theoretical Analyses," *Int. J. Fluid Power Syst.*, vol. 8, no. 2, pp. 76–81, 2014.
- [105] U. Scheuermann, R. Schmidt, and P. Newman, "Power cycling testing with different load pulse durations," in *Proc. PEMD*, 2014, pp. 1–6.

References

- [106] M. Simic and N. Herakovic, "Reduction of the flow forces in a small hydraulic seat valve as alternative approach to improve the valve characteristics," *Energy Convers. Manag.*, vol. 89, no. 1, pp. 708–718, 2015.
- [107] X. Song, L. Wang, and Y. Park, "Transient Analysis of a Spring-Loaded Pressure Safety Valve Using Computational Fluid Dynamics (CFD)," *J. Press. Vessel Technol.*, vol. 132, no. 5, pp. 54 501–54 505, 2010.
- [108] H. Sun, X. Wang, B. Tossan, and R. Dixon, "Three-dimensional thermal modeling of a lithium-ion battery pack," *J. Power Sources*, vol. 206, pp. 349–356, may 2012. [Online]. Available: <https://www.sciencedirect.com/science/article/pii/S0378775312001802>
- [109] J. Taylor, W. Rampen, A. Robertson, and N. Caldwell, "Digital Displacement ® Hydraulic Hybrids Parallel Hybrid Drives for Commercial Vehicles," in *JSAE Annu. Congr.*, no. 1, 2011.
- [110] H. Tian, P. Y. Li, and J. Van de Ven, "Valve Timing Control for a Digital Displacement Hydraulic Motor using an Angle-Domain Repetitive Controller - Final Version," *IEEE/ASME Trans. Mechatronics*, pp. 1–10, 2019. [Online]. Available: <https://ieeexplore.ieee.org/document/8671730/>
- [111] Toshihide Noguchi, H. Hirano, S. Kawabata, M. Shimizu, T. Hayashi, U. Stein, G. Voller, and W. Rampen, "POPPET VALVE, HYDRAULIC MACHINE, AND POWER GENERATING APPARATUS OF RENEWABLE-ENERGY TYPE," pp. 1–29, 2016.
- [112] H. C. Tu, M. B. Rannow, J. D. Van de Ven, M. Wang, P. Y. Li, and T. R. Chase, "High Speed Rotary Pulse Width Modulated On/Off Valve," in *ASME-IMECE*, no. January. Seattle, Washington USA: ASME, 2007, pp. 89–102. [Online]. Available: <http://proceedings.asmedigitalcollection.asme.org/proceeding.aspx?articleid=1599019>
- [113] H. C. Tu, M. B. Rannow, M. Wang, P. Y. Li, T. R. Chase, and J. D. Van de Ven, "Design, Modeling, and Validation of a High-Speed Rotary Pulse-Width-Modulation On/Off Hydraulic Valve," *J. Dyn. Syst. Meas. Control*, vol. 134, no. 6, p. 061002, 2012.
- [114] J. P. Uusitalo, V. Ahola, L. Soederlund, M. Linjama, and L. Kettunen, "Novel Bistable Hammer Valve For Digital Hydraulics," *Int. J. Fluid Power*, vol. 11, no. 3, pp. 35–44, 2010.
- [115] J. R. Valdés, J. M. Rodríguez, J. Saumell, and T. Pütz, "A methodology for the parametric modelling of the flow coefficients and flow rate in hydraulic valves," *Energy Convers. Manag.*, vol. 88, pp. 598–611, 2014.
- [116] J. A. Williams, "Wear and wear particles - some fundamentals," *Tribol. Int.*, vol. 38, no. 10, pp. 863–870, 2005.
- [117] B. Winkler, A. Plöckinger, and R. Scheidl, "A novel piloted fast switching multi poppet valve," *Int. J. Fluid Power*, vol. 11, no. 3, pp. 7–14, 2010.
- [118] B. Winkler and R. Scheidl, "Development of a fast seat type switching valve for big flow rates," *Tenth Scand. Int. Conf. Fluid Power*, pp. 137–146, 2007.

References

- [119] —, “Optimization of a Fast Switching Valve for Big Flow Rates,” in *Power Transm. Motion Control*. Bath: ASME, 2006, pp. 387–399.
- [120] D. Wu, R. Burton, and G. Schoenau, “An empirical discharge coefficient model for orifice flow,” *Int. J. Fluid Power*, vol. 3, no. 3, pp. 13–19, 2002.
- [121] S. Wu, X. Zhao, C. Li, Z. Jiao, and F. Qu, “Multiobjective Optimization of a Hollow Plunger Type Solenoid for High Speed On/Off Valve,” *IEEE Trans. Ind. Electron.*, 2018.
- [122] Y. P. Yang, J. J. Liu, D. H. Ye, Y. R. Chen, and P. H. Lu, “Multiobjective optimal design and soft landing control of an electromagnetic valve actuator for a camless engine,” *IEEE/ASME Trans. Mechatronics*, vol. 18, no. 3, pp. 963–972, 2013.
- [123] Y. Yang, H. Wang, A. Sangwongwanich, and F. Blaabjerg, *Reliability of Power Electronic Systems*, 4th ed. Elsevier Inc., 2018. [Online]. Available: <http://dx.doi.org/10.1016/B978-0-12-811407-0.00051-9>
- [124] Y. J. Yang, W. Peng, D. Meng, S. P. Zhu, and H. Z. Huang, “Reliability analysis of direct drive electrohydraulic servo valves based on a wear degradation process and individual differences,” *Proc. Inst. Mech. Eng. Part O J. Risk Reliab.*, vol. 228, no. 6, pp. 621–630, 2014.
- [125] B. Zardin, G. Cillo, C. A. Rinaldini, E. Mattarelli, and M. Borghi, “Pressure losses in hydraulic manifolds,” *Energies*, vol. 10, no. 3, 2017.
- [126] T. Zehetbauer, P. Foschum, A. Plöckinger, and B. Winkler, “Advancement and demonstration of the new generation of LCM’s FSVi4.1,” in *Proc. 9th Work. Digit. Fluid Power*, Aalborg, 2017.
- [127] K. Zhang, J. Yao, and T. Jiang, “Degradation assessment and life prediction of electro-hydraulic servo valve under erosion wear,” *Eng. Fail. Anal.*, vol. 36, no. 1, pp. 284–300, 2013.
- [128] L. Zhang, W. Zheng, J. Zhang, and M. Lian, “CFD Simulation of Flow Field for Pilot Operated Check Valve,” *Int. Conf. Inf. Sci. Mach. Mater. Energy*, pp. 1137–1140, 2015.

Appendix I

Design Optimization

“Premature optimization is the root of all evil.”

– Donald E. Knuth (1938 – x)

This appendix gives an example of how the revised modelling framework allows for a novel problem formulation where valve dynamics near the seat can be employed to include the fluid dynamical aspects in damping and stiction. The formulation also facilitates the knowledge gathered in previous work of both optimization and prototype measurements [5, 68, 98]. To do any type of optimization the objectives and requirement that are considered most suited for the DDU must be defined. These must be predictable by the models and in this case the objective function consist of implicit equations that are dynamic and coupled. Therefore, no discretized valve geometries (meshing) are used to locate candidate designs.

I.1 Objectives

The objective of a rotating machine is to convert mechanical energy (torque and rotation speed) to/from electric (voltage and current) or hydrostatic energy (flow and pressure). The task thus exists in doing this as effectively as possible, with a low volume and mass, preferably cheap and with sufficient robustness. The end-cost of a product under development is normally extremely difficult to predict, due to potential huge differences in costs related to manufacturing. The energy losses can be calculated to a sufficient level of certainty as can the machine mass. The combined durability is not possible to predict a priori at the current stage, but the factors influencing this are known, and some precautions can be made to avoid less durable designs. A series of metrics have been tested in this work, including: mass

of the plunger, total valve mass, plunger radius, RMS between the supply and chamber pressure, *impact velocity*, efficiency, *amount of power utilized compared to theoretical maximum*. The two highlighted in italic font are the ones resulting in most meaningful optimums, translated to the objectives

$$o_1^* = \min_{\mathbf{x} \in \mathbb{X}} E_{out,id} - (E_{out} - E_f - E_a) \quad (I.1)$$

$$o_2^* = \min_{\mathbf{x} \in \mathbb{X}} -\dot{z}_{H,imp} - \dot{z}_{L,imp} \quad (I.2)$$

where \mathbb{X} is the design vector space \mathbf{x} is the design vector.

Other authors have focused on the switching time and the overall machine efficiency [68,98], and to avoid a low power machine (which could still have high efficiency) a constraint is implemented to ensure a certain power output. The formulation of o_1^* inherently tries to maximize the power output of the DDU.

I.2 Design Variables and Constraints

The parameters that can be used to morph the machine are listed in Tab.I.1. The choices of parameter and corresponding lower and upper bounds (lb and ub) are determined from a priori systems knowledge, see similar studies [5] & [68]. This knowledge is combined with the sensitivity study presented in [Paper J] where significant parameters were found and basically when $lb = ub$ this is an easy way of disabling a parameter.

The constraints of the system relates to various features and are summarized in Tab. I.3. These either require a static or a dynamic evaluation to be checked and it is relevant to evaluate all static constraints initially, if these are inactive the dynamic simulation can be performed thus avoiding unnecessary computations.

The explanations of the allowable design variations are: $End_{on?}$ determines if an end-damping spring is included or not. $Cush_{on?}$ determines if cushioning grooves should be integrated or not. Act_{top} is able to choose between various actuators (the latter has been optimized in two separate routines due to faster convergence).

Decreasing the low pressure manifold (p_L) is an energy efficient way to increase the differential pressure without scaling leakage losses. Furthermore, if the energy of the low pressure line cannot be regenerated this is an effective way of increasing the machine efficiency. The issue arises if the pressure is too low and cavitation occurs, this typically occurs if the stiction period is too long compared to the value of p_L . Therefore, a constraint is formulated to avoid pressure below 1.5 bar.

The time for the actuators being on ($t_{A,H,on}$ and $t_{A,L,on}$) and the voltage step applied (u_H and u_L) are relevant in saving electrical energy and finding

I.2. Design Variables and Constraints

Table I.1: Parametrization of DDU design

x	Name	lb	ub	Unit
x_1	$End_{on?}$	0	1	[-]
x_2	$Cush_{on?}$	0	1	[-]
x_3	Act_{top}	0	1	[-]
x_4	p_L	3.00	10.00	[bar]
x_5	l_1	0.10	0.40	[mm]
x_6	l_2	0.10	0.40	[mm]
x_7	l_3	0.10	0.40	[mm]
x_8	l_4	0.10	0.40	[mm]
x_9	r_1	0.25	1.0	[mm]
x_{10}	r_2	0.25	1.0	[mm]
x_{11}	R	10.00	20.00	[mm]
x_{12}	l_s	1.00	5.00	[mm]
x_{13}	w_{in}	2.00	7.50	[mm]
x_{14}	l_B	0	1.00	[mm]
x_{15}	$A_{N,c1}$	0	0.85	[mm ²]
x_{16}	$A_{N,c2}$	0	0.85	[mm ²]
x_{17}	f_1	0.20	0.80	[-]
x_{18}	f_2	0.10	1.00	[-]
x_{19}	f_3	0.40	4.00	[-]
x_{20}	k_s	0	5.00	[N/mm]
x_{21}	θ_H	5.23	5.39	[rad]
x_{22}	θ_L	2.19	2.34	[rad]
x_{23}	$t_{A,H,on}$	0.05	0.52	[rad]
x_{24}	$t_{A,L,on}$	0.05	0.52	[rad]
x_{25}	$t_{A,H,reverse}$	0	0.35	[rad]
x_{26}	$t_{A,L,reverse}$	0	0.35	[rad]
x_{27}	u_H	-50.00	-5.00	[V]
x_{28}	u_L	-50.00	-5.00	[V]
x_{29}	$u_{H,reverse}$	30.00	50.00	[V]
x_{30}	$u_{L,reverse}$	30.00	50.00	[V]
Disabled parameters				
x_x	p_H	350.00	350.00	[bar]
x_x	r_e	16.50	16.50	[mm]
x_x	r_P	22.00	22.00	[mm]
x_x	N_{cyl}	5	5	[-]
x_x	$Material$	1	1	[-]

Table I.2: Objectives of DDU design

o	Name	Unit
o_1	Energy utilization	J
o_2	Impact speeds	m/s

Table I.3: Constraints of DDU design

g	Name
g_1	$F_{st} - F_f < 0$
g_2	$1 - \delta_H - \delta_L < 0$
g_3	$\sigma_{lim} - \sigma_s < 0$
g_4	$sim_{crash} < 0$
g_5	$\eta_{min} - \eta < 0$
g_6	$p_{min} - \min(p_C) < 0$
g_7	$\max(p_{H,cush}) - p_{cush,max} < 0$
g_8	$\max(p_{L,cush}) - p_{cush,max} < 0$
g_9	$\max(p_C) - p_{max} < 0$
g_{10}	$\dot{z}_{imp,H} - \dot{z}_{max} < 0$
g_{11}	$\dot{z}_{imp,L} - \dot{z}_{max} < 0$

Table I.4: Summary of design optimization formulation

Description	Value
Objective dimensions	length(o)
No. of constraints	length(g)
Parameters dimensions	length(x)
Population size (NP)	5 length(x)
No. of generations	≈ 300
GDE settings: CR, F	0.25, 0.75
Total computation time	3.5 days

the minimum required work. Furthermore, it is possible to reverse the force (for soft-landing control) and therefore the algorithm can tune the period of reverse force ($t_{A,H,reverse}$ and $t_{A,L,reverse}$ for both valves) and how much power should be used for this ($u_{H,reverse}$ and $u_{L,reverse}$). The durations are given in radians relative to the switching angle, θ_H and θ_L respectively. This corresponds to a constant time period since rotation speed is constant and is radians/sec.

$l_1, l_2, l_3, l_4, l_s, r_1, r_2, w$ and R are geometric parameters as depicted in Fig. 3.20, k_s is the stiffness of the spring ensuring the valve being normally open (only included when the MCA is used). The end-damping spring is determined from its stroke length l_B and f_1, f_2, f_3 governs its thickness and remaining dimensions as explained in section 3.3.

The current fixed values are for: the dimensions of the eccentricity (r_e, r_P), the high pressure manifold (p_H), number of cylinders (N_{cyl}) and material choice of the plunger (*Material*), which is set to be stainless steel.

Constraints with static dependencies

In g_1 it is checked if the valves are normally open as intended. The maximum flow force (F_f) of the specific machine type is predicted and this is compared to the static opening force (F_{st}) from either the spring assembly (in the MCA topology) or the latching magnet (in the MMA topology).

The stresses of the end-damping spring are not allowed to cross a given threshold. This can be computed based on the chosen design parameters and compared to the value of σ_{lim} .

The expressions of fluid losses over one cycle was derived in section 3.3 along with the ideal output energy. These are used to estimate the DDU efficiency and if this is not sufficient the design is discarded.

Constraints with dynamic dependencies

It occurs that the chosen design point give complex solutions or the numerical stiffness becomes so severe that the solution is not found within the time allocated per simulation (5 min). If this happens g_4 is activated.

The purpose of g_6 is to avoid cavitation, i.e. the algorithm will locate the lowest possible pressure in the manifold that is sufficient to activate the LP check valve without going into cavitation. $p_{min} = 1.5$ bar has been chosen.

If the algorithm chooses a cushion groove design a constraint is established which limits the fluid pressure to avoid too large pressures. This is ensured by g_7 .

The impact velocity is maintained under a given threshold to provide a durable design, this is furthermore used as an objective to reduce the stresses further.

Setting up the Optimization Algorithm

There exists various types of algorithms which are programmed to locate optimums in various types of problems. The definition of this optimization problem consists of several objective functions and computational tricks to avoid heavy simulations when not necessary. This calls for a versatile algorithm that can handle these requirements and is proven useful for similar problem formulations. This is the reason for choosing the Generalized Differential Evolution (GDE3) algorithm by [43].

The crossover rate (CR) and the control parameter (F) together governs the standard deviation in the populations, i.e. balancing between premature convergence and locating optimal solutions in a proper time-frame. The values of the two have been determined based on previous research of a similar problem [5] combined with the c -factor mentioned in [43] that when $c = 1$ no change in the populations diversity occurs as the generation number progresses, if $c < 1$ the diversity decreases (solution space converges) and if $c > 1$ the diversity increases (solution space is continually explored).

$$c = \sqrt{2F^2CR - 2CRNP^{-1} + CR^2NP^{-1} + 1} \quad (I.3)$$

The chosen values of CR and F and the population size (NP) results in $c = 1.13$ and the GDE3 does therefore explore more and more of the solution space over time.

I.3 Results

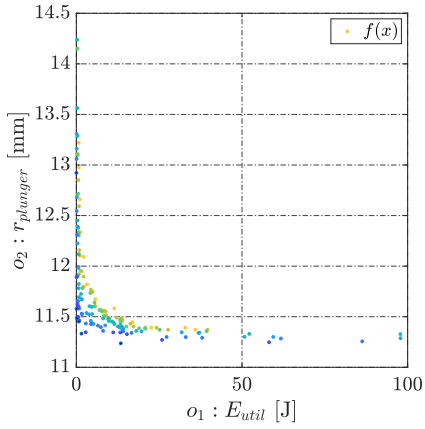
Initially two separate optimization studies were carried out each with two objectives. Hereafter, a study with three objectives was done to investigate the influence of another objective on the convergence time. Otherwise the formulation of the problem was identical. The objective evaluations of the optimization routine of the MMA are given in Fig. I.1. The results indicates that when three objectives are defined convergence to a Pareto front becomes slower/more difficult.

The achieved objectives are relevant to understand the obtainable performance and trade-off's.

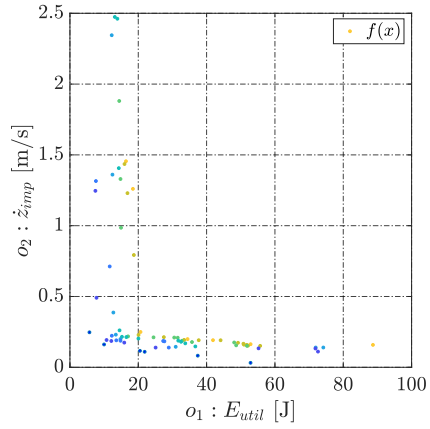
From Fig. I.1a it is observed that wider designs utilize the energy better in general. The two objective seems to be conflicting to some degree. However, slim designs with almost optimal values of energy utilization exists.

In Fig. I.1b the tendency is that reducing the impact speed is not directly conflicting with the energy utilization. Various designs exists which achieve almost the same impact speed, but large changes in the energy utilization are observed. A Utopian point is realistic for these objectives, i.e. the energy loss by introducing end-damping is marginal.

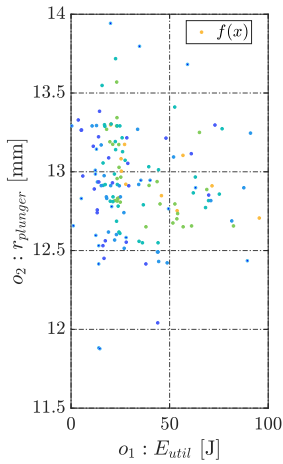
Appendix I. Design Optimization



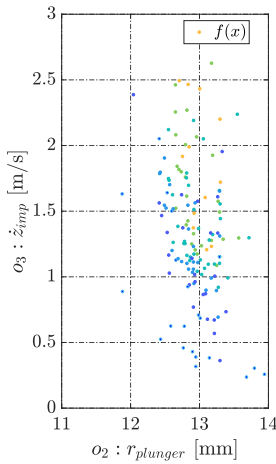
(a) Energy utilization vs plunger radius.



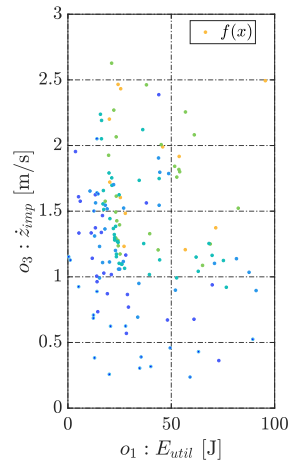
(b) Energy utilization vs plunger impact speed.



(c) 3 objectives.



(d) 3 objectives.



(e) 3 objectives.

Fig. I.1: Pareto fronts when optimizing the valves in a DDU with specifications given in Chapter 2. A MMA is applied to deliver the actuating force. Each Pareto rank is denoted with a color encoding with blue being best and yellow worst. The two plots in the top are optimized as two separate 2-objective formulations. The three at the bottom are from a 3-objective formulation.

I.3. Results

The analysis with three objectives does not reach the same performance points and additional computational time would be necessary. This was found after one week of optimization and it has been considered more feasible to use the results of Fig. I.1a or Fig. I.1b. The plunger radius is not as critical as durability for the considered application and therefore a design from I.1b has been chosen for verification purposes and the radius considered as a geometrical constraint. However, the results do indicate that a more compact design is possible while maintaining high efficiency and not crossing the defined constraints on the impact speed.

The distribution of the design variables for the latest generation shows if design parameters have converged to one level or if they are evenly distributed. The distributions of all parameters are given in Fig. I.2 with an estimated normal distribution on top which are valid for some values. Each parameter is displayed within the defined lower- and upper-bound.

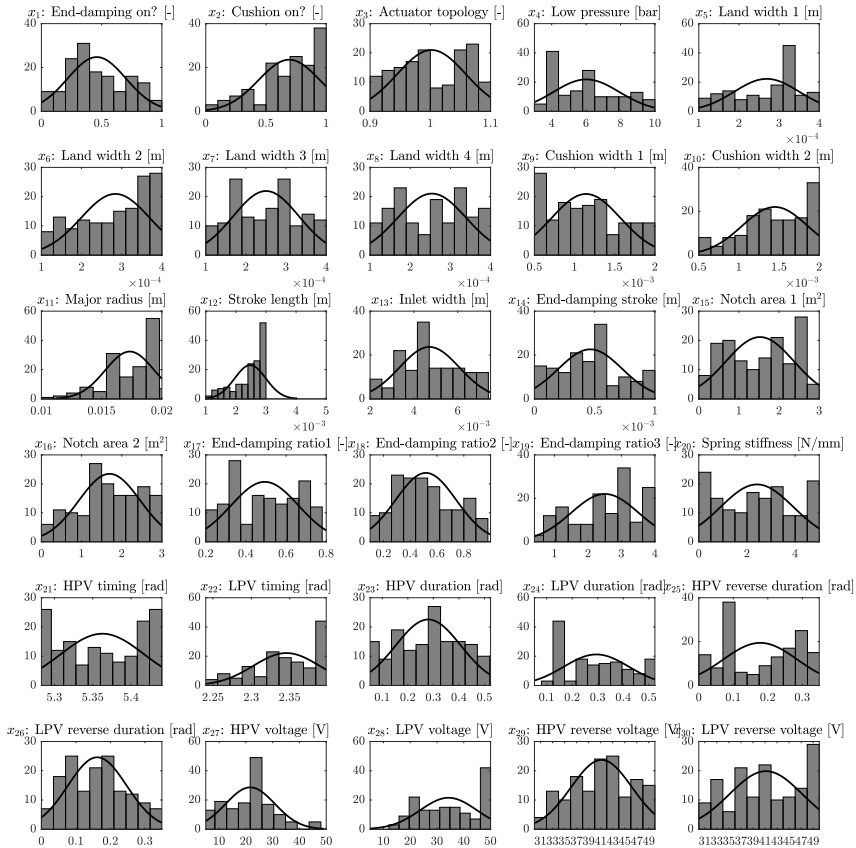


Fig. I.2: The design vector landscape corresponding to the objectives plotted in Fig. I.1b.

Appendix I. Design Optimization

The design points does not crowd toward any of the defined boundaries indicating that these have been defined 'wide enough' to capture the optimal region of the design space.

Appendix II

Plunger Surface Scans

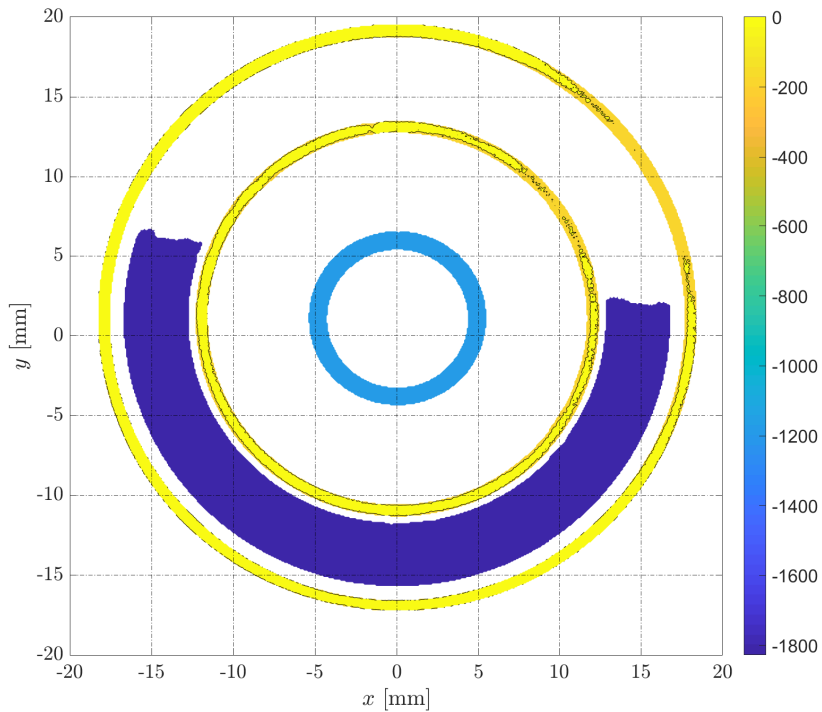


Fig. II.1: Distance to the plunger surface (concept 1) examined by ultrasound.

Appendix II. Plunger Surface Scans

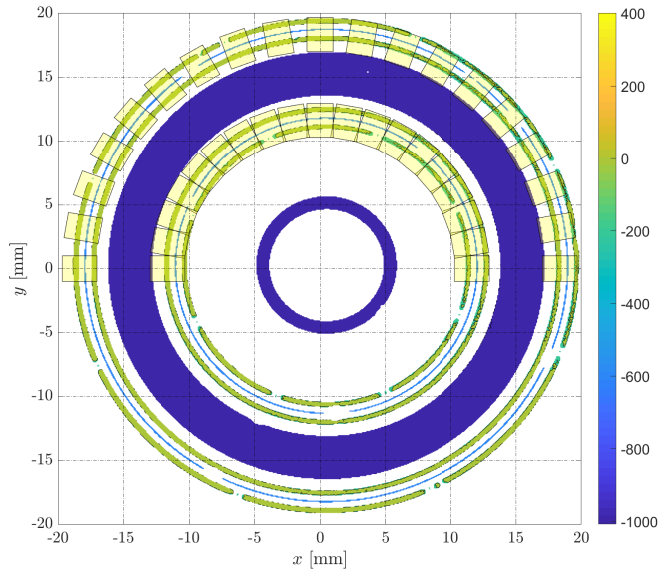


Fig. II.2: Distance to the plunger surface (concept 3) examined by ultrasound.

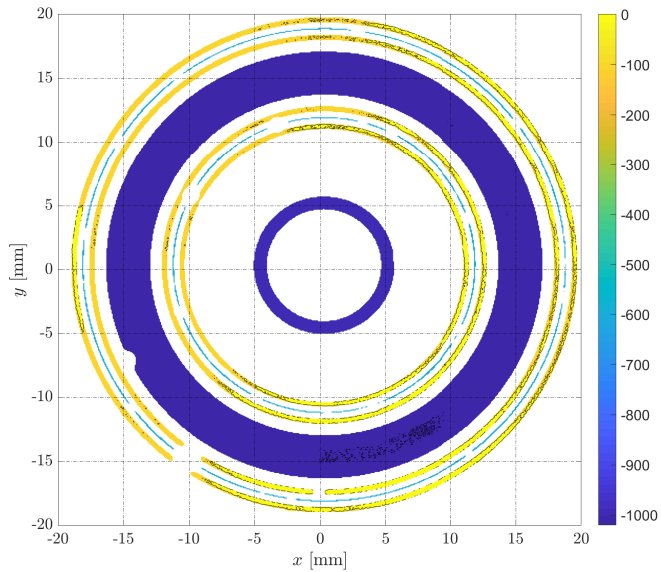


Fig. II.3: Distance to the plunger surface (concept 4) examined by ultrasound.

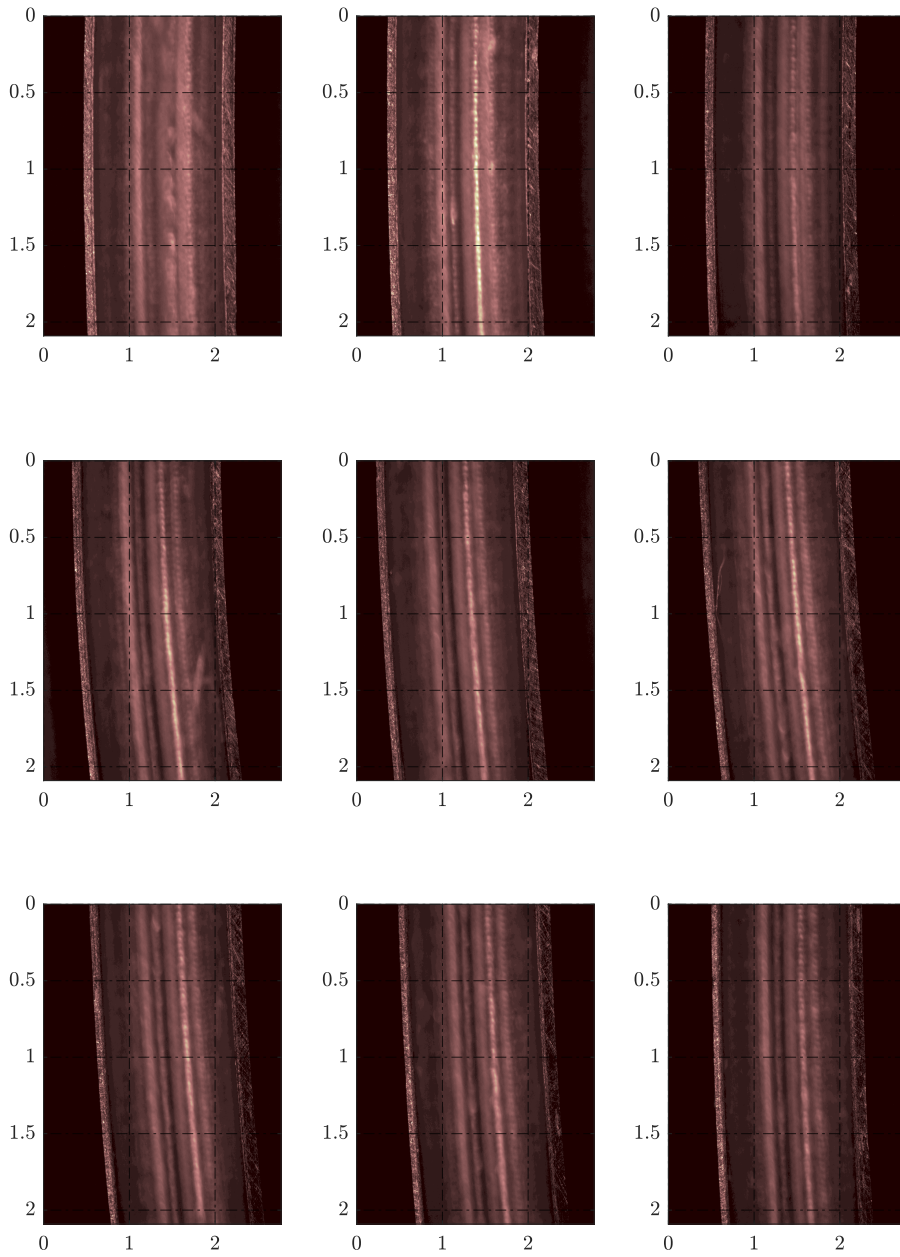


Fig. II.4: Valve plunger contact surface scans of concept 2, outer ring part 1.

Appendix II. Plunger Surface Scans

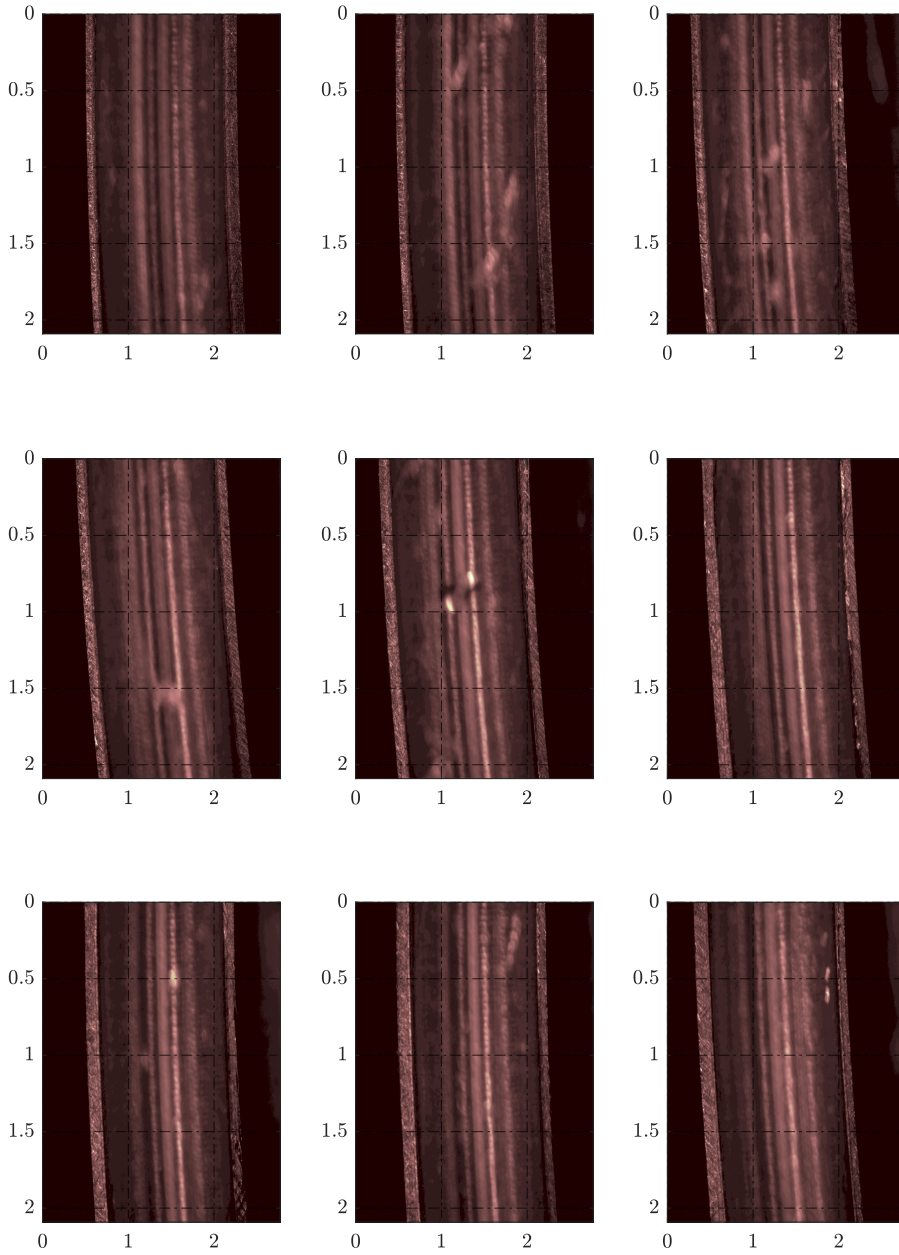


Fig. II.5: Valve plunger contact surface scans of concept 2, outer ring part 2.

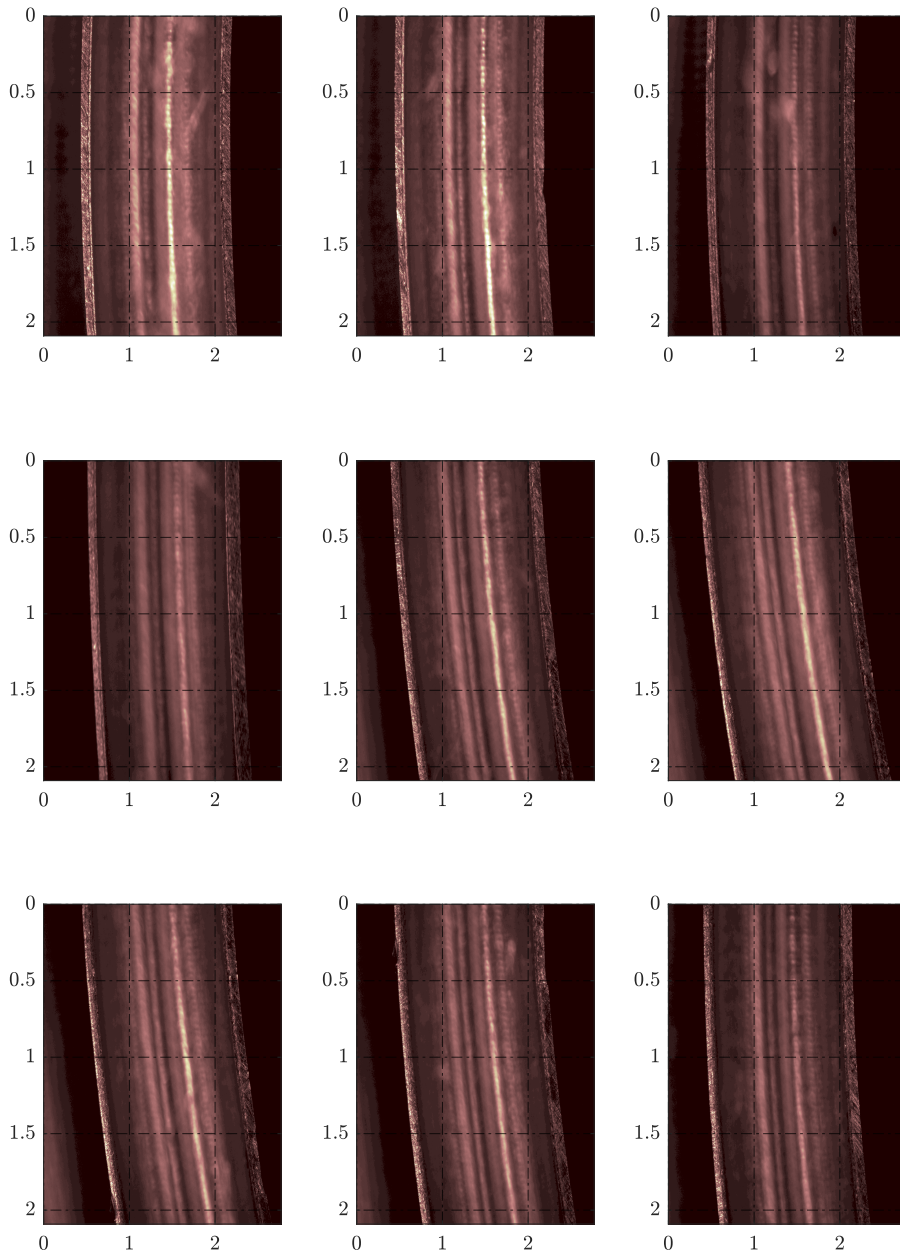


Fig. II.6: Valve plunger contact surface scans of concept 2, inner ring part 1.

Appendix II. Plunger Surface Scans

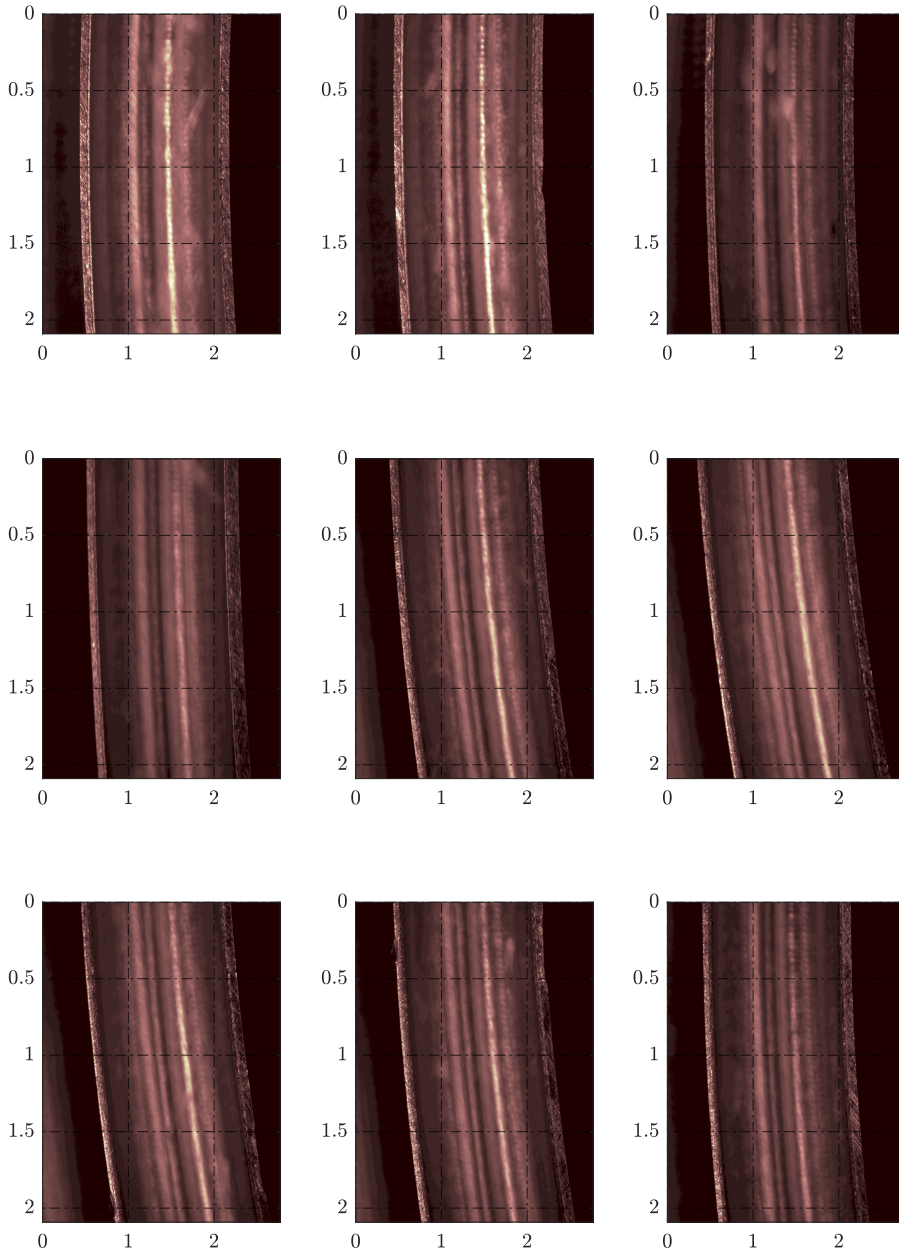


Fig. II.7: Valve plunger contact surface scans of concept 2, inner ring part 2.

Part II

Papers

Paper A

Experimental Validation of Flow Force Models for Fast Switching Valves

Niels C. Bender
Henrik C. Pedersen
Christian Nørgård

The paper has been presented and published in
*Proceedings of the 2017 ASME/BATH symposium on Fluid Power and Motion
Control*, Sarasota, USA, ISBN:978-0-7918-5833-2,
doi:10.1115/FPMC2017-4230.

©2017 ASME

The layout has been revised.

Paper B

Reliability Analysis of a Hydraulic on/off Fast Switching Valve

Niels C. Bender
Henrik C. Pedersen
Andreas Plöckinger
Bernd Winkler

The paper has been published & presented at
The Ninth Workshop on Digital Fluid Power, Aalborg, pp. 1–18, September 7-8,
2017.

2017 AAU, Energy Department
The layout has been revised.

Paper C

Towards a modelling framework for designing active
check valves a review of state of the art

Niels C. Bender
Henrik C. Pedersen
Andreas Plöckinger
Bernd Winkler

The paper has been published in
International Journal of Fluid Power, vol 19, issue 1, pp. 49–64 , 2017,
doi:10.1080/14399776.2017.1377027.

©2017 IJFP

The layout has been revised.

Paper D

Evaluating the Influence of Leaking Active Check Valves in Digital Displacement[®] Units

Niels C. Bender
Henrik C. Pedersen
Andreas Plöckinger
Bernd Winkler

The paper has been presented & published in
Proceedings of the 2018 IEEE Global Fluid Power Society PhD Symposium,
Samara, Russia, ISBN:978-1-5386-4785-1, doi:10.1109/GFPS.2018.8472399.

© 2018 GFPS

The layout has been revised.

Paper E

Numerical Investigation of Switching Features of a Hydraulic Seat Valve with Annular Flow Geometry

Niels C. Bender
Henrik C. Pedersen
Andreas Plöckinger
Bernd Winkler

The paper has been published in
International Journal of Fluid Power, vol 19, issue 3, pp. 152–164, 2018,
doi:10.1080/14399776.2018.1491755.

© 2018 IJFP

The layout has been revised.

Paper F

A Multi-agent Evolution Algorithm used for Input Shaping of a Repetitive Non-linear Dynamic System

Niels C. Bender
Henrik C. Pedersen
Michael M. Bech
Torben O. Andersen

The paper has been presented and published in
Proceedings of the 2018 ASME/BATH Symposium on Fluid Power and Motion Control, Bath, UK, ISBN:978-0-7918-5196-8, doi:10.1115/FPMC2018-8870

© 2018 ASME/BATH
The layout has been revised.

Paper G

Experimental Study of a Digital Displacement Machine Utilizing a Cushion Valve Topology

Niels C. Bender
Jeppe H. Christensen
Michael M. Bech
Henrik C. Pedersen

The paper has been published and presented at
the Tenth Workshop on Digital Fluid Power, Linz, Austria.

at 1-3 March 2019
The layout has been revised.

Paper H

Measurements of a Novel Digital Hydraulic Valve Comprising a Cushioning Feature

Niels C. Bender
Andreas Plöckinger
Paul Foschum
Bernd Winkler
Henrik C. Pedersen

The paper is accepted for publication and has been re-submitted for the
second review process

Journal of Dynamic Systems, Measurement and Control

©2019 ASME

The layout has been revised.

Paper I

Feasibility of Deep Neural Network Surrogate Models in Fluid Dynamics

Niels C. Bender
Torben O. Andersen
Henrik C. Pedersen

The paper has been published at
Modeling, Identification and Control, 2019

© 2019 MIC

The layout has been revised.

Paper J

Parameter Correlation by Static and Dynamic
Evaluations Utilizing a Mechatronic Design
Procedure for a Digital Displacement Unit

Niels C. Bender
Torben O. Andersen
Henrik C. Pedersen

The paper is under review since November 19th, 2018 for
the IEEE/ASME Transactions on Mechatronics

© 2018 IEEE/ASME
The layout has been revised.

ISSN (online): 2446-1636
ISBN (online): 978-87-7210-474-4

AALBORG UNIVERSITY PRESS